FUNctional characterisation of type 1 ryanodine receptor variants.

A thesis presented in partial fulfilment of the requirements for the degree of

Master of Science

in

Genetics

at Massey University, Manawatū, New Zealand.

Liam Scott Hewson

2021

Abstract

Malignant hyperthermia (MH) is a pharmacogenetic disorder that presents as a hypermetabolic response to volatile anaesthetics such as isoflurane, desflurane and sevoflurane, as well as the depolarising muscle relaxant succinylcholine. MH reactions are characterised by a wide variety of clinical symptoms, including but not limited to muscle rigidity, tachycardia, hyperthermia, and hyperkalaemia. If left untreated, an MH reaction can result in cardiac arrest; therefore, those with a family history of MH are encouraged to be tested for susceptibility. The current diagnostic procedure is the *in vitro* contracture test (IVCT), wherein the contractile response of a patient muscle biopsy after exposure to caffeine and halothane is measured. While considered the "gold-standard" for MH susceptibility testing, the reliance of the test on an excised muscle specimen makes it traumatic for the patient, and a financial burden on the healthcare system. As a result, a cheaper and less traumatic genetic test has been under development to one day replace the IVCT.

Genetic testing for MH susceptibility focuses on the allelic heterogeneity of a Ca^{2+} release channel known as the type 1 ryanodine receptor (*RYR1*). RyR1 functions to regulate Ca^{2+} release for the purposes of muscle contraction. Currently, between 50 and 86% of MH reactions can be attributed to variants in the *RYR1* gene. In order for MH susceptibility to be accurately diagnosed using a genetic test, known variants of RyR1 must meet a set of requirements to determine their pathogenicity, including being functionally characterised and shown to be hypersensitive to agonists.

Over the course of this project, six RyR1 variants, from families known to be susceptible to MH, were functionally characterised. Of these, one was located in the N-terminal hot spot domain (p.Phe539Leu), three were located in the central hot spot domain (p.Gly2183Glu, p.Cys2237Tyr, p.Arg2458Leu), while two flanked the central domain (p.Arg1707Cys, p.Pro2793Leu). The results obtained indicate that the substitutions p.Cys2237Tyr and p.Pro2793Leu produce hypersensitive channels, and while p.Pro2793Leu remains a variant of unknown significance, p.Cys2237Tyr has met the criteria to be classified as likely pathogenic for MH and should therefore be added to the list of MH diagnostic variants.

Acknowledgements

The work herein is dedicated to my family, without whom I could not succeed.

I would like to give special acknowledgements to my supervisors Prof. Kathryn Stowell and Dr Anja Schiemann who have been integral to my development as a scientist, and to my office mates, whose friendship I'll always appreciate.

Table of contents

List of figures

List of tables

Abbreviations

4-c*m*c	4-chloro *m* cresol
4E-BP1	4E-binding protein 1
ADP	Adenosine diphosphate
ATP	Adenosine triphosphate
axRyR1	pcDNA5/FRT/TO© full-length *RYR1* cDNA (using AvrII-XbaI)
bGH	Bovine growth hormone
BSA	Bovine serum albumin
BSS	Balanced salt solution
CaM	Calmodulin
CCD	Central core disease
cDNA	complementary deoxyribonucleic acid
CHCT	Caffeine-Halothane contracture test
CICR	Ca^{2+} induced Ca^{2+} release
CRAC	Ca^{2+} release-activated channel
Cryo-EM	Cryogenic-electron microscopy
CSQ	Calsequestrin
C-terminal	Carboxyl-terminal
DAPI	4', 6-diamidino-2-phenylindole
DEPC	Diethyl pyrocarbonate
DHPR	Dihydropyridine receptor
DIC	Disseminated intravascular coagulation
DMEM	Dulbecco's modified eagle media
DNA	Deoxyribonucleic acid
EC_{50}	Half maximal effective concentration
ECCE	Excitation-coupled Ca^{2+} entry
EC coupling	Excitation-contraction coupling
EDTA	Ethylenediaminetetraacetic acid
EMHG	European Malignant Hyperthermia Group
ER	Endoplasmic reticulum
ER-PM	Endoplasmic reticulum-plasma membrane
FBS	Foetal bovine serum

FITC	Fluorescein isothiocyanate
FKBP	FK-506 binding protein
FRET	Fluorescence resonance energy transfer
FRT	Flippase recombination target
ftRyR1	pcDNA5/FRT/TO© full-length *RYR1* cDNA
Fura2-AM	Fura2-acetoxymethyl
GC	Guanine-cytosine
GFP	Green fluorescent protein
GOI	Gene of interest
HEK293	Human embryonic kidney 293
HRP	Horseradish peroxidase
IP3R	Inositol 1,4,5-triphosphate receptor
IVCT	*In vitro* contracture test
LB	Lysogeny broth
MGS	Massey Genome Service
MH	Malignant hyperthermia
MHN	Malignant hyperthermia negative
MHS	Malignant hyperthermia susceptible
MHS_c	Malignant hyperthermia susceptible (caffeine)
MHS_h	Malignant hyperthermia susceptible (halothane)
MHS_{hc}	Malignant hyperthermia susceptible (caffeine and halothane)
Min	Minute
MMD	Multi-minicore disease
MMIC	Manawatū Microscopy and Imaging Centre
mTOR	Mammalian target of rapamycin
NAM	Native American Myopathy
N-terminal	Amino-terminal
P70s6k	Ribosomal protein S6 kinase beta 1
pBS	pBlueScript KS+
PBS	Phosphate buffered saline
PCR	Polymerase chain reaction
PDI	Protein disulphide isomerase
PKA	Protein kinase A
PTM	Post-translational modification

PVDF	Polyvinylidene difluoride
pVSD	Pseudo voltage-sensory domain
RNA	Ribonucleic acid
ROI	Region of interest
RyR1	Ryanodine receptor isoform 1
SDM	Site-directed mutagenesis
SDS	Sodium dodecyl sulphate
SERCA	Sarco/endoplasmic reticulum Ca^{2+} ATPase
SERCA2	Sarco/endoplasmic reticulum Ca^{2+} ATPase 2
SOC	Store-operated channel
SOCE	Store-operated Ca^{2+} entry
SPRY	Sp1A-Ryanodine receptor
SR	Sarcoplasmic reticulum
STAC3	SH3 and cysteine rich domain 3
STIM1	Stromal interaction molecule 1
SV40	Simian Virus 40
TAE	Tris-acetate-EDTA
TBST	Tris-buffered saline + Tween20
TE	Tris-ethylenediaminetetraacetic acid
TRITC	Tetramethylrhodamine
T-tubule	Transverse-tubule
UPR	Unfolded protein response
UV	Ultraviolet
VCEP	Variant Curation Expert Panel
U	Units
V	Volts
µg	Microgram
µL	Microlitre
µM	Micromole $litre^{-1}$
mL	Millilitre
Kb	Kilobase
bp	Base pair
s	Second

Chapter 1. Introduction

The RYR1 cDNA sequences referred to herein are Genbank accessions NM_000540.3 (Human) and NM_001101718.1 (Rabbit). RYR2 cDNA refers to Genbank accession NM_001035.3 (Human). Protein residues were determined by translating the respective cDNA sequences.

1.1 Principles of skeletal muscle contraction

1.1.1 Muscle structure and contraction process

Beginning with the detection of an action potential at the neuromuscular junction and ending with the compaction of the sarcomere, a range of processes occurring both out of and within the muscle fibre controls muscle contraction. Arranged in a repeating fashion within the myofibrils and comprised of a complex array of actin and myosin filaments, the fundamental unit of striated muscle fibre, known as the sarcomere (Fig. 1.1), contracts muscle via a sliding filaments model wherein the "thick" myosin filaments pull on the "thin" actin filaments resulting in the compaction of the sarcomere and thereby contraction of muscle[1].

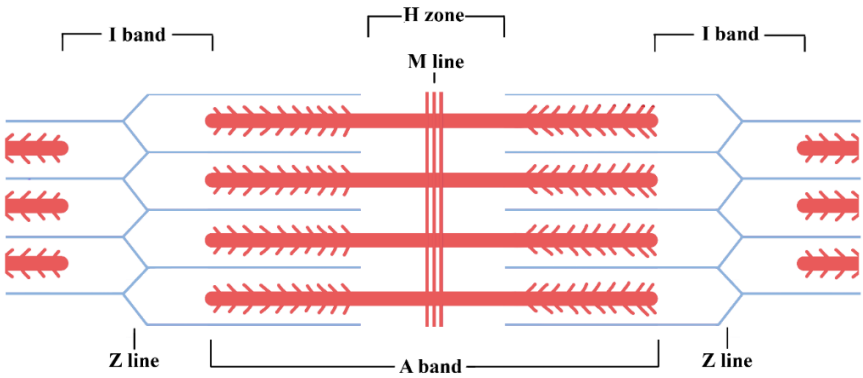

Figure 1.1. The sarcomere.

Schematic diagram of the sarcomere, the repeating unit comprising myofibrils. Shown are the thin filaments (blue), and the thick filaments (red). Labelled are the multiple regions of the sarcomere including the I bands, A band, Z lines and M line, as well as the H zone. Image was created in Adobe Photoshop.

Original artwork with reference to publication(s): [1]

Muscle contraction is the result of a complex set of events involving a wide variety of protein interactions regulated by a plethora of extra and intracellular processes. At the neuromuscular junction (also known as the motor end plate), an action potential travelling across the motor neuron is converted to a chemical signal in the form of acetylcholine. This neurotransmitter crosses the synaptic cleft and binds nicotinic receptors present in the muscle fibre membrane known as the sarcolemma. The binding of acetylcholine to these receptors induces the opening of Na^+ and K^+ channels within the sarcolemma causing its depolarisation[2]. The action potential produced as a result of this depolarisation is recognised by the voltage-gated channel Cav1.1, an L-type Ca^{2+} channel more commonly referred to as the dihydropyridine receptor (DHPR)[3, 4]. Once the depolarisation of the sarcolemma is detected, the DHPR undergoes a conformational change which activates the type 1 ryanodine receptor (RyR1), a large Ca^{2+} channel located transmembranously at the terminal cisternae of the sarcoplasmic reticulum[5].

Ca^{2+} plays an integral role in muscle contraction by binding to the troponin complex present on tropomyosin, a filamentous protein that comprises part of the thin filaments of the sarcomere (Fig. 1.2). According to the sliding filament model, the binding of Ca^{2+} to the troponin complex results in a conformational change that leads to the displacement of tropomyosin[6, 7]. As a result, myosin binding sites upon the actin are revealed, at which the thick filaments of the sarcomere then interact. The subsequent "pulling" of the thin filaments by myosin produces a contraction in a process known as the cross-bridge cycle[8, 9].

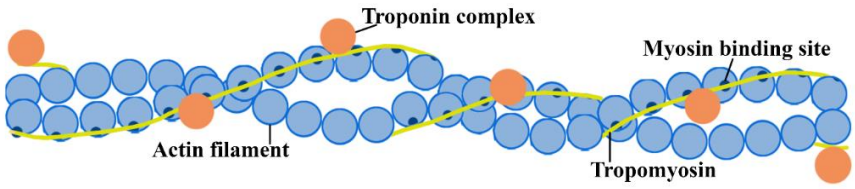

Figure 1.2. The thin filament of the sarcomere.

Schematic diagram of the thin filament of the sarcomere including the actin filament (blue) with the myosin binding sites (dark blue), the troponin complex (orange), and tropomyosin (yellow). Not shown are Ca^{2+} ions. Image was created in Adobe Photoshop.

Original artwork with reference to publication(s): [9, 10]

At the beginning of the cross-bridge cycle, when in the absence of ATP, myosin is tightly bound to actin in a transient state known as rigor (in death this state becomes permanent and is referred to as rigor mortis). In the next stage, ATP binds to the myosin head, causing a conformational change that results in the affinity of myosin

for actin being decreased. As a result, myosin dissociates from the actin filaments causing the myosin head to become "cocked" toward the end of the sarcomere. Subsequent hydrolysis of the ATP bound to myosin produces adenosine diphosphate (ADP) and an inorganic phosphate molecule. Both of these remain linked to the myosin head. From here, the myosin head binds a new site on the actin filament, producing a pulling motion that results in the shortening of the H zone of the sarcomere (Fig. 1.1). The cycle ends when ADP and the inorganic phosphate molecule are released from the myosin head, allowing the myosin to return to its original state of rigor, where it is bound to actin in the absence of ATP.

It should be noted that as long as Ca^{2+} remains bound to the troponin complex, cross-bridge cycling events will continue to occur. Relaxation of the muscle fibre only occurs when the intracellular [Ca^{2+}] decreases, causing Ca^{2+} to dissociate from the troponin complex. In the absence of Ca^{2+}, tropomyosin returns to its original position, blocking the myosin binding sites on the actin filaments, preventing interactions between the thick and thin filaments of the sarcomere. This sequence of events from the excitation of the muscle fibre to its contraction is termed excitation-contraction coupling (EC coupling) and although complex, is the central dogma for striated muscle contraction[6, 8].

1.1.2 Ca^{2+} homeostasis

Due to the integral role of Ca^{2+} in muscle contraction, its accumulation in and release from intracellular stores is a tightly regulated process. Indeed, the replenishment of Ca^{2+} stores after muscle contraction is controlled by multiple independent systems. Perhaps the most well understood mechanism for replenishing these stores is the sarco/endoplasmic reticulum Ca^{2+} ATPase (SERCA). This ATP-dependent Ca^{2+} pump binds cytosolic Ca^{2+} before transporting it into the lumen of the sarcoplasmic reticulum (SR) via a conformational change of its transmembrane region. Resolved at 2.6 Å, the transmembrane region (M) of the Ca^{2+} pump consists of 10 α-helices; of which, helices M4-M6 and M8 encompass 2 Ca^{2+} ion binding sites 5.7Å apart[11]. Ca^{2+} transport is highly dependent on these sites, specifically the side chain oxygen atoms present in residues Asn768 and Glu771 of M5, as well as Thr799 & Asp800 of M6 and Glu908 of M8. Indeed, mutation of these residues results in the complete loss of Ca^{2+} transport function[12].

While SERCA may be most affiliated with the replenishment of Ca^{2+} stores in the SR, Ca^{2+} is also replenished in multiple cell types via store-operated Ca^{2+} entry (SOCE). This is a process wherein the depletion of ER/SR Ca^{2+} stores is recognised by a diverse set of surface receptors that activate store-operated Ca^{2+} channels (SOCs). An example of this is seen with the Ca^{2+} release-activated channel (CRAC), a Ca^{2+}

channel present in the ER/SR which is activated by decreased luminal [Ca^{2+}]. This depletion of Ca^{2+} is recognised by stromal interaction molecule 1 (STIM1) which, once activated, localises to the endoplasmic reticulum-plasma membrane (ER-PM) junctions. Once localised, STIM1 rapidly recruits the Ca^{2+} release-activated Ca^{2+} channel protein 1 (Orai1) which moves in a coordinated fashion with STIM1 to produce open CRAC channels that provide an influx of Ca^{2+} after store depletion[13-15].

A third mechanism behind the replenishment of Ca^{2+} stores is a process known as excitation-coupled calcium entry (ECCE) wherein prolonged depolarisation of the sarcolemma results in an influx of extracellular Ca^{2+}[16]. While the exact mechanism behind this process is unknown, it is known that the Ca^{2+} channel protein, Orai1, is not involved. Importantly, dyspedic and dysgenic mouse myotubes that lack functional RyR1 and DHPR respectively do not exhibit ECCE, indicating that the recognition of membrane depolarisation is an important factor[16, 17]. Interestingly, unlike SOCE, ECCE does not depend on the state of Ca^{2+} stores within the ER/SR[18, 19]. While the replenishment of Ca^{2+} stores after muscle contraction is often attributed to SERCA, the gap in knowledge in regard to processes such as ECCE highlights the complexities of Ca^{2+} homeostasis, which may affect how muscles regulate contractions.

1.2 Mammalian ryanodine receptors

1.2.1 Overview

Ryanodine receptors (RyR) are large (>2 MDa) homotetrameric ion channels that mediate the release of Ca^{2+} from stores in the endo/sarcoplasmic reticulum[20]. There are 3 isoforms of ryanodine receptor present in mammals and while all 3 are expressed throughout different tissues, the current literature indicates each isoform as having specific expression patterns. RyR1 is found primarily in skeletal muscle, while RyR2 is found most abundantly in cardiac muscle. The third isoform (RyR3) is less understood but is found predominantly in neuronal tissue[21-23]. Each isoform of RyR provides a crucial role in mammalian physiological processes. RyR1 is a key regulator of skeletal muscle contraction, whereas RyR2 not only regulates cardiac muscle contraction, but is also involved in glucose homeostasis[24-26]. RyR3, while less studied than the other isoforms, has been implicated in regulating neurological function; however, it is also present in skeletal muscle, though it is not required for contraction[27, 28].

1.2.2 Ryanodine receptor isoform 1

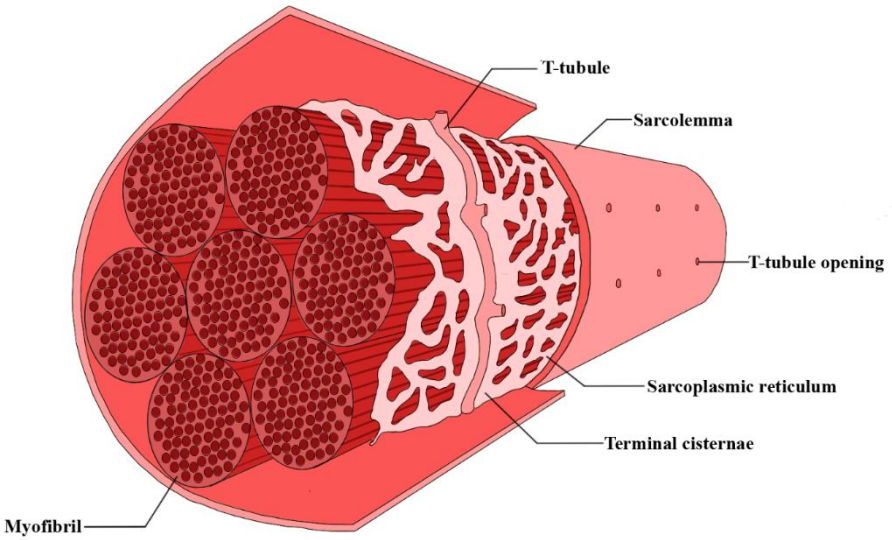

Figure 1.3. Anatomy of skeletal muscle fibre.

Schematic diagram of skeletal muscle fibre. Depicted are the myofibrils and the sarcoplasmic reticulum, as well as the sarcolemma with its invaginations known as transverse-tubules (T-tubules). Image was created in Adobe Photoshop.

Original artwork with reference to publication(s): [29]

Localised to the terminal cisternae of the sarcoplasmic reticulum (Fig. 1.3), RyR1 is the primary Ca^{2+} release channel involved in skeletal muscle contraction. Once activated, it mediates an efflux of Ca^{2+} from the sarcoplasmic reticulum to the cytosol of the cell where the ion then binds to contraction machinery comprising the myofibril. After muscle contraction has occurred, Ca^{2+} stores in the SR are replenished through a range of processes, including the aforementioned methods.

Resolved at 3.6Å, the four 565 kDa subunits of rabbit RyR1 form a transmembrane pore that is architecturally similar to that of the six-transmembrane cation channel family. The first four α-helices comprising the transmembrane region (S1-S4) form a helical bundle known as the pseudo voltage-sensory domain (pVSD) which is located parallel to the adjacent protomer, while the helices S5 and S6 interface with each subunit, forming the pore domain (Fig. 1.4)[30]. Although structurally similar to other Ca^{2+}-release channels present in the endoplasmic reticulum, such as the inositol-1, 4, 5 triphosphate receptor (IP3R), RyR1 can be differentiated by the presence of an S2S3 helical bundle in the transmembrane region of the protein[31]. Referred to as the S2S3 domain, this helical bundle is absent from IP3R and may be involved in $[Ca^{2+}]$-dependent regulation of RyR1 activity[32].

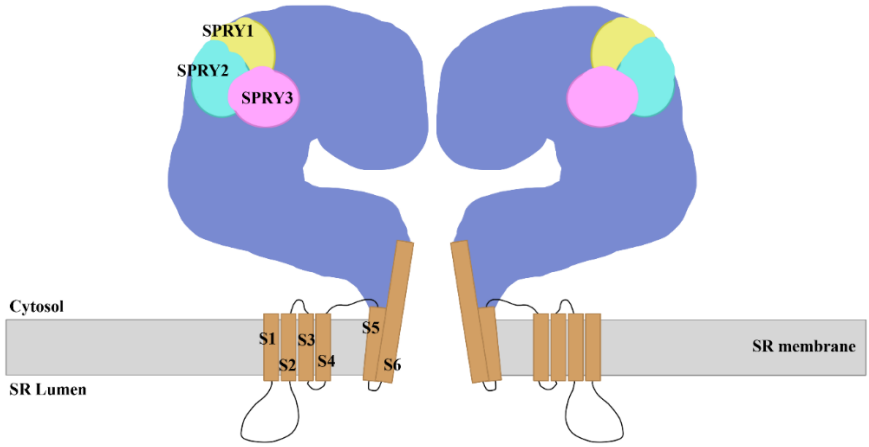

Figure 1.4. Structure of ryanodine receptor isoform 1

Schematic diagram of the type 1 ryanodine receptor with the transmembrane region consisting of the pseudo voltage-sensory domain (pVSD) (S1-S4) and the S5-S6 pore region in brown, the large cytosolic cap is shown in blue, the Sp1A-RyR (SPRY) domains in yellow (SPRY1), turquoise (SPRY2) and pink (SPRY3). Image was created in Adobe Photoshop.

Original artwork with reference to publication(s) [30, 33]

The vast majority of the RyR1 protein is comprised of the cytosolic cap; a large structure that extends into the cytoplasm and houses the three SPRY domains (residues Gly^{628}-Phe^{849} [SPRY1], Pro^{1055}-Ser^{1241} [SPRY2], Leu^{1242}-Arg^{1656} [SPRY3]) (rabbit: NM_001101718.1) as well as the possible binding sites for STAC3 and the 12 kDa FK-506 binding protein (FKBP12)[30, 34, 35]. FKBP12 is generally considered to stabilise the closed state of RyR1, while STAC3 has been shown to mediate the interactions between the DHPR and the ion channel, making it integral to EC coupling. However, while STAC3 and FKBP12 play important roles in maintaining RyR1 function, the SPRY2 domain of RyR1 is of particular interest[36, 37].

First discovered in the slime mould kinase, Sp1A and ryanodine receptors for which they get their name (Sp1A, RyR), SPRY domains are sequence repeats that act as protein interaction modules in a variety of different proteins[38]. Residues Leu720-Gln765 of the II-III loop structure of the α1s subunit of the DHPR (connecting the 2nd and 3rd of the 4 transmembrane helical bundles that comprise the DHPR) interact with the SPRY2 domain of RyR1 during activation of the channel[39]. This activation is aided by the 35 residue C-terminal tail of the β1a subunit of the DHPR, an interaction strengthened by a string of positively charged residues (Lys3494-Arg3502) present in the cytosolic cap of RyR1[40, 41].

1.3 The regulatory network of ryanodine receptors

As alluded to previously, RyR1 activity is controlled by a complex network of regulatory factors ranging from post-translational modifications to protein interactions such as those between RyR1 and DHPR/FKBP12/STAC3 as well as the Ca^{2+} binding proteins: calmodulin (CaM) and calsequestrin (CSQ)[42-44]. While not limited to these alone, these proteins are among the most well characterised in relation to RyR1 activity (Fig. 1.5).

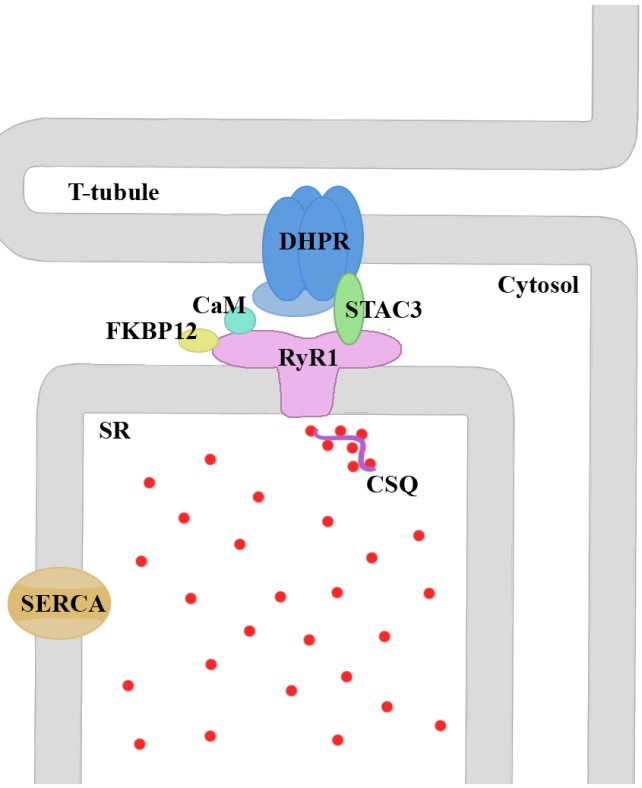

Figure 1.5. The regulatory network of RyR1.

Schematic diagram of the regulatory network of the type 1 ryanodine receptor (RyR1). Shown are the membrane bound proteins: RyR1 (lavender), the DHPR (blue) and SERCA (orange), along with the cytosolic proteins: calmodulin (CaM, teal), STAC3 (green), and FKBP12 (yellow) as well as calsequestrin (CSQ, purple), present in the SR lumen. Membranes are shown in grey, and Ca^{2+} depicted in red. Image was created in Adobe Photoshop.

CaM: *Calmodulin,* ***FKBP12:*** *FK506-binding protein 12,* ***STAC3:*** *SH3 and cysteine rich domain 3,* ***DHPR:*** *Dihydropyridine receptor,* ***SERCA:*** *Sarcoplasmic/endoplasmic reticulum* Ca^{2+} *ATPase,* ***SR:*** *Sarcoplasmic reticulum,* ***T-tubule:*** *Transverse-tubule.*

Original artwork with reference to publication(s): [29, 34, 35, 39-44]

1.3.1 FK506-binding protein 12/12.6

Present in all eukaryotes and ubiquitously expressed in most tissues, the FK506-binding proteins (FKBPs) are a group of proteins first described as receptors for the immunosuppressant drugs FK-506 and rapamycin. Termed immunophilins because of this function, FKBPs have a variety of roles within the cell, such as FKBP51 with its role as a protein chaperone, and FKBP25 as a regulator of the cell cycle[45, 46]. While the wide variety of roles displayed by the collective FKBPs is apparent, the 12kDa immunophilin (FKBP12) displays, in itself, a diverse set of functions in human physiology. While being implicated in processes such as embryogenesis, FKBP12 is perhaps most well-known for its role in the stabilisation of Ca^{2+} channels in the endo/sarcoplasmic reticulum as well as its mediation of rapamycin activity[37, 47-49].

The macrolide fungicide, rapamycin is a potent antimicrobial and anti-tumour drug which inhibits the translation of mRNAs into proteins required for conventional cell cycle function[50, 51]. Acting through the cis-trans peptidyl/prolyl isomerase domain characteristic of all FKBPs, FKBP12 binds rapamycin, forming a complex which blocks the protein kinase activity of the mammalian target of rapamycin (mTOR)[52]. The blocking of mTOR kinase activity prevents mRNA translation by affecting both the activity of the 40S ribosomal protein S6 kinase (p70s6k) and the function of the eukaryotic initiation factor 4E-binding protein-1 (4E-BP1) resulting in growth arrest in the G1 phase of the cell cycle[53, 54]. While FKBPs functionality in tumour suppression is of great significance, its role in Ca^{2+} homeostasis is arguably of equal, if not more importance. Indeed, FKBP12 and its isomer FKBP12.6 are deemed so integral to Ca^{2+} homeostasis, that together they are referred to as the calstabins for their interactions with the Ca^{2+} channels RyR and IP3R[37, 55].

FKBP12 and 12.6, while expressed ubiquitously throughout the body, are expressed substantially in skeletal and cardiac muscle respectively; however, the precise role of FKBP12 and 12.6 in their respective tissues is a highly contentious subject. The discordance between the roles of the calstabins in regard to RyR1/2 function is exacerbated by the close yet dissimilar findings of multiple laboratories. While it has been repeatedly shown that the calstabins interact with RyRs, the function of their interactions have been described in multiple conflicting ways. These include declarations that dissociation of FKBP12/12.6 from RyRs increases, decreases, and even has no effect on channel gating[37, 44, 56, 57].

Due to multiple discoveries that an absence of FKBP12 results in increased gating frequency of RyR1, the current literature surrounding the calstabins describes FKBP12/12.6 as having a “stabilising” effect on RyR1/2[37, 44]. However, others have shown that while FKBP12 may stabilise RyR1, dissociation of the isomers from

RyR2 has no effect on gating frequency[56]. Interestingly, while the general consensus is that dissociation of the calstabins from RyRs results in increased Ca^{2+} transients, a contradictory result indicated that RyR1 and RyR2 activity could be increased by the binding of FKBP12.6 and 12 respectively. The Sitsapesan laboratory proposes that RyR activity is regulated by the calstabins in an antagonistic manner. In cardiac muscle, they describe FKBP12 binding to RyR2, sensitising the channel to cytosolic Ca^{2+} until it dissociates from the channel by increased concentrations of FKBP12.6 which, when bound, stabilises RyR2 in the closed state[57]. Due to the high sequence identity between the two calstabins (83%) and their presence in both skeletal and cardiac muscle it is plausible that this occurs *in vivo*; however, it is generally accepted that the calstabins act as stabilisers of RyRs and that their dissociation leads to increased gating frequency.

It is accepted in the current literature that the FKBPs bind RyR in a stoichiometric ratio of 4:1; however, the precise binding site for FKBP has been a highly contentious subject. Initial reports indicated that residue Val2461 (Human) in the central domain of RyR1 is critical for FKBP12 binding; however, other analyses have shown that FKBP-RyR interactions occur at the N-terminus of the ion channel, specifically residues Cys305-Leu1937 (Human)[37, 58]. A third site has been proposed at the C-terminal end of RyR, proximal to the channel pore. Although this is a "sterically appropriate" location, cryo-EM reconstructions have shown FKBP localising to the cytoplasmic cap >100 Å from the transmembrane baseplate assembly of RyR1[59, 60].

Through the use of fluorescence resonance energy transfer (FRET) a fourth site has been proposed, that does not consist of a contiguous stretch of RyR1 but is rather comprised of sites at the N-terminus and central domain. Girgenrath *et al* observed a high degree of energy transfer ($E = 0.58$) between FKBP12 and RyR1 residue Val519, implicating this residue in the binding of FKBP12. They also found that insertions of green fluorescent protein (GFP) or the His-tag used in the FRET assay at position Asp619 eliminates FKBP12 binding, implying an integral role of residue in FKBP12-RyR1 interactions. FRET efficiencies from FKBP12 to residue Val2341 in the central domain of RyR1 ranged from 0.41 to 0.52 and inserting His tags at positions Glu2157 and Met2502 abrogated FKBP12-RyR1 interactions[61]. To summarise, these results display a binding pattern of FKBP12 that includes regions in the N-terminus and central domain that, while previously established as possible binding sites individually, had not been implicated together. Although the binding site for FKBP12 still remains highly contentious, the experimentation outlined previously by Girgenrath *et al.* implicates binding sites proposed by separate laboratories together, suggesting that the binding site arises as a product of the tertiary structure of RyRs as opposed to their primary structure.

1.3.2 STAC3

While the voltage sensor, Cav1.1 (DHPR) is accepted to be the primary activator of RyR1, another protein known as SH3 and cysteine-rich domain 3 (STAC3) has been implicated in the function of the DHPR. This 14 kDa protein is predominantly expressed in skeletal muscle where it is localised to the triads (junction between T-tubule and the terminal cisternae of the SR) of the sarcoplasmic reticulum and is thought to play an integral role in EC coupling[36]. STAC3 mediates the localisation of the DHPR to the membrane of the T-tubules where the voltage sensor then associates with RyR1[62]. In the cytosolic space between the T-tubule and the SR membrane, interactions between STAC3 and the II-III loop structure of the DHPR comprised of residues Gln747-Leu760 are thought to stabilise the binding of the DHPR to RyR1 and increase EC-coupling[35]. A p.Trp284Ser (NM_145064.3) homozygous substitution present in the DHPR binding region of STAC3 supports this claim by perturbing EC coupling and resulting in a disorder known as Native American myopathy (NAM) characterised by decreased EC-coupling, and severe muscle weakness[36].

1.3.3 Ca^{2+} binding proteins

Although interactions between RyR1 and its associated proteins are the primary regulatory factors in RyR1 activity, the role of Ca^{2+} itself in RyR1 activation cannot be overstated. Mediated predominantly through interactions with the Ca^{2+} binding proteins calmodulin and calsequestrin, Ca^{2+} has both an activating and inhibitory effect on RyR1. Comprised of two Ca^{2+} binding lobes connected by a 7-turn α-helix, the 17 kDa, dumbbell-shaped protein, calmodulin, displays a bifunctional effect on RyR1 activity. At nanomolar cytosolic [Ca^{2+}], CaM increases the open probability of RyR1, while at micromolar cytosolic [Ca^{2+}] CaM promotes its inhibition[42, 63]. Thought to bind at residues Lys3614-Leu3643 of RyR1, CaM is in a stoichiometric ratio of four proteins per subunit of RyR1 and along with calsequestrin, communicates intracellular [Ca^{2+}] to the RyR[64, 65].

Calsequestrin (CSQ) is the major Ca^{2+} binding protein present in the lumen of the sarcoplasmic reticulum. Localised to the junctional SR membrane via its interactions with the RyR associated proteins, junctin and triadin, CSQ communicates luminal [Ca^{2+}] to RyR1 and therefore plays a significant role in EC-coupling[66]. As Ca^{2+} concentrations within the SR increase, the 42 kDa protein polymerises, forming a ribbon-like quaternary structure capable of binding 50 mol Ca^{2+} per mol CSQ[67, 68]. It is thought that the tethering of CSQ to junctin and triadin results in high Ca^{2+} storage near the junctional SR membrane which would support fast Ca^{2+} release

during EC coupling. Despite this, the current literature on the function of calsequestrin is yet to reach a definitive consensus.

CSQ exhibits both an activating and inhibitory effect on RyR1 activity. Indeed, polymerised CSQ, in its dephosphorylated state, has been shown to increase the open probability of RyR1, suggesting a possible "on-off" switch that activates the Ca^{2+} channel[69]. While the phosphorylation of enzymes is a common regulator of protein activity, RyR1 has been observed to be active regardless of the phosphorylation state of CSQ, indicating its activity is likely regulated in another manner[43]. An increase in RyR1 activity has also been observed after depolymerisation of CSQ, suggesting that CSQ may provide an inhibitory role in RyR1 function, which is relieved when luminal [Ca^{2+}] decreases[70]. Regardless, what is known about CSQ is its importance in EC coupling by communicating to RyR1 the state of the SR Ca^{2+} stores and acting as a Ca^{2+} buffer to allow for rapid Ca^{2+} release.

1.3.4 Post-translational modifications

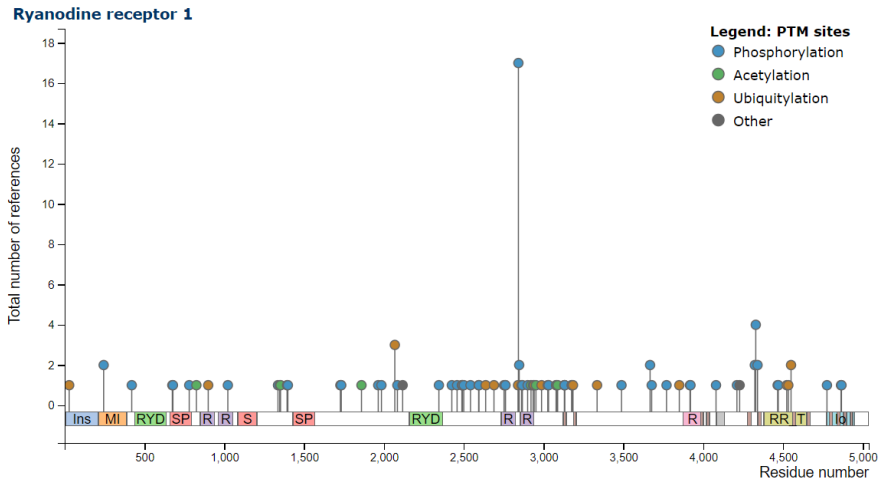

Figure 1.6. Map of post-translational modifications of RyR1.

A plot of the total number of publications referencing post-translational modifications of RyR1 at specific residues. Phosphorylations are shown in blue, acetylations in green, ubiquitylations in brown, and other post-translational modifications are shown in grey.

Ins: Ligand binding domain, **MI:** MIR(Protein mannosyltransferase, IP3R and RyR) domain, **RYD:** RIH (RyR and IP3R homology) domain, **SP:** SPRY domain, **R:** RyR domain, **S:** SPRY domain, **RRT:** Ryanodine receptor TM (transmembrane) 4-6, **Io:** Ion transport protein. *Figure was retrieved from Phosphosite Plus (https://www.phosphosite.org/proteinAction.action?id=5480&showAllSites=true)*

While it is clear that the activity of the ryanodine receptor is heavily controlled through a complex network of regulatory proteins, post-translational modifications (PTMs) also have a substantial effect on the open probability of RyRs. While there are many sites within RyRs that accommodate PTMs, residue Ser2843 (Human, homologous to Ser2809 in RyR2) is perhaps the most well characterised (Fig. 1.6). Phosphorylated by protein kinase A (PKA), Ser2843 phosphorylation disrupts FKBP12 binding and destabilises the ion channel; however, while some have found this results in a "leaky" channel, others have found that phosphorylation at this site alone is not enough to substantially alter RyR1 function[71, 72]. Instead, it seems, RyR activity is altered through hyperphosphorylation (defined as phosphorylation at Ser2843 on each of the RyR subunits) of the channel rather than single site modifications[44].

While PKA phosphorylates many sites in RyRs, the kinase plays another crucial role in Ca^{2+} homeostasis through one of its substrates, phospholamban. Phospholamban, in its unphosphorylated state, binds the cardiac sarco/endoplasmic reticulum Ca^{2+} ATPase (SERCA2) resulting in its inhibition[73]. Phosphorylation of phospholamban reverses this inhibition, implicating PKA in the regulation of Ca^{2+} store replenishment in cardiac muscle[74]. Although well-established in cardiomyocytes, the precise role of phospholamban in skeletal muscle is less understood; however, phospholamban has been observed in mouse soleus, where it has been heavily implicated in the super-inhibition of SERCA[75].

While phosphorylation is perhaps the most well established PTM, the lesser-known S-glutathionylation and S-nitrosylation PTMs have also been implicated in RyR function. Indeed, addition of these modifications has been reported to decrease binding of both FKBP12 and CaM to RyRs, resulting in increased Ca^{2+} transients[76]. These PTMs not only alter Ca^{2+} transients by interfering with the protein-protein interactions that regulate RyR1, but also through dismantling the regulatory effects of di-ionic cations. S-glutathionylation of cysteine residues has been shown to increase Ca^{2+} transients by diminishing the inhibitory role of Mg^{2+} on RyR1. In a similar manner, S-nitrosylation of separate cysteine residues has been observed to increase Ca^{2+} transients by modulating the activating role of Ca^{2+} on RyR1[77].

Importantly, while the aforementioned regulatory factors may increase Ca^{2+} release, they do so in a physiologically relevant manner. However, due to the critical role of RyR1 in muscle contraction, clinically relevant and substantial deleterious effects have been observed when either RyR1 itself or the modulation of RyR1 activity by these regulatory factors has been altered.

1.4 Malignant hyperthermia

1.4.1 Overview

Malignant hyperthermia (MH) is a pharmacogenetic disorder that presents as a hypermetabolic response to volatile anaesthetics used in surgery such as sevoflurane, isoflurane and desflurane as well as the depolarising muscle relaxant succinylcholine[78-81]. While an MH reaction may occur at any time during surgery, its onset is often rapid, occurring within 40 minutes of administration of the anaesthetic compound[82]. The presentation of an MH reaction is characterised by a wide variety of clinical symptoms, including muscle rigidity, and tachycardia as well as an increase in end-tidal CO_2. As the episode progresses hyperthermia, hyperkalaemia and acidosis present and if left untreated it can result in disseminated intravascular coagulation (DIC), widespread organ failure and cardiac arrest[83-85].

Due to the severity of malignant hyperthermia, the response to a suspected MH episode must be rapid and comprehensive. While initial treatment includes such measures as terminating the use of the volatile anaesthetic and decreasing the patient's body temperature; the administration of the drug dantrolene is the most effective measure[86]. Indeed, the introduction of dantrolene in 1979 has decreased the mortality rate of MH from 80% to 5%[85, 87]. Although other paralytic medications prevent muscle contraction by blocking post-synaptic acetylcholine receptors, it is thought that dantrolene arrests MH episodes by antagonising ryanodine receptors present in the sarcoplasmic reticulum, thus preventing Ca^{2+} release, and by extension, muscle contraction[88, 89].

Importantly, the dysregulation of Ca^{2+} release after exposure to volatile anaesthetics is the driving force behind MH episodes. Characterised by a substantial increase in Ca^{2+} transients from the SR, 70% of MH reactions are the result of an RyR1 channel hypersensitive to volatile anaesthetics. However, while a hypersensitive RyR1 channel may be conferred by point mutations in the *RYR1* gene itself, there is still a large proportion of MH cases that cannot be attributed to *RYR1* variants[84, 90].

1.4.2 Epidemiology

The incidence rate of malignant hyperthermia during general anaesthesia is a highly disputed subject with some estimates being as low as 1:250 000 and as high as 1:10 000 anaesthesias[91, 92]. The number of people who are MH susceptible is suspected to be much higher, with one estimate putting the prevalence at 1:3000 people[93]. However, we may never know the true prevalence of MH susceptibility as those who are susceptible can undergo several anaesthesias before a reaction takes place. It may

also be the case that those who are susceptible never get administered anaesthesia, or the duration of their exposure may be too short to trigger a response[94].

MH susceptibility is present in all races and although reactions occur in most demographics equally, males are affected at 2.5-4.5 times the rate of females[95]. It was also found in a review of cases from 1940 to 1992 that while the mean age at which an MH episode occurs was 18.3 years, 52.1% of cases occurred in children under the age of 15[96]. This is an important factor, as the current diagnostic protocol is not recommended for persons under the age of 10-12[97].

1.4.3 Diagnostic methods

The current diagnostic protocol for MH susceptibility (MHS) requires the use of a muscle biopsy taken from the *quadriceps femoris* of a patient for an *in vitro* contracture test (IVCT). During the IVCT, the roughly three cm biopsy is stretched to 120%-150% its resting length, electrically stimulated and exposed to cumulatively increasing concentrations of halothane (final concentrations: 0.11, 0.22, 0.44, 0.66 mmol L^{-1}) or caffeine (final concentrations: 0.5, 1, 1.5, 2.0, 3.0, 4.0 mmol L^{-1}). Exposure to these agonists results in a contraction of the muscle and it is this contraction which determines susceptibility to malignant hyperthermia. If the force generated by the contraction is greater than or equal to 2 mN when exposed to 0.44 mmol L^{-1} or less of halothane or 2 mmol L^{-1} or less of caffeine the patient is deemed MH susceptible (MHS). If no abnormal contraction occurs the patient is deemed MH negative (MHN). The MHS group can be further classified based on which agonist the muscle responds to. Those that respond to caffeine or halothane only are deemed MHS_c or MHS_h respectively whereas those that respond to both agonists are classified as MHS_{hc}[83].

With a 99% sensitivity and a 93.6% specificity, the IVCT is considered the "gold standard" diagnostic protocol[98]. While false positives are rare due to the high sensitivity, the specificity is low by design in order to limit the number of false negative diagnoses, because although a false positive diagnosis is not ideal, a false negative diagnosis can be fatal[83]. Despite the IVCTs standing as a "gold-standard" diagnostic tool, its reliance on a muscle biopsy makes it an invasive and traumatic experience which may act as a deterrent for those that need to be tested for MH susceptibility. Because of this, the development of a universal genetic test has been underway in order to provide a more appealing and cheaper option for diagnoses. Not only will the replacement of the IVCT with a universal genetic test make diagnosing MH susceptibility cheaper and less invasive, but it will also be more accessible; lowering the age at which testing can occur from 12 years to that of neonates through the use of cord blood[99].

Because roughly 70% of MH cases are attributed to a faulty RyR1 channel, genetic screening focuses mainly on the allelic variation of patient *RYR1*. While certain advancements in genetic screening such as the advent of next generation sequencing has made genetic testing faster, cheaper, and more accurate there are still drawbacks in the genetic screening process which has prevented the complete replacement of the IVCT with a universal genetic test. Although there is a high association between *RYR1* variants and MH reactions, the highly complex regulatory network controlling RyR1 function results in a pathological heterogeneity of malignant hyperthermia. In addition, the time, skill, and knowledge required to functionally characterise *RYR1* variants is the main bottleneck behind the development of a universal genetic test. Indeed, not only are 1% of MH episodes attributed to variations in the α1s subunit of the DHPR, of the over 300 *RYR1* variants associated with malignant hyperthermia, only 48 have been functionally characterised and deemed pathogenic for MH by the European Malignant Hyperthermia Group (EMHG)[100].

Operating since 1983, the EMHG have become a world-renowned group that act to assure the quality of research into the molecular aetiology of MH. The EMHG's goals are to improve the quality of diagnostic standards for MH susceptibility as well as, among others, to establish a common database of pathogenic *RYR1* variants. As a result, claims that variants are pathogenic have been exposed to immense scrutiny, making their database accurate and contemporary.

1.4.4 Functional characterisation of RyR1 variants

Before an RyR1 variant can be deemed pathological for malignant hyperthermia it must first meet a set of requirements outlined by the EMHG. These include, but are not limited to, displaying a gain of function effect on intracellular Ca^{2+} release and segregation with a positive IVCT phenotype in at least 4 individuals per family[101]. While whole exome sequencing allows those who have had a positive IVCT to be screened for associated *RYR1* variants, the size (15 kb) and GC rich nature of the transcript originally led to the preferential screening of 3 "hotspots"; these being the N-terminal (residues p.Met1-p.Arg614), central (residues p.Arg2163-p.Arg2458) and C-terminal (residues p.Arg4136-p.Pro4973) regions[102]. Of the 48 recognised MH-causative *RYR1* variants, only 5 have been found outside of these hotspots, highlighting their importance in RyR1-related muscle disorders[100]. Once an associated variant has been identified, it must be functionally characterised to determine its effect on intracellular Ca^{2+} release. There are a range of systems that can be used in order to perform functional analyses, including *ex vivo*, *in vitro*, and *in vivo* techniques.

Ex vivo techniques that have been used for functional analyses include the use of primary myotubes derived from the muscle of patients, as well as immortalised β-lymphoblastoid cells originating from patient blood samples. While β-lymphoblastoid cells may help elucidate previously unknown mechanisms involved in malignant hyperthermia, such as the possible role of IL-1β in producing MH symptoms, their lack of machinery involved in muscle contraction makes them an imperfect physiological representation of RyR1 activity[103]. A more accurate physiological depiction of RyR1 activity is found in patient-derived myotubes. Primary myotubes differentiate into fast and slow twitch muscle fibres and therefore contain the majority of proteins involved in muscle contraction, including those that interact with RyR1. Although seen as a relatively simple system due to it not requiring the cloning of *RYR1* variants, the use of primary myotubes does have its drawbacks. For instance, the system requires a muscle biopsy and is therefore expensive, while also being traumatic for the patient, and although the use of myotubes allows for a better physiological characterisation of RyR1, it cannot discriminate between a faulty RyR1 channel and its associated proteins. Not only this, but if a patient displays compound heterozygosity for *RYR1* or multiple variants at the same locus, this system is unable to determine which variant is causing the channel to fault. In short, while *ex vivo* studies characterise variants in a physiological manner, they are also limited by the genetic background of the patient.

For the most accurate representation of RyR1 activity, a complete physiological model is required. The mouse model has long been a quintessential system for physiological studies in the biological sciences, and unlike the aforementioned *ex vivo* techniques, a mouse model allows for the characterisation of individual variants with the associated contraction machinery in living muscle tissue[104]. This is normally performed by inducing episodes of malignant hyperthermia, or by measuring muscle strength of the soleus[105, 106]. However, due to the high price and difficulty involved in producing transgenic mice, only highly specialised laboratories have the equipment and funding required to generate *RYR1* knock-in mice. Indeed, only 6% of the *RYR1* variants deemed pathogenic for malignant hyperthermia were characterised using a mouse model[100, 107]. In addition, mice do not necessarily behave in the same way as humans. Indeed, many *RYR1* variants characterised to date exhibit somewhat different functions in the mouse models compared to human MH[108, 109].

Perhaps the most pervasive model used in studies of RyR1 related myopathies is that of HEK293 cells. This *in vitro* system not only requires the cloning of *RYR1* variants, but also does not contain the machinery required for muscle contraction. Subsequently, studies that utilise this system focus solely on the RyR1 channel itself; therefore, variants which may result in a faulty channel due to the disruption of

interactions between RyR1 and its associated proteins cannot be accurately characterised. On the upside of this, the use of HEK293 cells allows RyR1 to be assayed in isolation using an isogenic background. While the process of cloning *RYR1* variants is the primary drawback of using this system, the relatively inexpensive requirements and ease of maintaining HEK293 cell lines makes them a widely used cell line for *in vitro* assays of RyR1 function[107]. As with assays utilising myotubes and immortalised β-lymphoblastoid cells, the characterisation of RyR1 variants in HEK293 cells is centred around the use of fluorescent Ca^{2+} dyes to measure Ca^{2+} release after exposure to RyR1 agonists such as 4-chloro *m* cresol (4-c*m*c), caffeine, or halothane[110].

1.5 Other RyR1 related myopathies

1.5.1 Central core disease

First described in 1956 by Shy and Magee, central core disease (CCD) is a autosomal dominantly inherited, congenital myopathy characterised by central cores present in muscle biopsies[111]. These central cores are areas running along the longitudinal axis of the muscle fibre where there is reduced oxidative activity brought on by a decreased presence of mitochondria[112]. Presenting in infants as hypotonia and motor development delay, CCD displays proximal weakness (weakness in muscles closest to the body's midline) pronounced in the hip girdle and leads to orthopaedic complications and malignant hyperthermia susceptibility.

CCD and MH susceptibility are allelic conditions both caused by variations in RyR1. Subsequently, those afflicted by CCD are presumed to be MH susceptible and precautions during administration of anaesthesia should be taken. While CCD is regarded as an autosomal dominantly inherited disorder, recessive alleles have been found to be pathogenic for CCD[113]. It should be noted that unlike MH susceptibility, CCD is the result of loss of function mutations, rather than the gain of function mutations seen in patients who are susceptible to MH.

1.5.2 Multi-minicore disease

Inherited in an autosomal recessive manner, multi-minicore disease (MMD) is characterised similarly to CCD by the presence of "cores" of decreased oxidative activity due to depleted mitochondria in histochemically stained muscle. These cores, unlike CCD, do not run the entirety of the longitudinal axis of the muscle fibre but instead present as multiple "groups" of cores for which the myopathy gets its name[114]. MMD presents much like CCD, with hypotonia and muscle weakness, and is usually diagnosed in infancy or childhood. While generally considered to be a

relatively benign disorder, MMD has been associated with cardiomyopathy; however, the authenticity of this claim should be reflected on due to the small sample size used in the study[115].

1.5.3 Native American myopathy

Native American myopathy (NAM) was first described in 1987 by Bailey and Bloch and is named after the Lumbee Native American tribe in which it was discovered. Bailey and Bloch's case report described an MH reaction in a three-month-old, female descendant from the Lumbee tribe presenting with multiple congenital anomalies, including cleft palate, talipes equinus (club foot) and arthrogryposis (congenital joint contractures)[116]. NAM is an autosomal recessive disorder and is now characterised by the aforementioned anomalies, along with short stature, and progressive debilitating muscle weakness, and scoliosis. A 2008 report concluded a 36% mortality rate by the age of 18, and a prevalence of approximately 2:10 000 Lumbee tribe members; however, the true prevalence of NAM remains unknown[117]. A p.Trp284Ser (human) mutation in STAC3 is the most characterised variant to cause this disorder. STAC3 bearing this variant abrogates the binding of DHPR with concomitant reduced EC-coupling that is likely the principal cause of the muscle weakness seen in those suffering from NAM[36].

The current literature states that NAM can be characterised by an increase in susceptibility to MH. While those suffering from NAM may have experienced an MH episode in the past, it is important to recognise that the defining feature of MH susceptibility is a gain of function effect on Ca^{2+} release in response to agonists. Due to NAM resulting from a loss of function effect on EC coupling, it is likely that the underlying mechanism behind the MH episodes described in patients suffering from NAM is mutually exclusive from that which results in the decreased EC coupling that defines the disorder.

1.6 Project outline

1.6.1 Significance of project

Malignant hyperthermia, while uncommon, is a relevant and deadly occurrence those in the medical field must deal with. Although the incidence rate of MH is disputed, as many as 1 in 10 000 anaesthesias can result in an MH reaction. In addition, for every 150 anaesthetics administered at Palmerston North hospital, one patient will need to be treated as MH-susceptible and be given a non-triggering anaesthetic[118]. Because of this, diagnostic protocols have been developed in order to determine one's susceptibility to MH. Known as the *in vitro* contracture test (IVCT) in Europe and the caffeine-halothane contracture test (CHCT) in North America, this diagnostic protocol is commonly referred to as the "gold-standard" for diagnosis of MH susceptibility. However, the requirement of a muscle biopsy from the *quadriceps femoris* of the patient means that many who need to determine their susceptibility to MH are discouraged from undergoing the test, due to the traumatic and expensive nature of the procedure as well as the limited number of centres dedicated to performing the IVCT.

A faulty RyR1 channel is the most common cause of MH reactions due to its central role in regulating the release of Ca^{2+} from intracellular stores. With the advent of next generation sequencing, it has become possible for a new test to be developed which, through the use of a blood sample, scans patients for pathogenic variants in the *RYR1* gene. For a variant to be classified as pathogenic for MH, its inheritance pattern and effect on Ca^{2+} release must be characterised. Although this genetic test is often performed in conjunction with the IVCT/CHCT, the need for functional characterisation of *RYR1* variants is preventing its complete replacement of the contracture test. Importantly, functional characterisation of *RYR1* variants can take months to accomplish. Indeed, to date, of the over 300 RyR1 variants associated with MH, only 48 have been classified as pathogenic by the EMHG. Due to this substantial gap, it is most evident that more variants require functional characterisation. This would increase the chances of correctly diagnosing a patient via a genetic test, thus saving them from undergoing a traumatic muscle biopsy and decreasing the cost of diagnoses.

1.6.2 Hypothesis

Single nucleotide changes in *RYR1* identified in malignant hyperthermia susceptible patients result in altered Ca^{2+} release in response to the agonist 4-chloro *m* cresol.

1.6.3 Objectives

- Generate variants in human *RYR1* cDNA.
- Sub-clone newly generated variants into full length *RYR1* cDNA.
- Produce mammalian cell lines that stably express *RYR1* variants.
- Characterise Ca^{2+} release mediated by new RyR1 variants.
- Characterise Ca^{2+} release in RyR1 variants in the presence of FKBP12

Chapter 2. Materials and methods

2.1 Materials

Unless otherwise stated, chemicals were of analytical grade or better

2.1.1 Antibiotics

Item	Supplier
Ampicillin	Sigma Aldrich
Blasticidin	Invitrogen
Hygromycin B	Roche
Tetracycline	Sigma Aldrich
Zeocin™	Invitrogen

2.1.2 Antibodies

Item	Derived from	Cat #	Supplier
α-Mouse:FITC	Goat	115-093-003	Jackson ImmunoResearch
α-Mouse:HRP	Rabbit	A9044	Sigma
α-PDI	Rabbit	P7496	Sigma
α-Rabbit:TRITC	Goat	111-025-003	Jackson ImmunoResearch
α-RyR1 34 C	Mouse	Ab2868	Abcam
α-α-Tubulin	Mouse	T9026	Sigma

2.1.3 Reagents for Ca^{2+} release assays

Item	Supplier
4-chloro-*m*-cresol (4-c*m*c)	BDH Chemical Ltd
Zellkultur microplate (96-well)	Greiner Bio-One
Fura2-AM	Thermo Fisher
Pluronic® F-127	Sigma

2.1.4 DNA modifying enzymes

Item	Supplier
AvrII-HF	New England Biolabs (NEB)
BamHI-HF	New England Biolabs (NEB)
EcoRI-HF	New England Biolabs (NEB)
HindIII-HF	New England Biolabs (NEB)
KpnI-HF	New England Biolabs (NEB)
MfeI-HF	New England Biolabs (NEB)
NdeI-HF	New England Biolabs (NEB)
NotI-HF	New England Biolabs (NEB)
NsiI-HF	New England Biolabs (NEB)
SphI-HF	New England Biolabs (NEB)
XbaI	New England Biolabs (NEB)
T4 DNA ligase	New England Biolabs (NEB)

2.1.5 DNA processing and manipulation

Item	Supplier
1Kb+ DNA ladder	Invitrogen
5x HOT FIREpol® master mix	Solis BioDyne
5x KAPA HiFi ready mix	KapaBiosystems
6x Gel loading dye (purple)	New England Biolabs (NEB)
Agarose	Hydragene
ChargeSwitch™ Pro plasmid miniprep kit	Thermo Fisher
DNA primers	Integrated DNA Technologies
Ethidium Bromide	Sigma Aldrich
ExoSAP-IT™	Thermo Fisher
PureLink™ HiPure plasmid filter midiprep kit	Thermo Fisher
RNase H	Invitrogen
ZymoClean™ DNA recovery kit	Zymo Research

2.1.6 Immunoblotting/SDS-PAGE

Item	Supplier
β-mercaptoethanol (BME)	Aldrich
40% polyacrylamide 29:1 acrylamide/Bis	BioRad
Ammonium persulfate (APS)	Sigma Aldrich
ECL™ prime	Amersham
Immunobilon® PVDF membrane	Sigma Aldrich
Pierce ECL Western Blotting substrate	Thermo Fisher
Precision Plus Protein™ Dual Colour Standard	BioRad
Sodium dodecyl sulphate (SDS)	Merck
TEMED	SIGMA
Whattman paper	GE Healthcare Lifesciences

2.1.6.1 SDS-polyacrylamide gel recipe

Stacking gel (4%)	
H_2O	3.15 mL
40% polyacrylamide	500 µL
0.5M Tris-HCl (pH 6.8)	1.25 mL
10% SDS	50 µL
10% APS	25 µL
TEMED	5 µL
Resolving gel (7.5%)	
H_2O	5.5 mL
40% polyacrylamide	1.9 mL
1.5M Tris-HCl (pH 8.8)	2.5 mL
10% SDS	100 µL
10% APS	50 µL
TEMED	10 µL

2.1.7 Immunofluorescence assays

Item	Supplier
Nunc® Lab-Tek® II 8 well chamber slide	Thermo Scientific
ProLong™ Gold antifade mountant containing DAPI	Thermo Fisher

2.1.8 Miscellaneous

Item	Supplier
Bacteriological agar	LAB Supply
Bromophenol blue	Sigma Aldrich
Bovine Serum Albumin (BSA)	Merck
$CaCl_2$	Sigma
Chloroform	BDH Laboratory Supplies
DEPC	BDH Laboratory Supplies
Dimethyl sulfoxide (DMSO)	Sigma
Dulbecco's Modified Eagle Media (DMEM)	Sigma Aldrich
EDTA	Ajax Finechem
EGTA	Sigma Aldrich
Ethanol (Absolute)	Merck
Ethanol (Denatured)	Merck
Fugene HD	Promega
Glacial acetic acid	Merck
Glucose	Merck
Glycerol	Sigma
Glycine	US Biochemical Corp
HEPES	Carl Roth GmBH & Co
iScript reverse transcription supermix for RT-qPCR	BioRad
Isopropanol	Fischer Chemical
KCl	Merck
KH_2PO_4	Merck
LB broth base	Life Technologies
Methanol	Fisher Scientific
$MgCl_2$	Merck
Na_2HPO_4	Merck
NaCl	Merck
Paraformaldehyde	Prosci Technologies
Potassium acetate	Merck
CELLSTAR® 15 cm round cell culture dish	Greiner bio-one
T25 Nunc™ EasYflask	Thermo Fisher
Tris-HCl	PureScience Ltd
Triton X-100	Merck
TRIzol™ reagent	Life Technologies
TrypLE™ Express enzyme	Life Technologies
Turbo DNAse kit	Ambion
Tween20	Sigma

2.1.9 Plasmids

Item	Supplier
pBlueScript KS+	Stratagene
pcDNA™3.1(+)	Invitrogen
pcDNA5/FRT/TO©	Thermo Fisher
pcFKBP12	Gift from Dr Peter Jones (University of Otago)
pOG44	Thermo Fisher

2.2 Methods

2.2.1 DNA processing

2.2.1.1 Bacterial transformation

DH5-α *E.coli* cells made chemically competent via treatment with $CaCl_2$ following the method outlined by Chang *et al* (2017) were transformed with plasmid DNA following a modified protocol outlined in the same methodology[119]. Although the mechanism behind this method is unknown, it is hypothesised the Ca^{2+} acts as a cation bridge between the bacterial membrane and DNA. The Ca^{2+} facilitates the binding of DNA to the membrane which is then transported into the cell via a brief period of heatshock. Cells were transformed by incubating 50 µL of competent cells with 50 ng to 100 ng of plasmid DNA on ice for 20 minutes before being transferred to a 42°C heat block for 1 minute, then cooled on ice for a further 10 minutes. Cells were then spread on LB-agar plates containing 100 µgµL^{-1} ampicillin and incubated overnight at 37°C. Glycerol stocks were made using 50% glycerol at a final concentration of 25% and stored at -80°C.

2.2.1.2 Preparation of plasmid DNA

Plasmid DNA was extracted from 1.5 mL of a 5 mL LB-amp overnight *E.coli* culture for the confirmation of site-directed mutagenesis (SDM). Plasmid DNA for use in cloning was extracted from 50 mL overnight cultures as more DNA was required for these steps. Extraction from the 5 mL culture was performed using the Invitrogen ChargeSwitch™ plasmid mini-prep kit, while the Invitrogen PureLink™ midiprep kit was used for the 50 mL cultures. Plasmid DNA was stored in TE buffer at -20°C.

2.2.1.3 DNA sequencing

Sanger sequencing of DNA samples was performed by the Massey Genome Service (MGS) (Palmerston North, New Zealand) using a capillary ABI3730 DNA analyser with BigDye™ terminator 3.1 (Applied Biosystems). Primers used for the sequencing reactions are outlined in (Appendix I, Table. 2 and Table. 3 and Appendix III, Table. 6). Sequencing reactions consisted of 500 ng template DNA and 5 µM primer (final concentration = 0.25 µM) in a total volume of 20 µL. Sequence alignments were performed using emboss needle (https://www.ebi.ac.uk/Tools/psa/emboss_needle/). RyR1 sequences were aligned to a human RyR1 transcript (NM_000540.3), while the pcFKBP12 sequence was aligned to a human FKBP12 transcript (NM_000801.5).

2.2.1.4 Site-directed mutagenesis

Site-directed mutagenesis is a process wherein primers containing the mutation of choice are used for PCR amplification of template DNA, thereby incorporating the mutation in a PCR-dependent manner. In this case the primers are complementary to the template DNA with exception of a single nucleotide substitution. After PCR amplification, only a small fraction of original wild type template DNA should remain, with the vast majority of DNA present now containing the nucleotide substitution. While the remaining template DNA is low in concentration, it can still interfere with downstream applications of the PCR products, therefore the sample is treated with the restriction enzyme, DpnI. Dpn1 digests DNA only when its recognition site is methylated. Due to the unmethylated nature of the PCR products, it therefore selectively digests the template DNA, and as a result, purifies the newly synthesised variant DNA.

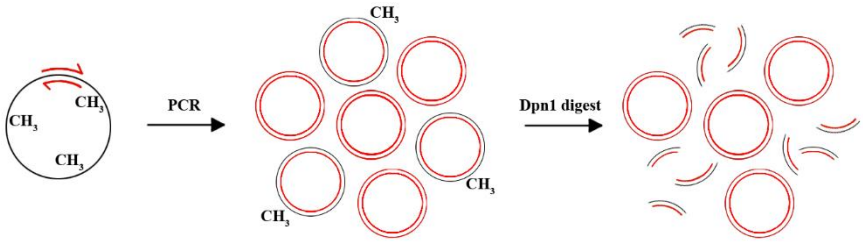

Figure. 2.1. Site-directed mutagenesis

Schematic diagram depicting the process through which nucleotide substitutions were incorporated into human *RYR1* cDNA. Template DNA shown in black with CH_3 denoting methyl groups. Primers containing the nucleotide substitution and newly synthesised DNA shown in red. Image was created in Adobe Photoshop.

This is an original artwork.

70 ng of template DNA with 0.65 µL of mutagenic primer (final concentration = 0.26 µM) was used for site-directed mutagenesis. Kapa HiFi HotStart Readymix (Kapa Biosystems) was used because of the high fidelity of the polymerase. The PCR protocol was as follows:

95°C	5 min	
98°C	50 s	
57°C-67°C	20 s	18 cycles
72°C	1 min Kb^{-1}	
72°C	5 min	

Due to the GC rich nature of *RYR1*, dimethyl sulfoxide was added at a final concentration of 2% to facilitate amplification by lowering the melting temperature of the primers. Mutagenic primer sequences can be found in Appendix I, Table. 1.

2.2.1.5 RYR1 sub-cloning

Sub-cloning of *RYR1* variants was performed via a restriction endonuclease cloning process wherein *RYR1* cDNA was "cut" from the vector and separated from the vector backbone and any remaining cDNA via gel electrophoresis (Fig. 2.2). The cDNA containing the variant of interest as well as the vector in which the cDNA will be incorporated were then purified from the gel according to the guidelines set out by the Zymoclean™ gel DNA recovery kit (Zymo Research). The digested vector and cDNA insert were then ligated overnight at 16°C using T4 DNA ligase (New England Biolabs).

Cloning the *RYR1* cDNA from the pBSH+ vector into the pBSKX+ vector was achieved by performing a double digestion using restriction endonucleases XbaI and SphI. Cloning of the *RYR1* cDNA from pBSKO+ into the pBSKX+ vector required a triple digestion as digestion with the chosen endonucleases (NsiI and MfeI) alone produced two bands of indistinguishable sizes. NotI was used in conjunction with these two enzymes in order to separate the *RYR1* insert from the backbone. pBSKX+ was digested with NsiI and MfeI for sub-cloning of the insert from the pBSKO+ vector. Generation of the pcDNA/FRT/TO© vector containing full-length *RYR1* cDNA was conducted by double digestion of the pBSKX+ half-length vector with KpnI and XbaI. Due to the presence of multiple XbaI sites in the full-length construct, AvrII was used in conjunction with XbaI to digest the pcDNA/FRT/TO© vector as AvrII and XbaI digestion produces compatible cohesive ends.

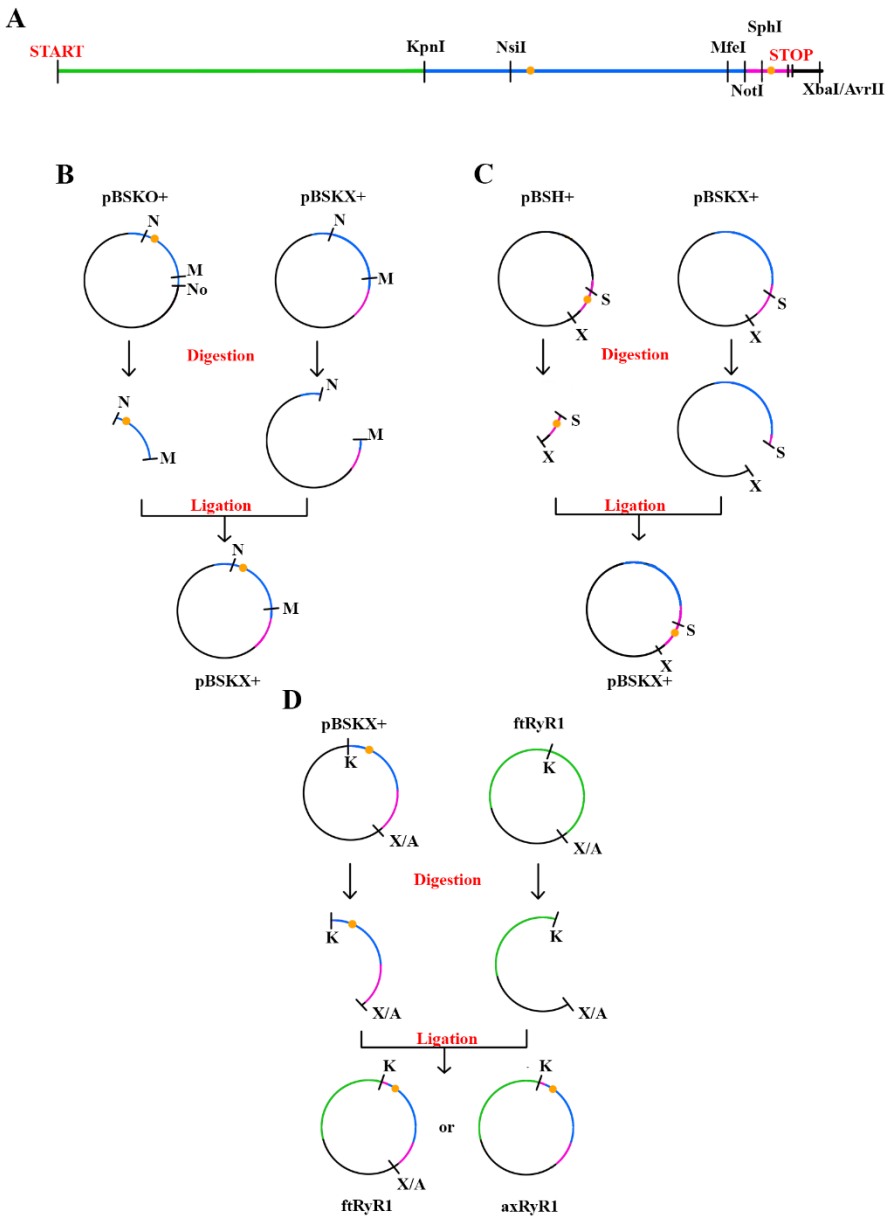

Figure. 2.2. Cloning process of *RYR1* variants.

Sub-cloning process of *RYR1* variants from the mutagenic plasmid to full-length construct (ftRyR1/axRyR1). **(A)** *RYR1* cDNA with N-terminal half shown in green, the pBSH+ insert shown in pink, the pBSKO+ insert shown in blue, and the mutation shown in orange. **(B)** Initial sub-cloning step of the variant pBSKO+ construct into the wild type pBSKX+ vector containing the C-terminal half of *RYR1*. N = NsiI, M = MfeI, No = NotI. **(C)** Initial sub-cloning step of the variant pBSH+ construct into the wild type pBSKX+ vector containing the C-terminal half of *RYR1*. S = SphI, X = XbaI. **(D)** Final cloning step of the newly constructed pBSKX+ plasmid containing the variant of interest into pcDNA5/FRT?TO© containing the full-length wild type *RYR1* cDNA, creating either ftRyR1 (Kpn1 + XbaI) or axRyR1 (AvrII + XbaI). K = KpnI, X = XbaI, A = AvrII. Image was created in Adobe Photoshop.

This is an original artwork with reference to publication(s): [120]

2.2.1.6 Amplification of genomic DNA

Polymerase chain reaction (PCR) was performed to amplify variant DNA using primers that flank each *RYR1* variant (Appendix III, Table. 6). The resulting amplicons were then purified by incubation with ExoSAP-IT™ for 45 minutes at 37°C before being sent to the MGS (Palmerston North, New Zealand) for Sanger sequencing using a capillary ABI3730 DNA analyser with BigDye™ terminator 3.1 to confirm the presence of the variant. 100 ng of genomic DNA was amplified using 0.5 µL of primer (final concentration = 0.1 µM) in a total volume of 20 µL. Amplicons were separated on a 0.8% agarose gel in 1x TAE for 45 minutes at 100 V to determine successful amplification of variant *RYR1* in transfected HEK293 cells. The PCR protocol was as follows:

94°C	4 min	
94°C	30 s	
55°C-67°C	30 s	35 cycles
72°C	30 s	
72°C	4 min	

2.2.1.7 cDNA synthesis and multiplex PCR

RNA was incubated with 1 µL turbo DNAse (0.04 $UµL^{-1}$) for 25 minutes at 37°C then treated with 5 µL DNAse inactivation reagent. The solution was then centrifuged for 1.5 minutes at 10 000 x g and the supernatant was transferred to a new tube. Reverse transcription of 500 ng of RNA extract was accomplished following the guidelines in the Biorad i-Script™ cDNA biosynthesis kit, using a blend of both oligo(dT) and random primers sequences to accomplish cDNA synthesis. Expression of FKBP12 in transiently transfected cell lines was confirmed through multiplex PCR using a 5 µM primer solution specific for *FKBP12* and *β-tubulin* at a final concentration of 0.2 µM (Appendix IV, Table. 13). The PCR protocol was as follows:

95°C	5 min	
95°C	15 s	
54°C	20 s	25 cycles
72°C	30 s	
72°C	7 min	

The amplicons were separated on a 2% agarose gel for 2 hours at 70 V in 1x TAE buffer. A densitometric analysis was performed using ImageJ to calculate the extent of FKBP12 expression in comparison to the endogenous expression of β-tubulin, the data were compiled using Graphpad Prism 9™.

2.2.2 Mammalian cell culture

2.2.2.1 Stable cell line transfections

Flp-In™ T-REx™ cells were grown in Dulbecco's modified eagle media (DMEM) (Sigma-Aldrich), 10% Foetal bovine serum (FBS), 15 μgmL^{-1} blasticidin and 100 μgmL^{-1} zeocin™ until confluent in T25 flasks. The medium was replaced with 3 mL of DMEM, 10% FBS and 15 μgmL^{-1} blasticidin and incubated for 2 hours. After incubation, transfection reagent containing 2.7 µg ftRyR1 or axRyR1 DNA, 300 ng pOG44 DNA and 12 µL Fugene HD made up to 300 µL with uncompleted DMEM was added to the medium. The following day 2 mL DMEM, 10% FBS and 15 μgmL^{-1} blasticidin were added to the media and after 24 hours the cells were used to re-seed two new T25 flasks. On day four the medium was replaced with DMEM, 10% FBS, 15 μgmL^{-1} blasticidin and 30 μgmL^{-1} hygromycin (Complete selection media). The medium was replaced every three to four days before 1 mL of cell culture was used to seed a round 15 mL cell culture dish. Single colonies were isolated using cloning rings before being trypsinised and used to seed a poly-D-lysine-treated 96-well plate. Isolated colonies were then used to seed a T25 flask and grown until confluent before being frozen as described in section 2.2.2.4. Successful transfections were confirmed by immunoblot analysis as well as sequencing of genomic DNA to confirm the presence of the appropriate *RYR1* variant.

2.2.2.2 Transient transfections

Transient transfections of pcDNA™3.1(+) vector containing *FKBP12* cDNA were carried out for the analysis of FKBP12 overexpression in Flp-In™ T-REx™ 293 cells. A poly-D-lysine-treated 96-well Zullkutur microplate was seeded with each cell line before 10 µL of transfection reagent containing 1.8 µg plasmid DNA + 20 µL Fugene® HD made up to 200 µL with uncompleted DMEM was added. Cells were left to grow for 72 hours before being functionally characterised.

2.2.2.3 Maintaining cell lines

Cell lines were maintained following general tissue culture practice. Cells were passaged every 3-4 days with DMEM + 15 μgmL^{-1} blasticidin, 30 μgmL^{-1} hygromycin, and 10% FBS and grown in T25 flasks or 96-well plates sourced from ThermoFisher Scientific at 37°C and 5% CO_2.

2.2.2.4 Storing cell lines

Cell lines were grown in T25 flasks until 80%-100% confluent before being resuspended by gently pipetting up and down in old medium. The cell suspension was then centrifuged for 5 minutes at 110 x g. The supernatant was removed, and the cell pellet was resuspended in 900 µL FBS + 100 µL DMSO. The cells were then frozen at -80°C within a freezing container before being moved to a liquid nitrogen Dewar for long-term storage.

2.2.2.5 Genomic DNA extraction

Each cell line was grown in a T25 flask until ≥80% confluent then mechanically detached by pipetting before being centrifuged for 5 minutes at 110 x g. The supernatant was removed, and the pellet was resuspended in 600 µL nuclei lysis buffer (Promega) + 3 µL RNase A (10 $mgmL^{-1}$) sourced from Invitrogen. The suspension was incubated at 37°C for 15 minutes before adding 200 µL protein precipitation buffer (Promega) and centrifuging for 3 minutes at 13 000 x g. Six hundred µL of isopropanol was then added before centrifuging for 1 minute at 13 000 x g. The pellet was washed in 200 µL 70% ethanol then air dried before being resuspended in 50 µL Tris EDTA (TE) buffer.

2.2.2.6 RNA extraction

RNA was extracted from confluent cells pooled from 6 wells from a 96-well plate using 50 µL TrypLE™ (Gibco) as well as a confluent T25 flask 72 hours post transfection with FKBP12. Cells were centrifuged for 5 minutes at 110 x g then resuspended in 1 mL TRIzol™ (Ambion) and incubated at room temperature for 5 minutes before adding 250 µL chloroform. The suspension was then centrifuged for 10 minutes at 8000 x g at 4°C. The clear aqueous RNA phase was precipitated with an equal volume isopropanol and the RNA was collected by centrifugation for 10 minutes at 13 000 x g. The pellet was resuspended in 20 µL of diethyl pyrocarbonate (DEPC) treated water.

2.2.2.7 Protein extraction

Protein expression was induced over the course of 72 hours through the addition of tetracycline to a final concentration of 1 μgmL^{-1}. After induction, cells were mechanically detached from the T25 flask via pipetting before being centrifuged for 5 minutes at 110 x g. The supernatant was discarded, and the pellet resuspended in 150 µL cell lysis buffer + 20 µL 7x cOmplete™ mini protease inhibitor (Roche). The lysate was then centrifuged for 30 minutes at 12 000 x g at 4°C. The supernatant was then divided into 20 µL aliquots and stored at -80°C.

2.2.3 Protein expression

2.2.3.1 Immunoblot analysis

RyR1 expression was confirmed via immunoblot analysis. Approximately 200 µg of protein extract from induced and uninduced cells were electrophoresed in 1x Tris-Glycine-SDS (TGS) buffer on a 7.5% SDS-polyacrylamide gel for 2 hours and 30 minutes at 120 V alongside 7 µL of Precision Plus Protein™ dual colour standard (Biorad). Protein was then transferred to a polyvinylidene difluoride (PVDF) membrane (Immunobilon®) overnight at 70 mA at 4°C in Tris-Glycine (TG) buffer + 10% methanol. The membrane was blocked at room temperature with 5% skim milk in tris buffered saline + 0.1% Tween20 (TBST) for 3 hours with gentle agitation. The membrane was then incubated overnight at 4°C with 34C mouse anti-RyR1 (1:1000) and anti-α-tubulin (1:5000) primary antibody + 2.5% skim milk in TBST. The following day, the membrane was washed for 40 minutes in 1x TBST, changing the buffer every 10 minutes before adding 5 mL 2.5% skim milk in TBST + horse radish peroxidase (HRP) conjugated anti-mouse secondary antibody (1:5000). Following a one hour incubation at room temperature, the membrane was washed in 1x TBST for 40 minutes, replacing the buffer every 10 minutes.

ECL™ prime western blotting detection reagent (Amersham™) (Fig. 3.5) and Pierce ECL western blotting substrate (Thermo Fisher) (Fig. 3.6) were used in accordance with the guidelines set out by the respective companies. Images were developed using the Azure c600 (Azure Biosystems) and compiled in Adobe Photoshop.

2.2.3.2 Immunofluorescence staining

Cells were grown until confluent in a poly-D-lysine-treated 8-well Nunc™ Lab-Tek II chamber slide (Thermo Fisher) with complete media + 1 µgmL^{-1} tetracycline. After a 72-hour induction the medium was removed, and the cells were washed with 1x PBS before being fixed for 15 minutes with 4% paraformaldehyde. Following 3x wash steps with 1x PBS, the cells were permeabilised with 0.2% Triton X-100 for 10 minutes then washed a further 2x with PBS. A 5% bovine serum albumin (BSA) + 0.1% Tween20 blocking solution was then added to each chamber and left to incubate with slight agitation for 30 minutes. The cells were then incubated with rabbit α-protein disulphide isomerase (α-PDI) (1:1000) and 34C mouse α-RyR1 (1:1000) antibody for one hour at room temperature. Following 3x wash steps with PBS, the cells were incubated at room temperature for two hours with goat tetramethylrhodamine (TRITC) conjugated α-rabbit (1:200) and fluorocein isothiocyanate (FITC) conjugated α-mouse (1:200) secondary antibody. The cells were then washed another 3x with PBS before the chambers were removed and the slide was mounted with ProLong™ Gold containing DAPI (Thermo Fisher) for visualisation of the nucleus.

Imaging of the cells was performed via confocal microscopy at the Manawatū Microscopy and Imaging Centre (MMIC) (Palmerston North, New Zealand) using the Zeiss LSM900 with Airyscan 2 super resolution microscope and the Leica SP5 DM6000B scanning confocal microscopes.

2.2.4 Functional analysis

2.2.4.1 Characterising Ca^{2+} release

Functional analysis of each variant was carried out on uninduced cell lines as the Ca^{2+} profiles for induced wild type and variant cell lines were indistinguishable (Appendix IV, Fig.7.13). The inability to distinguish variants based off Ca^{2+} transients was novel to this project and correlated with the use of a new microscope system. This new system was substantially more sensitive than the former and resulted in inaccurate fluorescence data being gathered from induced cell lines.

Ca^{2+} release was detected using the ratiometric Ca^{2+} dye, fura2. Uninduced cells were grown in a poly-D-lysine-treated 96-well Zellkultur microplate in complete medium until roughly 70% confluent, the medium was removed, and the cells were washed with 100 µL 1x balanced salt solution (BSS). The cells were then incubated at 37°C for 45 minutes with 1x BSS buffer + Ca^{2+} (final concentration 0.2 M) + fura2-AM (final concentration = 2 µM). Pluronic® F-157 was also added at the same final concentration as fura2-AM to aid in the uptake of the Ca^{2+} dye by the cells.

After incubation, the cells were washed with 100 µL Ca^{2+}-free 1x BSS before 100 µL of Ca^{2+}-free 1x BSS was added to each well. Ca^{2+} release was induced by the addition of 100 µL of the RyR1 agonist 4-c*m*c to increasing final concentrations ranging from 0 µM to 1000 µM in 200 µM increments.

Cells were visualised using an Olympus I X 2 UCB microscope and cellSens™ Dimension visualisation software. Fura2-AM is excited at wavelengths of 340 nm and 380 nm for bound and unbound Ca^{2+} respectively and fluorescence is detected at 510 nm emission. To facilitate measurements, the cells were exposed to light at 340 nm for 25.04 ms and 380 nm for 2.04 ms and the resulting emission at 510 nm was detected to measure Ca^{2+} transients. Exposure times were detected empirically. A ratiometric analysis with background correction was then performed on the resulting images using the ratio analysis tool in the cellSens Dimension software. Fluorescence data for each variant were normalised against maximum fluorescence achieved at 1000 µM 4-c*m*c. Data was compiled in Graphpad prism 9™.

Chapter 3. Results

3.1 Generation of *RYR1* variants

3.1.1 Overview

Variants in human *RYR1* cDNA were generated via site-directed mutagenesis using mutagenic primers containing a single nucleotide substitution (Appendix 1. Table. 1). Due to the large size of *RYR1*, these variants were made in vectors containing smaller fragments of the *RYR1* cDNA and subsequently cloned into vectors containing larger portions of *RYR1*. Site-directed mutagenesis was performed on two sub-clones representing the regions of the C-terminal half of *RYR1* cDNA inserted into pBluescript KS+. These were pBSH+ which contains the last 2.2 Kb of the *RYR1* C-terminal coding region, and pBSKO+ which holds 5.9 Kb of *RYR1* cDNA beginning at the unique KpnI site and ending at the C-terminal NotI site.

Over the course of this project eight variants in total were introduced into *RYR1*, four into the pBSKO+ construct (p.Arg2458Leu, p.Val2627Met, p.Arg2676Trp, p.Arg3348His), and two into the pBSH+ construct (p.Phe4808Ser, p.Gly4835Glu). The cDNA of three *RYR1* constructs (p.Arg2458Leu, p.Arg2676Trp, p.Gly4835Glu) were sub-cloned into pBSKX+, a vector containing the entirety of the C-terminal half of *RYR1* cDNA beginning at the KpnI site. One was further cloned into pcDNA5/FRT/TO© containing full length *RYR1* cDNA (ftRyR1) (Fig. 2.2). A further two constructs (p.Gly2183Glu and p.Cys2237Tyr) were generated and cloned into ftRyR1 by Dr Anja Schiemann.

3.1.2 Mutagenesis

3.1.2.1 pBSH+ constructs

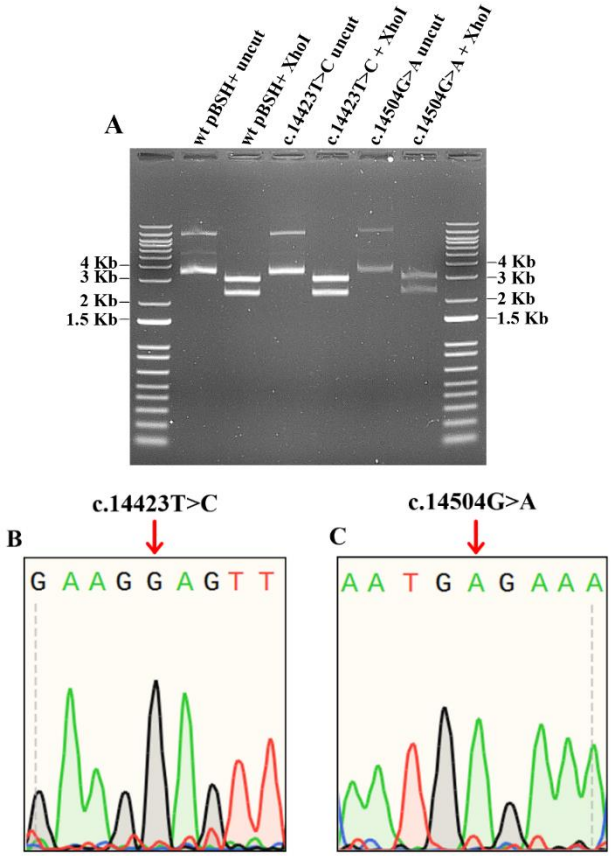

Figure 3.1. Mutagenesis of pBSH+ constructs.

Mutagenesis of the C-terminal variants c.14423T>C (p.Phe4808Ser) and c.14504G>A (p.Gly4835Glu) in pBSH+ **(A)** Restriction endonuclease digestion of wild type pBSH+ and mutated pBSH+ with XhoI. Electrophoresis was performed on a 0.8% agarose gel for 45 minutes at 100 V with 5 µL 1Kb+ DNA ladder. **(B)** Chromatogram showing the presence of the c.14423T>C nucleotide substitution (red arrow) in the complementary DNA strand. **(C)** Sequence chromatogram showing the presence of the c.14504G>A nucleotide substitution (red arrow). Chromatograms were generated in SnapGene®5.3. Images were compiled in Adobe photoshop. Primers used for sequencing of the constructs can be found in Appendix I, Table. 3. List of expected fragment sizes can be found in Appendix II, Table. 4.

Digestion of the wild type pBSH+ vector resulted in two bands that upon comparison to the 1Kb+ DNA ladder were shown to be of the expected lengths. The same fragments are seen in both plasmids with the *RYR1* variants while being absent from the uncut DNA controls, indicating they are a product of the restriction endonuclease digest. The presence of the nucleotide substitution in the sequence, along with the XhoI digestion proves that the variants c.14423T>C and c.14504G>A have been successfully incorporated into the pBSH+ vector.

3.1.2.2 pBSKO+ constructs

Identity of the pBSKO+ constructs was confirmed by digestion with NsiI, MfeI, and NotI to produce 3 fragments of 4340 bp, 3245 bp, and 1234 bp in length. The *RYR1* cDNA of pBSKO+ was then sequenced to confirm the presence of the nucleotide substitutions.

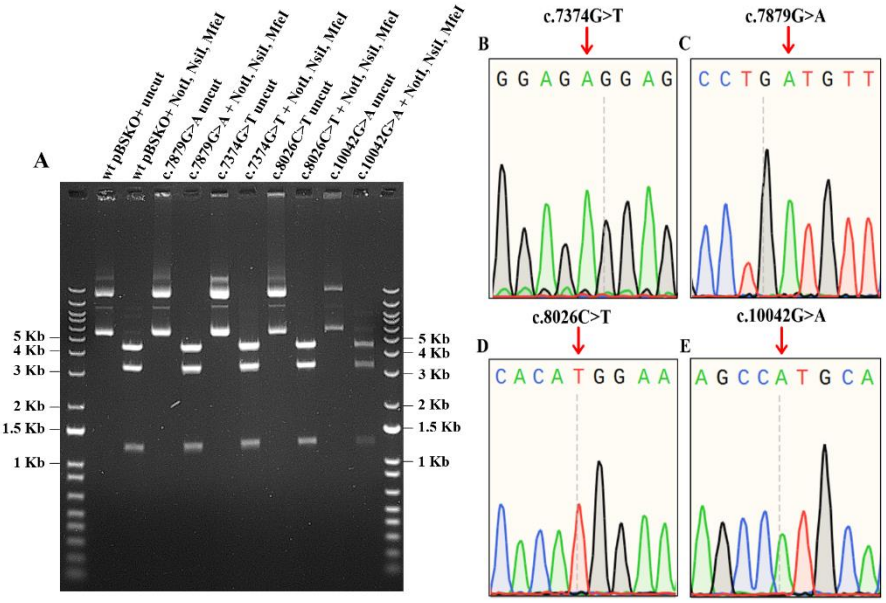

Figure 3.2. Mutagenesis of pBSKO+ constructs

Mutagenesis of the pBSKO+ constructs to produce variants c.7374G>T (p.Arg2458Leu), c.7879G>A (p.Val2627Met), c.8026C>T (p.Arg2676Trp), and c.10042G>A (p.Arg3348His). **(A)** Restriction endonuclease digestion of wild type pBSKO+ and mutated pBSKO+ with NsiI, MfeI, and NotI. Electrophoresis was performed on a 0.8% agarose gel at 100 V for 45 minutes with 5 µL 1Kb+ DNA ladder. Sequence chromatograms showing the presence of the **(B)** c.7374G>T (complementary DNA strand), **(C)** c.7879G>A, **(D)** c.8026C>T, **(E)** c.10042G>A nucleotide substitutions (red arrows). Chromatograms were generated in Snapgene®5.3. Images were compiled in Adobe photoshop. Primers used for sequencing constructs can be found in Appendix 1, Table. 3. List of expected fragment sizes can be found in Appendix II, Table. 4.

Digestion of the wild type pBSKO+ vector produced three fragments that are of the expected lengths. These fragments are seen in each of the mutated pBSKO+ constructs, while being absent from the wells containing undigested DNA. Sequence confirmation of the nucleotide substitution along with the restriction endonuclease digests indicate that the c.7374G>T, c7879G>A, c.8026C>T, and c.10042G>A nucleotide substitutions had each been successfully incorporated into the pBSKO+ vector.

3.1.3 Sub-cloning of RYR1 constructs

While the primers used for site-directed mutagenesis incorporate the variant of interest, the PCR process itself has the capacity to introduce variations in the template DNA due to errors made by the DNA polymerase. If unwanted PCR-induced mutations are present, then it will be unknown whether the Ca^{2+} release profile observed during functional analysis is due to the variant of interest or PCR-induced mutations. To confirm the absence of unwanted PCR-induced mutations, sections of *RYR1* cDNA to be sub-cloned into pBSKX+ were sequenced and mapped to wild type *RYR1* (NM_000540.3). Once unwanted PCR-induced mutations were confirmed to be absent from the variant *RYR1* cDNA, restriction enzyme based cloning was carried out to generate full-length *RYR1* constructs. This began with the cloning of inserts from the pBSH+ and pBSKO+ constructs into the pBSKX+ construct containing the C-terminal half of *RYR1* cDNA. Full-length *RYR1* constructs were then generated by cloning the *RYR1* cDNA from the pBSKX+ vector into pcDNA5/FRT/TO© containing the entire *RYR1* cDNA sequence (ftRyR1) (Fig. 2.2).

3.1.3.1 Generation of half-length RYR1 vairants

As the pBSH+ and pBSKO+ constructs contain different sections of *RYR1* cDNA, different restriction enzymes were used for sub-cloning of each construct into the pBSKX+ vector. Cloning of the pBSH+ and pBSKO+ constructs into pBSKX+ was carried out as outlined in chapter 2.2.1.5 where the small, variant-containing cDNA inserts from pBSH+/pBSKO+ were purified after gel electrophoresis and then ligated into the appropriately prepared pBSKX+ construct overnight at 16°C.

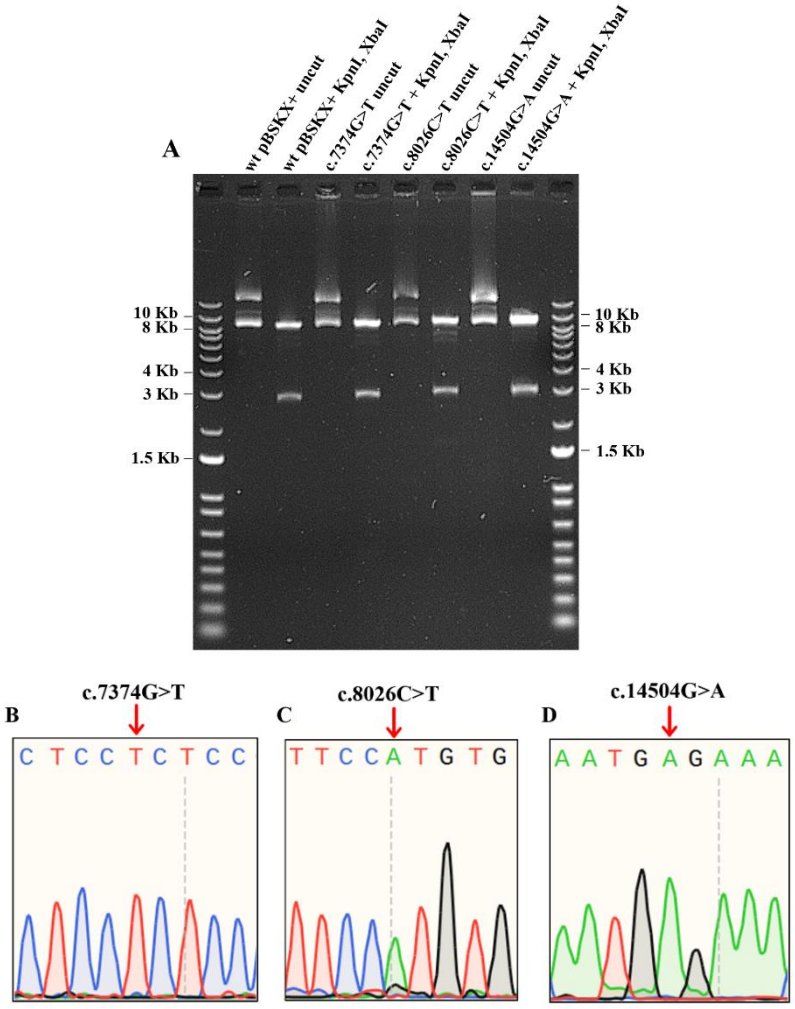

Figure 3.3. Cloning of *RYR1* variants into pBSKX+

Confirmation of *RYR1* variants being cloned into the pBSKX+ vector containing half length *RYR1* cDNA. **(A)** Restriction endonuclease digest of wild type pBSKX+ and the three variant pBSKX+ constructs c.7374G>T (p.Arg2458Leu), c.8026C>T (p.Arg2676Trp) and. C.14504G>A (p.Gly4835Glu). Fragments were separated via 0.8% agarose gel electrophoresis at 100 V for 45 minutes. **(B-D)** Chromatograms showing the presence of the desired nucleotide substitution **(B)** c.7374G>T **(C)** c.8026C>T (complementary strand) **(D)** c.14504G>A. Primers used for sequencing constructs can be found in Appendix 1, Table. 2 and Table. 3. List of expected fragment sizes can be found in Appendix II, Table. 4.

Successful ligation of *RYR1* cDNA into the pBSKX+ vector was confirmed via restriction endonuclease (RE) digestion with XbaI and KpnI. Digestion of the pBSKX+ vector with these enzymes was expected to produce two fragments of 8308 bp and 2884 bp in length which can be seen in each digest of both the wild type pBSKX+ vector as well as the newly constructed plasmids containing the variants, while importantly also being absent from the undigested controls. Sequencing of each variant confirmed that each newly generated construct contained the desired nucleotide substitution. Sequencing of the c.8026C>T variant was carried out on the complementary strand and therefore appears as an adenine. Together these results confirm the successful generation of three variant pBSKX+ constructs.

3.1.3.2 Generation of full-length RYR1 variants

Cloning pBSKX+ variants into ftRyR1 was performed using the restriction endonucleases KpnI, XbaI, and AvrII. XbaI and AvrII produce compatable cohesive ends, and therefore the products of XbaI and AvrII digestion can be ligated together. ftRyR1 was digested with KpnI and AvrII, rather than XbaI due to the presence of multiple XbaI sites in the pcDNA5/FRT/TO© vector. The pBSKX+ vector containing the c.7374G>T (p.Arg2458Leu) variation was digested with KpnI and XbaI and the products of each digest were separated by electrophoresis on a 0.8% agarose gel. The 8 kb fragment was then purified and ligated to the KpnI/AvrII digested ftRyR1 vector backbone. Variants p.Cys2237Tyr and p.Gly2183Glu were cloned into ftRyR1 using KpnI and XbaI by Dr Anja Schiemann.

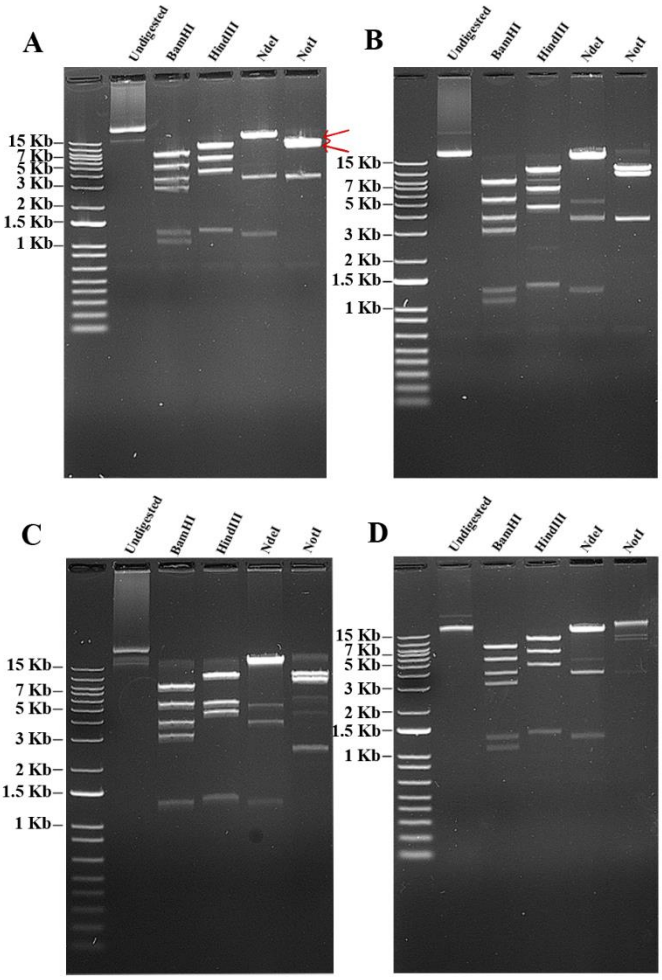

Figure 3.4. Confirmation of full-length *RYR1* constructs

Restriction endonuclease digest of the ftRyR1 plasmid containing full length human *RYR1* cDNA. Resctriction endonucleases used are BamHI, HindIII, NdeI, and NotI. Reaction mixtures were incubated for 1 hour at 37°C then separated on a 0.8% agarose gel at 100 V for 45 minutes. (**A)** RE digest of ftRyR1 plasmid containing the p.Gly2183Glu variant. Red arrows denote location of two separate fragments. (**B)** RE digest of ftRyR1 plasmid containing the p.Cys2237Tyr variant. (**C)** RE digest of axRyR1 plasmid containing the p.Arg2458Leu variant. (**D)** RE digest of ftRyR1 plasmid containing full length wild type human *RYR1* cDNA. Expected fragment sizes and sequence confirmation shown in Appendix II, Table. 5.

Each full length construct displays fragments of expected lengths (Appendix II, Table. 5) after restriction endonuclease digestion with BamHI, HindIII, NdeI, and NotI. Some non-specific or partial digestion by NotI can be seen as a faint band roughly 5 kb in length in the p.Cys2237Tyr (Fig. 3.4B), p.Arg2458Leu (Fig. 3.4C) and wild type (Fig. 3.4D) constructs. Undigested plasmid DNA can be seen as a high molecular weight band (>15 Kb) in each digest of the p.Cys2237Tyr (Fig. 3.4B) and p.Arg2458Leu (Fig. 3.4C) constructs as well as the NotI digest of the wild type construct (Fig. 3.4D). Incubation of the p.Arg2458Leu construct with NotI also resulted in non-specific/partial digestion as shown by two faint bands with sizes of

roughly 5 Kb and 6 Kb each (Fig. 3.4C). Faint bands of roughly 0.7 Kb can also be seen in each lane of the gel; however, its presence in the undigested plasmid control would indicate it is not a product of digestion.

The presence of the nucleotide substitution was confirmed via pairwise alignment of the construct's nucleotide sequence and human *RYR1* cDNA (NM_000540.3) using the emboss needle pairwise alignment tool (https://www.ebi.ac.uk/Tools/psa/emboss_needle/). These images, along with the nucleotide alignment (Appendix II, Fig. 7.9), confirm full length *RYR1* constructs containing the p.Gly2183Glu, p.Cys2237Tyr, and p.Arg2458Leu variants had been generated and were ready for introduction into the Flp-In™ T-REx™ host cell line for functional analysis.

3.2 Generation of cell lines stably expressing RyR1 variants

3.2.1 Overview

Generation of mammalian cell lines stably expressing variant *RYR1* cDNA was accomplished via the Flp-In™ system from Invitrogen. In this system the cell line was co-transfected with the gene of interest (GOI, *RYR1* cDNA) and a vector containing Flp recombinase (pOG44). The *RYR1* cDNA is then subsequently incorporated into the Flp-In™ T-REx™ host cell genome via recombination at Flp recombination target (FRT) sites. Cell lines were generated in this fashion as opposed to transient transfection of *RYR1* cDNA as it allowed for more consistent and accurate control of expression of RyR1. Expression of the GOI in transiently transfected cells is dependent on the transfection efficiency of the plasmid, which can vary between transfection reactions; as a result, RyR1 expression is likely to vary depending on the success of each transfection. While the data gathered in this fashion can be normalised in the same manner for stably expressing lines, the use of cell lines stably expressing RyR1 streamlines the functional analysis process and prevents potential technical problems and time wastage that may arise as a result of failed transfections.

Cell lines stably expressing RyR1 were generated as outlined in chapter 2.2.2.1. Multiple colonies for each variant were selected and the extent of RyR1 expression was characterised to select the colonies that express RyR1 most abundantely. That colony was then used to propagate the cell lines and to conduct all further analyses.

3.2.2 Confirmation of successful transfections

Successful transfections were confirmed through sequencing of PCR amplicons made from genomic DNA extracts. Like all mammalian somatic cells, the *RYR1* gene is endogenously present in the host cell line, therefore amplification and subsequent sequencing of endogenous *RYR1* may falsely confirm a successful transfection. In order to prevent this, primers that are complementary for the cDNA sequence of *RYR1* were used for PCR amplification. As a result of the presence of introns in the gene, endogenous *RYR1*, if amplified, would result in a substantially larger PCR product than the non-endogenous cDNA. Successful transfections of variant *RYR1* were therefore confirmed as outlined in chapter 2.2.1.6

The cell lines containing substitutions c.1615T>C (p.Phe539Leu), c.5119C>T (p.Arg1707Cys), c.8378C>T (p.Pro2793Leu), and c.14477C>T (p.Thr4826Ile) were generated by previous students and were sequenced to confirm the correct variants were present. Due to an error during cell culture occuring in a previous project, the correct identity of the cell line containing the p.Phe539Leu variant was unknown. PCR amplification and sequencing of this cell line using primers that flank the location of the c.8378C>T substitution confirmed that the variant present was p.Pro2793Leu, rather than p.Phe539Leu (Appendix III, Fig. 7.10).

3.2.3 Selection of stable cell lines

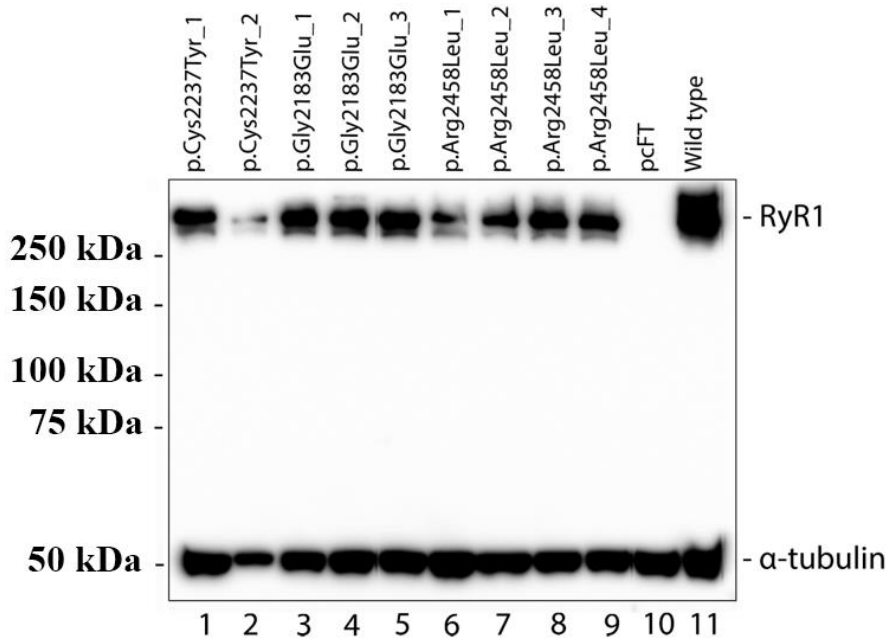

Figure 3.5. Induced RyR1 expression in Flp-In™ T-REx™ colonies

Immunoblot of protein extracts made from colonies generated by *RYR1* transfection in Flp-In™ T-REx™ 293 cell lines after a 72 hour induction with tetracycline (1 μgmL^{-1}). ~250 µg of total protein extract was resolved at 120 V for 2½ hours using 7.5% SDS-PAGE before being transferred to a PVDF membrane. RyR1 and α-tubulin were detected using 34C anti-RyR1 (mouse) and anti-α-tubulin (mouse) and a horseradish peroxidase-conjugated anti-mouse secondary antibody. The membrane was developed using the Azure c600 from Azure biosystems and the resulting images were compiled using Adobe Photoshop.

After the generation of stable cell lines, protein extracts were harvested for each colony as outlined in chapter 2.2.2.6 and electrophoresed by 7.5% SDS-PAGE, before being transferred to a PVDF membrane for visualisation as outlined in chapter 2.2.3.1. The 565 kDa RyR1 monomer can be seen in each lane above the 250 kDa marker, while being absent from the cell line transfected with vector only (pcFT). α-tubulin can be seen at the 50 kDa marker in each lane, confirming protein extract from the pcFT cell line is present and thus the lack of RyR1 is due to the absence of *RYR1* cDNA.

Clones were selected for further analysis based on their relative abundance of RyR1. Clones p.Gly2183Glu_1 and p.Arg2458Leu_4 were chosen as the stable cell lines for p.Gly2183Glu, and p.Arg2458Leu respectively to use for further analysis, while the clone p.Cys2237Tyr_2 was chosen for the p.Cys2237Tyr construct. In preliminary analysis the p.Cys2237Tyr_2 clone displayed more abundant RyR1 expression than p.Cys2237Tyr_1 (Appendix III, Fig. 7.11) thus the p.Cys2237Tyr_1 cell line stock

was prematurely discarded. The p.Cys2237Tyr_2 clone was therefore chosen despite showing reduced RyR1 expression in comparison to p.Cys2237Tyr_1. Interestingly, while this clone shows less RyR1, it also displays reduced α-tubulin expression, indicating that the decrease in RyR1 seen in the p.Cys2237Tyr_2 clone may be due to an overall reduction in protein expression in that cell line or a gel loading artifact.

3.2.4 RYR1 expression and co-localisation to the endoplasmic reticulum

3.2.4.1 Stable expression of variant RyR1

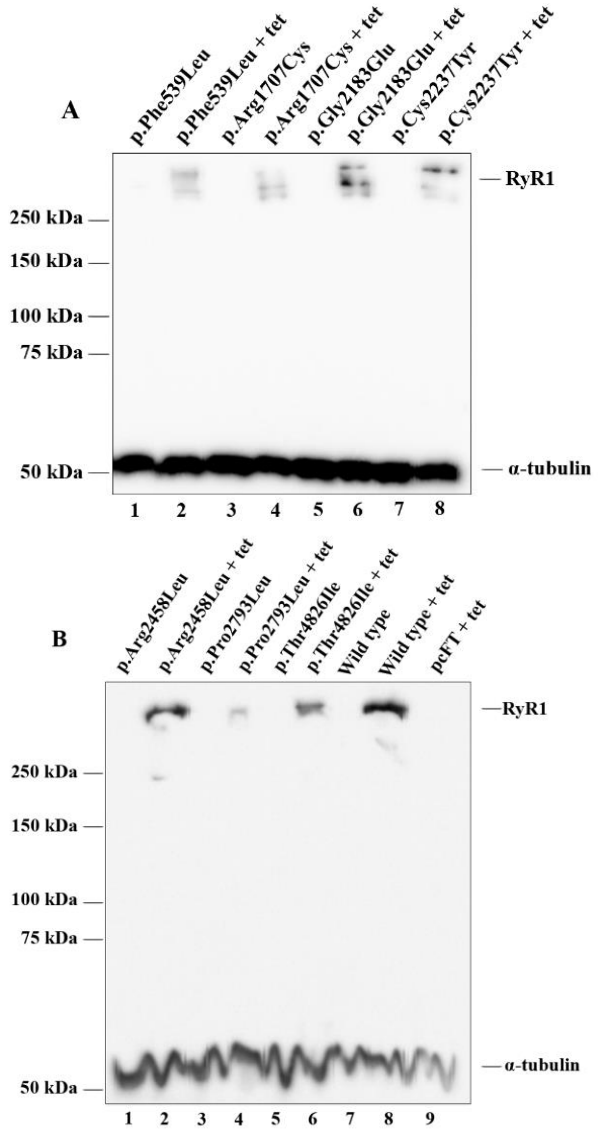

Figure 3.6. RyR1 expression in Flp-In™ T-REx™ 293 cell lines

Immunoblot analysis of protein extracts retrieved from Flp-In™ T-REx™ 293 cell lines stably expressing RyR1 variants. ~200µg total protein extract from uninduced and induced (1 µgmL^{-1} tetracycline) cell lines were separated using 7.5% SDS-PAGE then immunoblotted for RyR1 and α-tubulin as outlined in chapter 2.2.3.1. **(A)** cell lines p.Phe539Leu, p.Arg1707Cys, p.Gly2183Glu, p.Cys2237Tyr. **(B)** cell lines p.Arg2458Leu, p.Pro2793Leu, p.Thr4826Ile, wild type, and pcFT. pcFT = cell line transfected with vector only (pcDNA5/FRT/TO©). Lanes are numbered beneath each figure.

Each cell line transfected with *RYR1* cDNA was confirmed to express RyR1 via immunoblot analysis as outlined in chapter 2.2.3.1. As inducible systems such as the tet-repressor system used for this project have been known to express transgenes in the absence of the inducer, protein extracts from uninduced and induced cell lines were examined for RyR1 expression. Distinct bands correlating to the sizes of RyR1 and α-tubulin could be seen in each lane, indicating the presence of RyR1 and tubulin in each cell line. Multiple bands corresponding to RyR1 in Fig.3.5 and Fig.3.6A could be seen in each lane. The precise reasoning behind this was not established; however, duplex bands are a common occurrence when visualising RyR1 through immunoblot analysis[121-123]. Variation in the intensities of the bands corresponding to protein extracted from the p.Gly2183Glu, p.Arg2458Leu, and wild type cell lines was observed between Fig. 3.5 and Fig. 3.6. While the protein extracts used for each electrophoresis were identical, the total protein mass loaded into the gel was lower in Fig. 3.6 (200 µg) than in Fig. 3.5 (250 µg) which may explain this discrepancy.

While all cell lines expressed RyR1 in the presence of tetracycline, the abundance of expression varied between them. Cell lines p.Phe539Leu, and p.Arg1707Cys appeared to express RyR1 to a slightly lesser extent than the other cell lines, while p.Pro2793Leu displayed substantially less expression of the Ca^{2+} channel than the other cell lines. No band correlating to RyR1 could be seen in the pcFT cell line indicating it lacked RyR1. Importantly, a band of equal size to RyR1 in the uninduced p.Phe539Leu cell line was observed after over-exposure of the image. This result indicates the cell lines are likely to express the transgene in the absence of tetracycline (Appendix III, Fig. 7.12), even though bands are not obvious on the immunoblot.

3.2.4.2 Co-localisation of RYR1 to the endoplasmic reticulum

RyR1 mediates the release of Ca^{2+} from stores in the sarcoplasmic reticulum (SR) of muscle cells, making its localisation to the membrane of the endo/sarcoplasmic reticulum paramount in maintaining its function. Appropriate analysis of variant RyR1 is therefore dependent on its localisation to the endoplasmic reticulum (fibroblast equivalent of the sarcoplasmic reticulum) of the host cell line. To confirm targeting of RyR1 to the endoplasmic reticulum, immunofluorescence staining was performed using 34C anti-RyR1 (mouse) and anti-PDI (rabbit). Protein disulfide isomerase (PDI) is an endoplasmic reticulum-targeted enzyme responsible for the catalysis of disulfide bonds between cysteine residues during protein folding. As a result, PDI is often used as a marker for the endoplasmic reticulum, and was used here for co-localisation analysis. Visualisation of RyR1 and PDI was achieved as outlined in chapter 2.2.3.2.

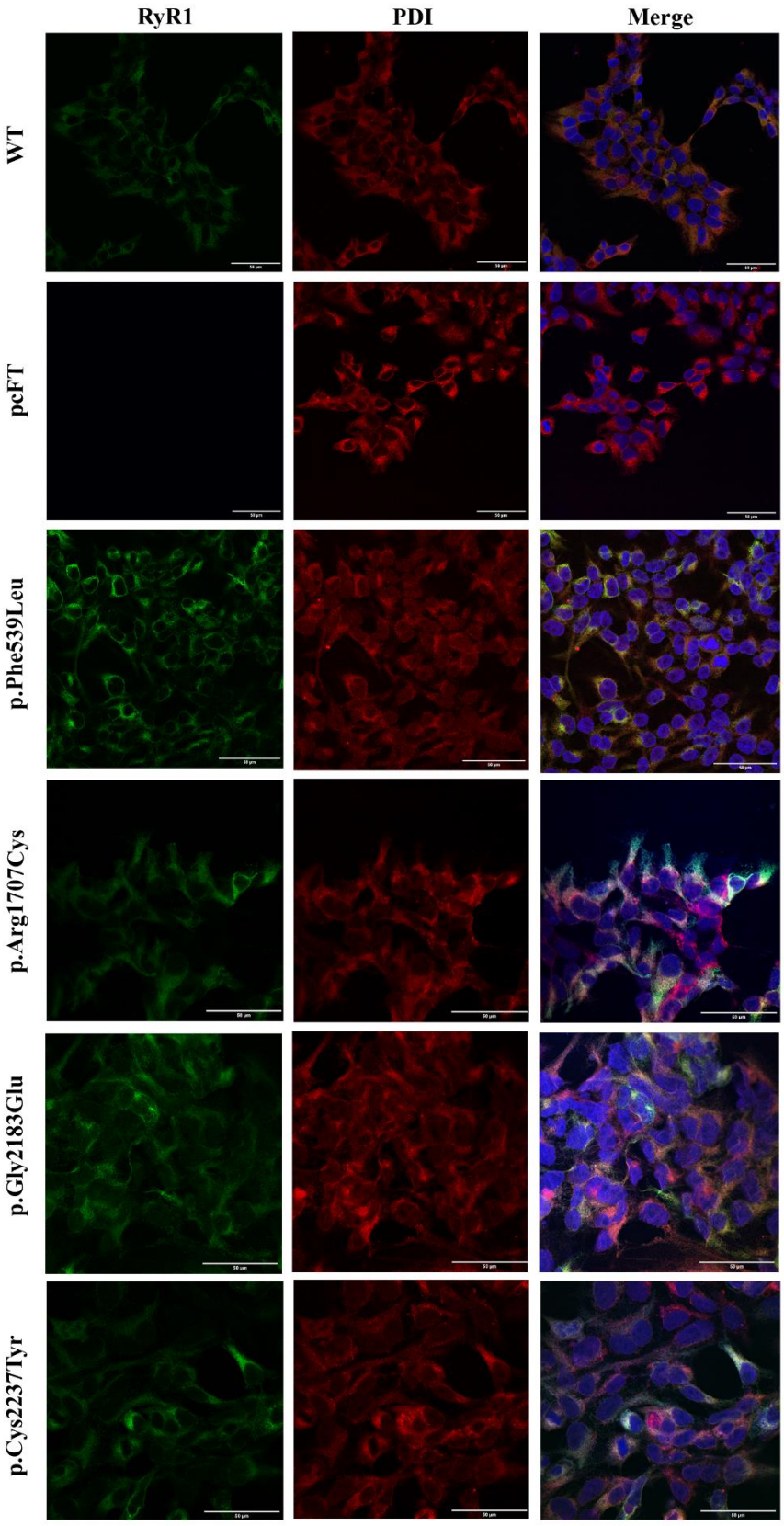
RyR1
PDI
Merge
WT
pcFT
p.Phe539Leu
p.Arg1707Cys
p.Gly2183Glu
p.Cys2237Tyr

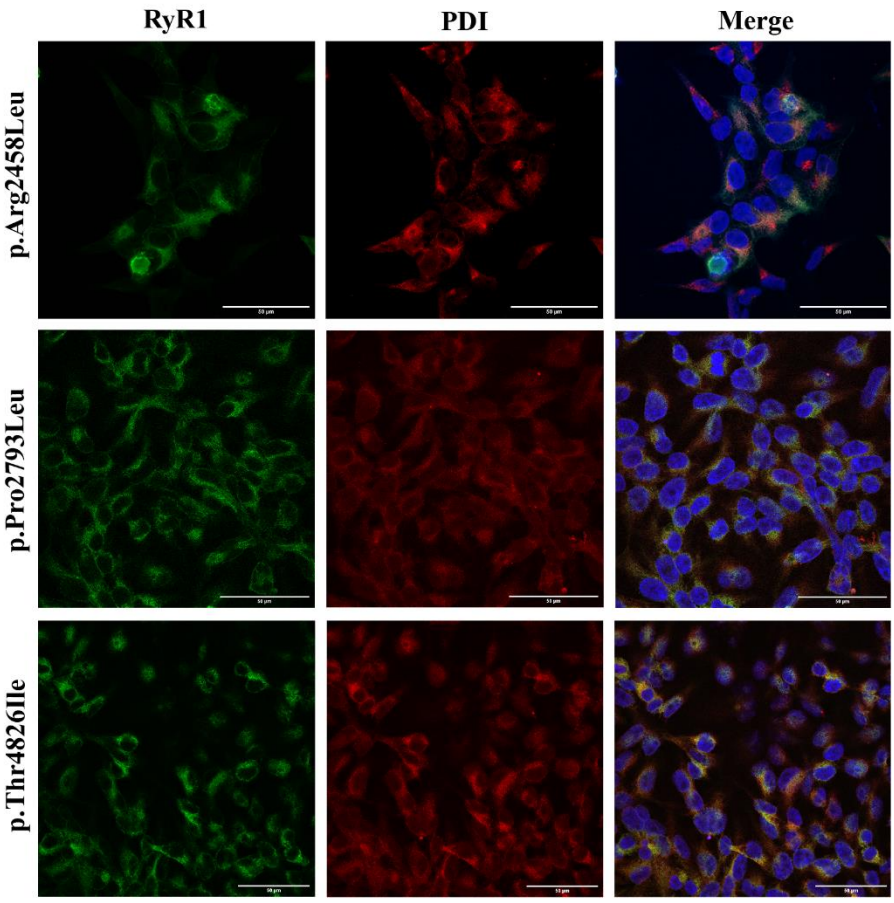

Figure 3.7. Immunofluorescence assay of cell lines stably expressing RyR1

Confocal images of immunofluorescence staining showing RyR1 co-localisation with PDI to the endoplasmic reticulum membrane. Stable cell lines are denoted by the RyR1 amino acid substitution with pcFT denoting cells transfected with vector only. RyR1 is stained green with FITC conjugated α-mouse antibody, PDI is stained red with TRITC conjugated α-rabbit antibody. The nucleus is stained blue with Prolong gold containing DAPI. Scale bar denotes 50 microns. Images compiled in ImageJ.

RyR1 can be seen to co-localise with PDI in each cell line as evident by the merged images (Fig. 3.7). All cell lines visually display similar fluorescence, including variants p.Phe539Leu, p.Arg1707Cys, and p.Pro2793Leu which contradictively display reduced RyR1 expression in immunoblot analysis. As expected the pcFT cell line does not display any RyR1 expression. These images confirm that RyR1 localises to the endoplasmic reticulum in each transfected cell line and therefore these lines could be used for functional analysis of RyR1.

3.3. Functional analysis of RyR1 variants

3.3.1 Overview

Functional analysis of RyR1 variants was carried out as outlined in chapter 2.2.4.1. The variant p.Thr4826Ile has been deemed pathogenic for MH by the EMHG and was therefore analysed as a hypersensitive control. Cells transfected with wild type *RYR1* and vector only (pcFT) were used as controls to display "normal" Ca^{2+} release and to show that Ca^{2+} transients were indeed mediated by RyR1. Data were normalised to the fluorescence obtained after exposure to 1000 µM 4-c*m*c and represented as a % of the fluorescence detected at this concentration. Hypersensitivity was determined by the concentration of agonist at which 50% of the maximal response was reached, also known as the half maximal effective concentration (EC_{50}).

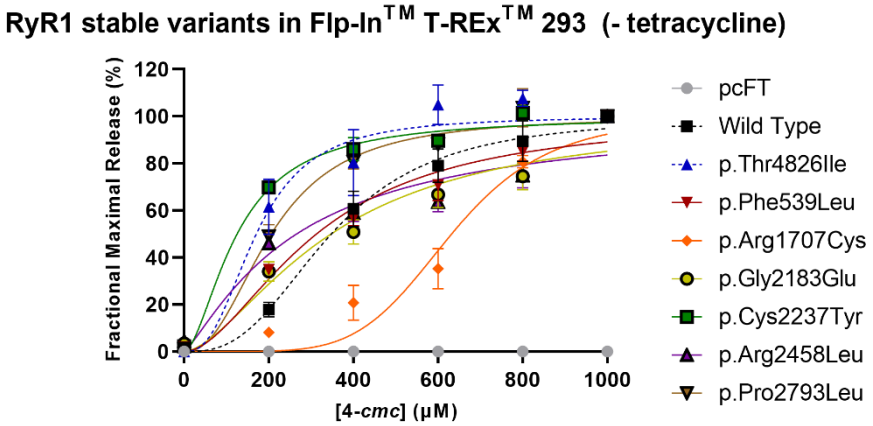

Figure 3.8. Ca^{2+} release profiles of cell lines stably expressing RyR1.

Ca^{2+} release profiles of variant RyR1 after exposure to 4-c*m*c. Data were normalised to maximum Ca^{2+} release established at maximal 4-c*m*c concentration (1000 µM). Data are represented as a % of maximal Ca^{2+} release ± SEM and fitted to an [agonist] vs normalised response (variable slope) curve. Variants are depicted as their amino acid substitutions with the hypersensitive control (p.Thr4826Ile) and wild type control depicted as dashed lines. pcFT is vector only. Created using Prism9 (Graphpad).

p.Thr4826Ile displayed a hypersensitive response to 4-c*m*c, with an EC_{50} of 221.32 µM 4-c*m*c ± 38.32. Wild type RyR1 displayed an EC_{50} of 377.1 µM 4-c*m*c ± 31.73 making the p.Thr4826Ile variant significantly different to wild type ($p = 0.00605$) and therefore appropriate to use as a control. The pcFT cell line did not produce a response to 4-c*m*c as expected as endogenous *RYR1* is not expressed in a functional form.

3.3.2 p.Phe539Leu RYR1

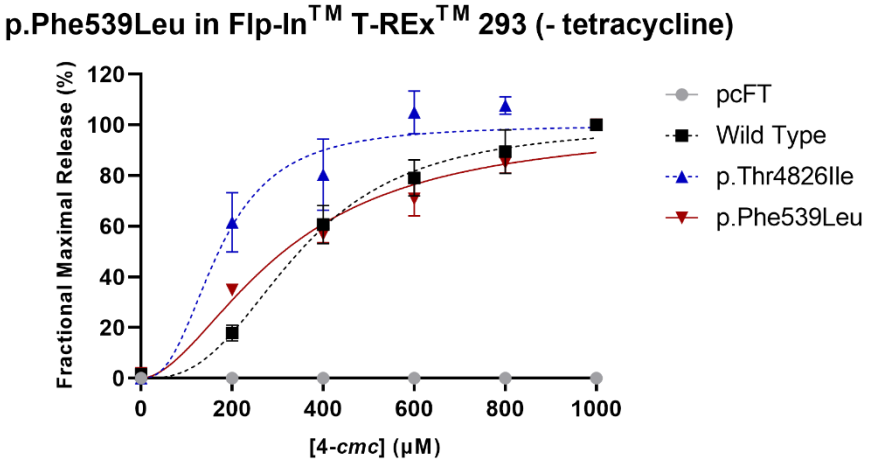

Figure 3.9. p.Phe539Leu Ca^{2+} release profile

Ca^{2+} release profile of the RyR1 variant p.Phe539Leu. Data were normalised to maximal Ca^{2+} release established at maximal 4-c*m*c concentration (1000 µM) and represented as a % ± SEM (Fractional maximal release). Hypersensitive and wild type channels are represented as dashed blue and black lines respectively, with p.Phe539Leu depicted as purple. pcFT is solid grey. Data compiled in Prism9 (Graphpad).

Functional characterisation of the p.Phe539Leu variant showed that it behaves similarly to wild type, with an EC_{50} of 304.82 µM 4-c*m*c ± 18.12 (Fig. 3.9). After performing a Bonferroni correction for multiple tests there was no significant difference seen between the variant and the wild type cell line ($p = 0.039677$, $\alpha = 0.01$). While this variant did not display a hypersensitive response to 4-c*m*c, the proximity of the variant to a putative binding site for FKBP12 makes it a relatively good control during experimentation on the effects of the calstabin on RyR1 function. Therefore it was analysed further in the presence of over-expressed FKBP12. (Fig. 3.17).

3.3.3 p.Arg1707Cys RYR1

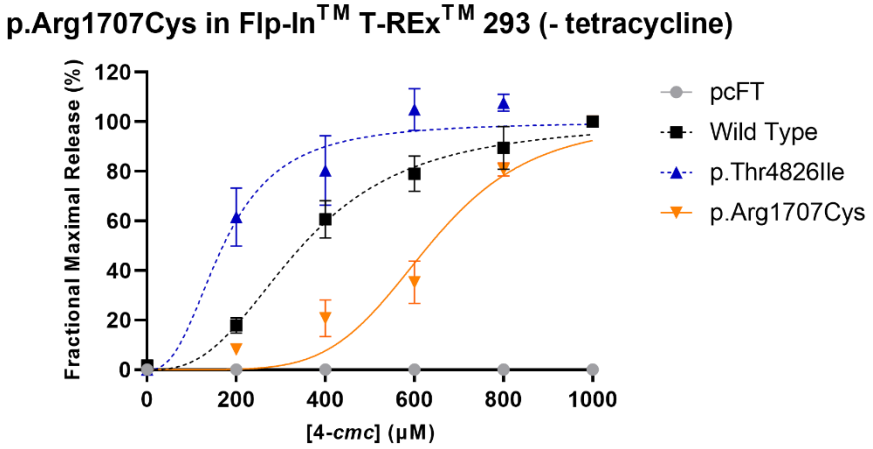

Figure 3.10. p.Arg1707Cys Ca^{2+} release profile

Ca^{2+} release profile of the RyR1 variant p.Arg1707Cys. Data were normalised to maximal Ca^{2+} release established at maximal 4-c*mc* concentration (1000 µM) and represented as a % ± SEM (Fractional maximal release). Hypersensitive and wild type channels are represented as dashed blue and black lines respectively, with p.Arg1707Cys depicted as orange. pcFT is solid grey. Data compiled in Prism9 (Graphpad).

The p.Arg1707Cys cell line had proven difficult to functionally characterise, displaying fluorescence so diminished that it was unable to be easily detected by the experimental system. With perseverance however, the uninduced p.Arg1707Cys cell line produced an EC_{50} of 621.55 µM 4-c*mc* ± 29.50. This suggests that the p.Arg1707Cys variant may substantially diminish the response to 4-c*mc*; however, further analysis should be performed due to the very poor response to the agonist. After a Bonferroni correction, this response was deemed not significantly different to wild type ($p = 0.024682$, $\alpha = 0.01$).

3.3.4 p.Gly2183Glu RYR1

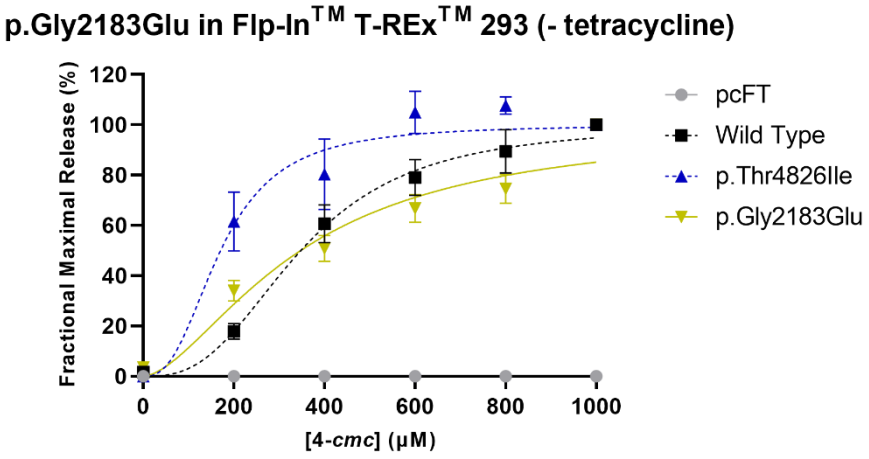

Figure 3.11. p.Gly2183Glu Ca^{2+} release profile

Ca^{2+} release profile of the RyR1 variant p.Gly2183Glu. Data were normalised to maximal Ca^{2+} release established at maximal 4-c*m*c concentration (1000 µM) and represented as a % ± SEM (Fractional maximal release). Hypersensitive and wild type channels are represented as dashed blue and black lines respectively, with p.Gly2183Glu depicted as yellow. pcFT is solid grey. Data compiled in Prism9 (Graphpad).

The p.Gly2183Glu variant displayed a Ca^{2+} release profile very similar to that of wild type. While exposure of p.Gly2183Glu to 200 µM 4-c*m*c produced a similar response to wild type, exposure to higher concentrations of 4-c*m*c resulted in a diminished response. The EC_{50} of p.Gly2183Glu was 358.42 µM 4-c*m*c ± 38.11, and in this regard was closest in comparison to wild type RyR1 out of all the cell lines assayed. However, the p.Phe539Leu variant was more closely aligned with the fitted curve (Fig. 3.9). After a Bonferroni correction, the differences seen between the p.Gly2183Glu variant and wild type RyR1 were not deemed statistically significant ($p = 0.35759$, $\alpha = 0.01$).

3.3.5 p.Cys2237Tyr RYR1

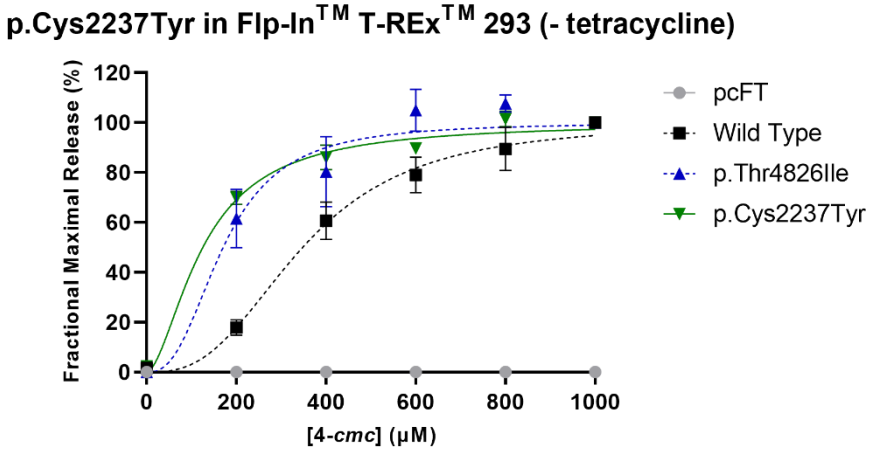

Figure 3.12. p.Cys2237Tyr Ca^{2+} release profile

Ca^{2+} release profile of the RyR1 variant p.Cys2237Tyr. Data were normalised to maximal Ca^{2+} release established at maximal 4-c*m*c concentration (1000 µM) and represented as a % ± SEM (Fractional maximal release). Hypersensitive and wild type channels are represented as dashed blue and black lines respectively, with p.Cys2237Tyr depicted as green. pcFT is solid grey. Data compiled in Prism9 (Graphpad).

Out of all the variants tested, none were more hypersensitive to 4-c*m*c than p.Cys2237Tyr (Fig. 3.8). With an EC_{50} of 128.66 µM 4-c*m*c ± 13.37, the p.Cys2237Tyr variant displayed a Ca^{2+} release profile that, after a Bonferroni correction for multiple tests, was deemed significantly different to wild type ($p = 4.56x10^{-5}$, $\alpha = 0.01$) (Fig. 3.12). The significantly low EC_{50} indicates that substituting the cysteine at position 2237 for tyrosine produces a response to 4-c*m*c that is characteristic of a variant pathogenic for MH. Due to the proximity of this variant to a putative FKBP12 binding site as well as its hypersensitive nature, further analysis in the presence of the calstabin was performed (Fig. 3.18).

3.3.6 p.Arg2458Leu RYR1

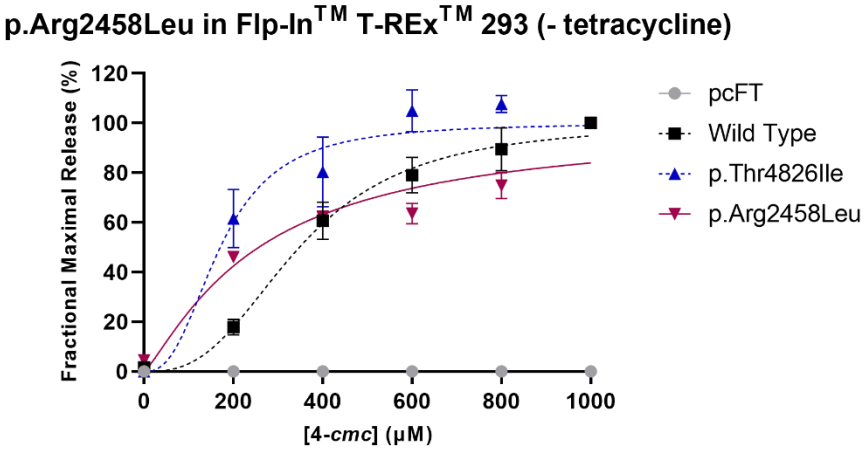

Figure 3.13. p.Arg2458Leu Ca^{2+} release profile

Ca^{2+} release profile of the RyR1 variant p.Arg2458Leu. Data were normalised to maximal Ca^{2+} release established at maximal 4-c*m*c concentration (1000 µM) and represented as a % ± SEM (Fractional maximal release). Hypersensitive and wild type channels are represented as dashed blue and black lines respectively, with p.Arg2458Leu depicted as pink. pcFT is solid grey. Data compiled in Prism9 (Graphpad).

The p.Arg2458Leu variant displayed an unusual Ca^{2+} release profile, appearing hypersensitive to 4-c*m*c at low concentrations and less sensitive than wild type at higher concentrations (Fig. 3.13). The EC_{50} of p.Arg2458Leu was 283.86 µM 4-c*m*c ± 18.71, making it substantially different to wild type; however, the difference did not reach statistical significance after correcting for multiple tests via a Bonferroni correction ($p = 0.016098$, $\alpha = 0.01$). This suggests p.Arg2458Leu does not result in a hypersensitive channel in this study, but further analysis is warranted as other variants at this amino acid position result in a hypersensitive channel[124, 125]

3.3.7 p.Pro2793Leu RYR1

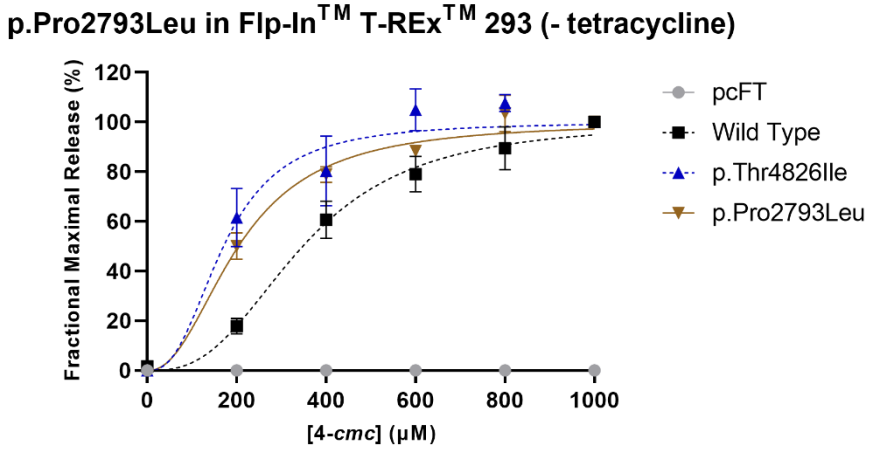

Figure 3.14. p.Pro2793Leu Ca^{2+} release profile

Ca^{2+} release profile of the RyR1 variant p.Pro2793Leu. Data were normalised to maximal Ca^{2+} release established at maximal 4-c*m*c concentration (1000 µM) and represented as a % ± SEM (Fractional maximal release). Hypersensitive and wild type channels are represented as dashed blue and black lines respectively, with p.Pro2793Leu depicted as brown. pcFT is solid grey Data compiled in Prism9 (Graphpad).

The p.Pro2793Leu substitution in RyR1 produced a channel that is hypersensitive to 4-c*m*c (Fig. 3.14). With an EC_{50} of 218.97 µM 4-c*m*c ± 17.67, the p.Pro2793Leu variant resulted in the second most hypersensitive channel assayed (Fig. 3.8). Though not as hypersensitive as p.Thr4826Ile, p.Pro2793Leu displayed a difference to wild type that was deemed statistically significant after a Bonferroni correction for multiple tests and could therefore be considered pathogenic for MH ($p = 9.21x10^{-4}$, $\alpha = 0.01$). Due to the hypersensitive nature of the variant and its proximity to a putative FKBP12 binding site, further analysis in the presence of the calstabin was performed (Fig. 3.19).

3.4 Effects of FKBP12 on RyR1 function

3.4.1 Overview

Due to three of the assayed variants being present near putative binding sites of FKBP12, over-expression of the calstabin in these cell lines was induced to indirectly characterise the variants effect on FKBP12 binding. Cell lines stably expressing RyR1 variants p.Phe539Leu, p.Cys2237Tyr, and p.Pro2793Leu were each transiently transfected with pcDNA^{TM}3.1(+) vector containing *FKBP12* cDNA. After 72 hours, Ca^{2+} release was characterised as outlined in section 2.5.1. The variant, p.Thr4826Ile, was also characterised in the presence of over-expressed FKBP12 as a negative control due to its distal location to the proposed calstabin binding site.

3.4.2 p.Thr4826Ile RYR1 + FKBP12

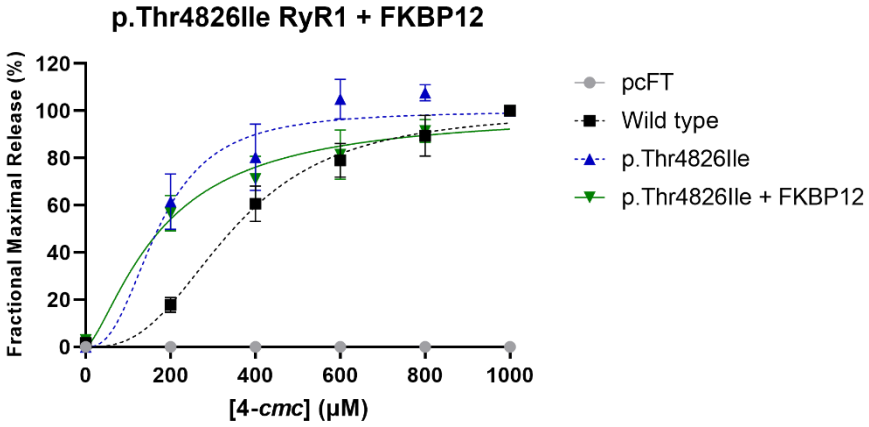

Figure 3.15. p.Thr4826Ile RyR1 + FKBP12 Ca^{2+} release profile

Ca^{2+} release profile of RyR1 variant p.Thr4826Ile in the presence of FKBP12. Data were normalised to maximum Ca^{2+} release established at maximal 4-*cm*c concentration (1000 µM) and represented as a % ± SEM (Fractional maximal release). Ca^{2+} release by p.Thr4826Ile RyR1 before FKBP12 over-expression and wild type RyR1 are represented by blue and black dotted lines respectively. Ca^{2+} release by p.Thr4826Ile RyR1 after over-expression of FKBP12 is depicted in green. Stable cell lines not expressing RyR1 (pcFT) is depicted in grey. Data compiled using Prism9^{TM} (Graphpad).

Over-expression of FKBP12 resulted in decreased sensitivity to 4-*cm*c for the p.Thr4826Ile variant. While not evident from the fitted curve (Fig. 3.15), the EC_{50} increased to 305.54 µM 4-*cm*c ± 60.65 (Appendix IV, Table 8 and Table 11.), making the difference between the hypersensitive channel and wild type RyR1 no longer significant ($p = 0.0607$). While the difference between p.Thr4826Ile and wild type RyR1 was no longer statistically significant, p.Thr4826Ile mediated Ca^{2+} release pre- and post-over-expression of FKBP12 was also not significantly different ($p = 0.286$).

3.4.3 Wild type RYR1 + FKBP12

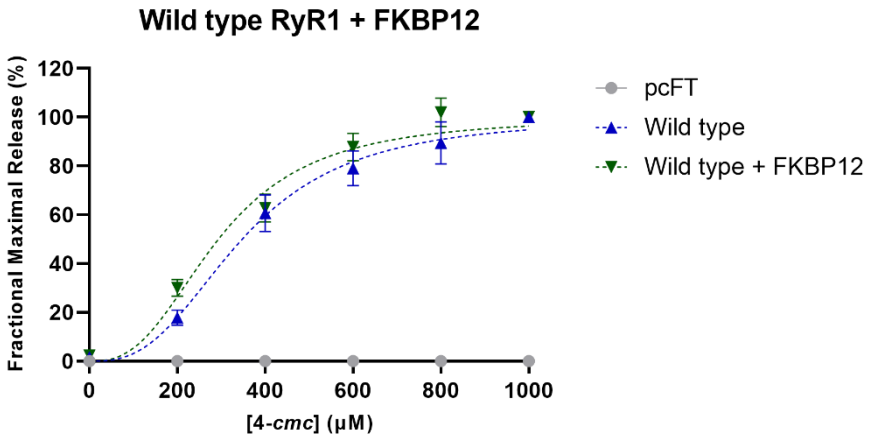

Figure 3.16. Wild type RyR1 + FKBP12 Ca^{2+} release profile

Ca^{2+} release profile of wild type RyR1 in the presence of FKBP12. Data were normalised to maximum Ca^{2+} release established at maximal 4-c*m*c concentration (1000 µM) and represented as a % ± SEM (Fractional maximal release). Ca^{2+} release by wild type RyR1 before FKBP12 over-expression is represented by blue lines. Ca^{2+} release by wild type RyR1 after over-expression of FKBP12 is depicted in green. A stable cell line not expressing RyR1 (pcFT) is depicted in grey. Data compiled using Prism9™ (Graphpad).

Over-expression of FKBP12 had no effect on wild type RyR1 (Fig. 3.16). With an EC_{50} of 293.80 µM 4-c*m*c ± 10.86, there was no significant difference in Ca^{2+} release when FKBP12 was over-expressed ($p = 0.0210$) ($\alpha = 0.01$ after Bonferroni correction). Over-expression of FKBP12 did, however, result in wild type RyR1 no longer being significantly different to the p.Thr4826Ile variant ($p = 0.0642$).

3.4.4 p.Phe539Leu RYR1 + FKBP12

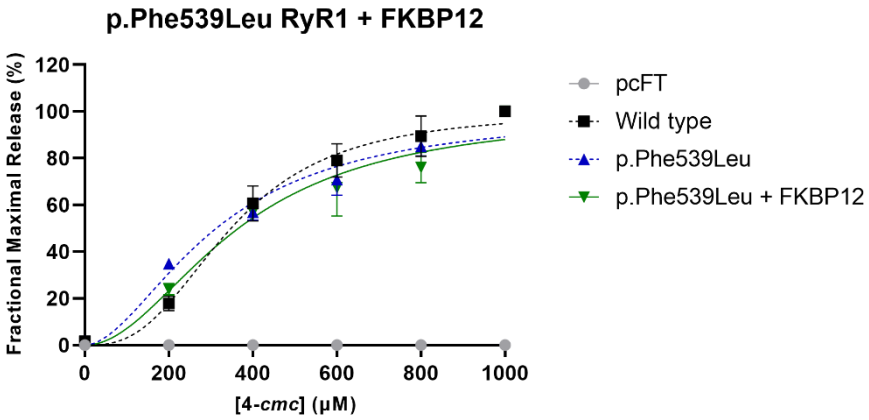

Figure 3.17. p.Phe539Leu RyR1 + FKBP12 Ca^{2+} release profile

Ca^{2+} release profile of RyR1 variant p.Phe539Leu in the presence of FKBP12. Data were normalised to maximum Ca^{2+} release established at maximal 4-*cmc* concentration (1000 µM) and represented as a % ± SEM (Fractional maximal release). Ca^{2+} release by p.Phe539Leu RyR1 before FKBP12 over-expression and wild type RyR1 are represented by blue and black dotted lines respectively. Ca^{2+} release by p.Phe539Leu RyR1 after over-expression of FKBP12 is depicted in green. A stable cell line not expressing RyR1 (pcFT) is depicted in grey. Data compiled using Prism9 (Graphpad).

Over-expression of FKBP12 had no significant effect on Ca^{2+} release for the p.Phe539Leu variant ($p = 0.0217$) (Fig. 3.17). With an EC_{50} of 367.57 µM 4-*cmc* ± 16.62, addition of FKBP12 resulted in the p.Phe539Leu variant displaying a Ca^{2+} release profile almost identical to wild type, with no significant difference being seen between the two ($p = 0.398$).

3.4.5 p.Cys2237Tyr RYR1 + FKBP12

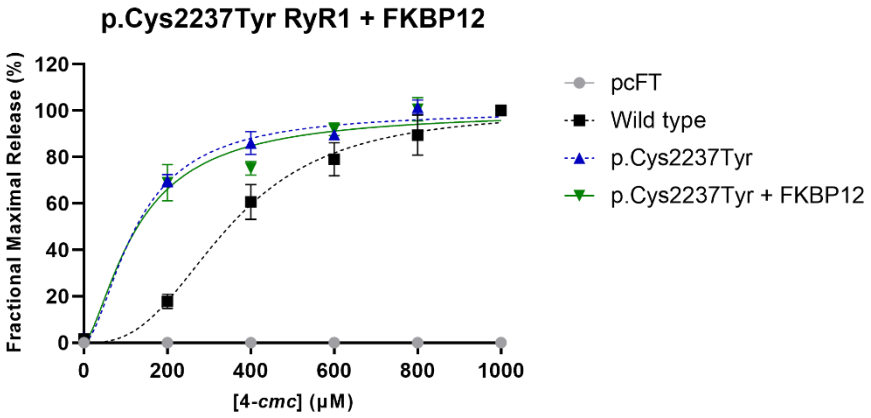

Figure 3.18. p.Cys2237Tyr RyR1 + FKBP12 Ca^{2+} release profile

Ca^{2+} release profile of RyR1 variant p.Cys2237Tyr in the presence of FKBP12. Data were normalised to maximum Ca^{2+} release established at maximal 4-*cm*c concentration (1000 µM) and represented as a % ± SEM (Fractional maximal release). Ca^{2+} release by p.Cys2237Tyr RyR1 before FKBP12 over-expression and wild type RyR1 are represented by blue and black dotted lines respectively. Ca^{2+} release by p.Cys2237Tyr RyR1 after over-expression of FKBP12 is depicted in green. A stable cell line not expressing RyR1 (pcFT) is depicted in grey. Data compiled using Prism9™ (Graphpad).

Interestingly, over-expression of FKBP12 had no effect on Ca^{2+} release mediated by the p.Cys2237Tyr variant (p = 0.449) (Fig. 3.18). With an EC_{50} of 123.07 µM 4-c*m*c ± 37.56 the variant remained significantly different to wild type (p = 0.00178). In the absence of FKBP12, this variant displays a Ca^{2+} release profile similar to that of the p.Thr4826Ile positive control variant. With no significant difference seen between the two (p = 0.0356), the variant can therefore be confirmed as hypersensitive, with the possibility that it disrupts FKBP12 binding.

3.4.6 p.Pro2793Leu RYR1 + FKBP12

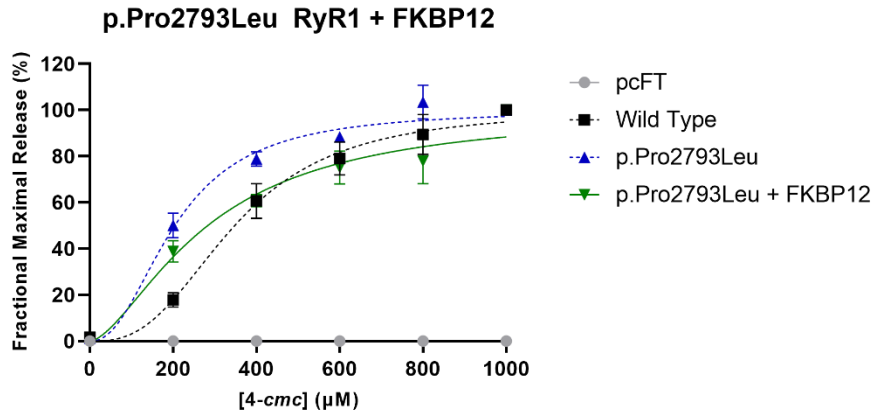

Figure 3.19. p.Pro2793Leu RyR1 + FKBP12 Ca^{2+} release profile

Ca^{2+} release profile of RyR1 variant p.Pro2793Leu in the presence of FKBP12. Data were normalised to maximum Ca^{2+} release established at maximal 4-c*m*c concentration (1000 µM) and represented as a % ± SEM (Fractional maximal release). Ca^{2+} release by p.Pro2793Leu RyR1 before FKBP12 over-expression and wild type RyR1 are represented by blue and black dotted lines respectively. Ca^{2+} release by p.Pro2793Leu RyR1 after over-expression of FKBP12 is depicted in green. A stable cell line not expressing RyR1 (pcFT) is depicted in grey. Data compiled using Prism9™ (Graphpad).

The Ca^{2+} release profile of the p.Pro2793Leu variant in the presence of FKBP12 was unusual. With an EC_{50} of 282.77 µM 4-c*m*c ± 32.97, over-expression of FKBP12 appeared to result in a Ca^{2+} release profile that was no longer significantly different to wild type ($p = 0.0424$) ($\alpha = 0.01$ after Bonferroni correction). However, while no longer significantly different to wild type, over-expression of FKBP12 did not produce a significant difference to the p.Pro2793Leu variant in the absence of the calstabin ($p = 0.0933$). This discrepency likely arose as a function of the small sample size used ($n = 3$); therefore, further analysis should be performed in the presence of over-expressed FKBP12.

In summary, six variants were incorporated into *RYR1* cDNA via site-directed mutagenesis. Three were cloned into half-length constructs, while one was successfully cloned into the full-length construct. This variant (p.Arg2458Leu), along with two others generated by Dr Anja Scheimann (p.Gly2183Glu, p.Cys2237Tyr) were successfully transfected into a Flp-In™ T-REx™ 293 cell line and were shown to stably express the variant *RYR1*. The localisation of the protein to the endoplasmic reticulum was confirmed and the variants were functionally characterised along with three previously generated variants (p.Phe539Leu, p.Arg1707Cys, p.Pro2793Leu). Of these variants, p.Cys2237Tyr, and p.Pro2793Leu were deemed hypersensitive to 4-c*m*c, with the p.Cys2237Tyr variant being implicated in the disruption of FKBP12 binding.

Chapter 4. Discussion

4.1 Overview

The overall aim of this project was to functionally characterise RyR1 variants associated with malignant hyperthermia. To do this, variants were generated via SDM and full-length *RYR1* cDNA constructs were subsequently produced through a set of sub-cloning steps. The resulting constructs were used to generate cell lines for stable expression of variant RyR1 before being functionally characterised. A myriad of technical difficulties occurred over the course of this project; however, most were resolved, allowing for the functional characterisation of 6 variants, 3 of which were newly generated during this project. While the causes of many errors were not determined, action was taken to allow the progression of the project, the results of which are discussed herein.

4.2 Mutagenesis of RYR1 variants

During initial separation of the SDM products, large molecular weight bands were present that did not move from the wells of the agarose gel (Appendix 1, Fig. 7.1A). It was unknown what these large artifacts were; however, it was noticed that successful amplification of the plasmid resulted in a decrease in their presence. Amplification controls were performed to diagnose this issue. PCRs performed in the absence of enzyme or primers did not produce the large molecular weight bands, indicating that they are a product of amplification and not an artifact of the gel. Confusingly, the large molecular weight bands were also present in the water control with no template DNA, suggesting DNA contamination. To curtail this, new PCR grade water was used for subsequent SDM; however, this had no effect on the presence of the bands, indicating that DNA contamination may have occurred elsewhere.

Over the duration of the mutagenesis stage, multiple SDM reactions were performed until products of equal size to the pBSH+/pBSKO+ vectors were generated. While DNA contamination may be deleterious in other PCR mediated methods, the overlapping design of the primers used for SDM should always result in the product re-circularising, thereby theoretically allowing only successful SDM products to transform bacteria and express the antibiotic selectivity marker. Because of this, SDM samples exhibiting a product of the expected plasmid size were used to transform *E.coli* regardless of the presence of these high molecular weight bands (or non-specific amplification such as the case with variants p.Arg2458Leu, and

p.Arg2676Trp). It should also be noted that the subsequent sequencing of the constructs and purification of both vector backbones and the variant *RYR1* cDNA during the cloning process resulted in only the desired constructs being present in downstream applications.

Another problem that arose during the mutagenesis of variants was the repeated incorporation of the mutagenic primer sequence in both the pBSH+ and pBSKO+ constructs (Appendix I, Fig. 7.1B). Variants p.Arg2458Leu, p.Phe4808Ser, and p.Gly4835Glu each displayed this repeating primer sequence, although the extent of the repetition varied between constructs. Due to the nature of the repeats which seem to occur randomly as both direct repeats of the full primer sequence and as truncated sequences, it was assumed that the polymerase was slipping during the initial stages of amplification, resulting in the random and repeated incorporation of the primer sequence into the newly synthesised DNA. Though this reasoning may not entirely explain this result, polymerase slippage normally occurs at areas of unstable DNA, such as stretches of mono-, di-, or trinucleotide repeats; motifs that are present at the locus at which the primers anneal. Therefore, it may be having an effect on the faithful replication of the plasmid.

The occurrence of the primer repeats in conjunction with the large molecular weight bands seen after electrophoresis highlights pitfalls of the site-directed mutagenesis process used in this experimentation. These pitfalls may have arisen as a consequence of the *RYR1* coding sequence, which has a high GC-content and many regions of mono and dinucleotide repeats. Regardless, selection of alternative colonies after transformation of *E.coli* provided constructs without the primer repeats present which were used for downstream applications.

4.3 Cloning of RYR1 variants

Restriction enzyme-based cloning was performed to generate full-length variant *RYR1* constructs as opposed to other techniques, such as Gibson assembly, or Gateway® recombination. While Gibson assembly is a common and powerful tool for incorporating PCR products into vectors and allows for the incorporation of large fragments into said vectors, a restriction endonuclease-oriented system for cloning of full-length constructs was already established in the laboratory. Therefore, it may have been more laborious to design and test a new system using Gibson assembly which would require a complete re-development of the system in place. Restriction enzyme-based cloning was chosen over Gateway® recombination due to the latter requiring the presence of recombination sites that flank the fragment being cloned. While not dissimilar to restriction enzyme cloning in that the fragment being cloned also must be flanked by specific sites, the restriction sites used for cloning in this case

are a feature of the *RYR1* sequence itself, rather than the Gateway attB1 and attB2 sites used for recombination which must be incorporated into the 5' and 3' end of each fragment. Due to the variants being incorporated in sub-clones of *RYR1*, the incorporation of the recombination sites required for Gateway® recombination would change the *RYR1* cDNA, and therefore the product.

After producing the 6 small *RYR1* constructs, a series of cloning steps was carried out to incorporate the newly generated variants into pcDNA5/FRT/TO© containing full-length *RYR1* cDNA (ftRyR1). The initial stage required cloning of both the pBSH+ and pBSKO+ constructs into the pBSKX+ vector containing the C-terminal half of *RYR1* cDNA, starting at the central KpnI site. Due to pBSH+ and pBSKO+ containing separate sections of *RYR1*, different enzymes were used for the cloning process of each construct. To confirm the desired nucleotide substitution was the only change present after SDM, sequencing of the region between the restriction sites used for cloning was performed on each variant construct (Appendix 1, Fig 7.2-Fig. 7.7). Multiple single nucleotide changes were detected during this process; however, these had no effect on the amino acid sequence of RyR1.

The pBSH+ vector was digested with restriction endonucleases SphI and XbaI, producing 2 fragments that were 3200 bp, and 2049 bp in length. The roughly 2 kb fragment (*RYR1* sequence) was purified after separation via gel electrophoresis. The process of gel purification resulted in a substantial loss of DNA and therefore a total of 4 digestion reactions (1 µg DNA per digest) were conducted and then pooled to generate an adequate concentration of DNA. The pBSKX+ vector was digested with SphI and XbaI resulting in 2 fragments of 9079 bp, and 2113 bp in length (Appendix II, Fig.7.8). The ~9 kb backbone + partial *RYR1* sequence containing fragment was purified in the same process as the pBSH+ insert and the two fragments were ligated together with T4 DNA ligase, overnight at 16°C. During the cloning process, DH5-α *E.coli* were also transformed with ligation products that lack the insert DNA. As the cloning strategy employed during this project was directional, theoretically the vector should not re-ligate as the cohesive ends produced after digestion are incompatible, thus preventing the formation of colonies when plated on LB-agar. This process acts as a control for the activity of the restriction endonucleases as well as the products of the digestion and determines that the cohesive ends are not altered by possible contamination by exonucleases.

The substantial loss of DNA after gel purification can be attributed to several factors including the size of the fragment being purified (larger fragments resulted in greater DNA loss), and the presence of undissolved agarose. While care was taken to ensure complete dissolution of the agarose, it is still possible undissolved agarose was present during purification. According to the manufacturer, undissolved agarose can interfere with DNA purification by clogging the spin column, preventing the elution

of DNA. Larger fragments of *RYR1*/vector backbone were increasingly difficult to purify, being most evident when cloning the pBSKX+ sequence into the full length *RYR1* construct. This may be as a result of the length of time the DNA fragments were incubated with the elution buffer. Fragments over 10 Kb in length require contact with the elution buffer for a minimum of 1 minute for maximal elution of the DNA; a function of the kit which was overlooked during the purification process. Although the gel extraction kit used is capable of purifying fragments between 50 bp and 23 kb, fragments exceeding 11 kb have an estimated 50%-70% recovery rate. During the purification process, the true recovery rate of the ftRyR1 backbone was only ~11%. While this made it difficult to obtain sufficient DNA for cloning of the variant into ftRyR1, enough DNA was eventually purified to perform the ligation.

Cloning of the pBSKO+ construct into pBSKX+ required a triple digestion using restriction endonucleases NsiI, MfeI, and NotI. While digestion with NsiI and MfeI produces the variant containing fragment to be inserted into pBSKX+, digestion with these enzymes alone produces two fragments of indistinguishable sizes (4479 bp, and 4340 bp) when separated on an agarose gel. NotI was therefore chosen to produce a 3rd fragment of 1234 bp in length, thus making the insert (4340 bp) and backbone (3245 bp) distinguishable and thereby allowing purification of the insert (Appendix II, Fig. 7.8). NotI digests the *RYR1* fragment present in pBSKO+ outside of the region between NsiI and MfeI, therefore cloning of the pBSKO+ insert into pBSKX+ using NsiI and MfeI results in no loss of the coding sequence of *RYR1*.

As the sizes of the DNA fragments being cloned increase, so too does the difficulty in successfully producing a complete construct. As a result, while three variants were able to be cloned into the pBSKX+ vector over the course of this project (p.Arg2458Leu, p.Arg2676Trp, p.Gly4835Glu), only 1 was successfully cloned into the full-length construct (p.Arg2458Leu). The generally accepted and supplier recommended method for ligating DNA fragments is to perform the reaction in a solution containing a total DNA mass of 100 ng with a vector:insert molar ratio of 1:3; however, a vector:insert molar ratio of 1:10 was found to be required for cloning of the large pBSKX+ fragment into the full-length construct. As the DNA fragments were so large, the ligation efficiency was diminished, therefore the increased concentration of insert DNA should counteract this decreased efficiency.

While unsuccessful generation of the full length *RYR1* constructs can be a result of the ligation process itself, wherein the larger fragments of DNA make it more difficult for the DNA ligase to find and successfully ligate cohesive ends; a successful ligation may occur but be lost during the transformation process. Bacteria such as DH5-α *E.coli*, although widely accepted as a prime organism for the long-term storage, and growth of plasmid DNA, have their limitations. Indeed, the inverse correlation between plasmid size and transformation efficiency determines that a decrease in the

number of transformants during the end stages of *RYR1* cloning should be expected, as a result of successful ligations being inadvertently discarded[126].

The success of a ligation reaction can be determined by separating the products via gel electrophoresis. Doing this could have provided information as to why the transformations failed which could have been used to further optimise the cloning process. For instance, had the ligation products been electrophoresed, it may have revealed that a vector:insert ratio of 1:3 was adequate in generating sub-clones, and that the main bottleneck experienced during this stage was in fact a function of the transformation efficiency of the *E.coli*, rather than the ligation itself.

Generation of the full-length c.7374 G>T (p.Arg2458Leu) *RYR1* construct was performed by ligating the 8.3 kb fragment produced after KpnI, XbaI double digestion of pBSKX+ to the 12.1 kb fragment of ftRyR1 produced after double digestion with KpnI, and AvrII. AvrII and XbaI digestion produces compatible cohesive ends that can be ligated together; however, this does destroy the AvrII site. The AvrII site present in the ftRyR1 vector is present outside of the *RYR1* cDNA sequence and therefore this disruption should not influence RyR1 structure or function (Appendix V, Fig. 7.19). Cloning in this manner does, however, remove a 1 kb fragment of the ftRyR1 vector backbone, meaning constructs generated via XbaI/KpnI digestion alone contain an extra 1 kb of vector backbone.

Constructs p.Gly2183Glu, and p.Cys2237Tyr were generated by XbaI/KpnI digestion but for consistency each of the full-length constructs should have been produced in an identical manner. The 1kb fragment in question contains an f1 origin of replication, a KS primer sequence, a Simian virus 40 (SV40) origin of replication and a bGH poly(A) signal. While the 1 kb fragment lost does not contain any features of the vector that are essential for replication of the plasmid or expression of RyR1, it was discovered at a later date that it does contain the SV40 promoter utilised for expression of hygromycin resistance (Appendix V, Fig. 7.20). Unfortunately, this was realised too late; however, interestingly this vector still conferred hygromycin resistance onto cells during stable cell line generation, suggesting at least basal expression of the antibiotic resistance gene had occurred.

AvrII digestion of ftRyR1 was chosen over XbaI as the vector contains multiple XbaI sites (Appendix V, Fig.7.19). Therefore, ligation of the insert from pBSKX+ into ftRyR1 would be semi-random, occurring at 3 different loci and as a result producing 3 separate vectors. As AvrII is a unique cutter, ligation of the insert into ftRyR1 would occur at an identical locus in all reactions. While cloning of *RYR1* into ftRyR1 with XbaI would produce 3 slightly varied vectors, transformation of bacteria would theoretically "purify" a single vector as a result of the transformation and subsequent single colony isolation. While this may be the case, the specific isolated vector will

depend on which colony is selected for isolation, therefore producing a library of *RYR1* variants inserted into slightly different vectors. As hygromycin resistance is still conferred using the AvrII cloning strategy and RyR1 expression was successful, it may be more consistent to commit to this method for future generation of *RYR1* variants to standardise the constructs.

Confirmation of each full-length construct was determined by individual restriction digests of each vector with the enzymes BamHI, HindIII, NdeI and NotI. These enzymes were chosen solely because the fragments they produce vary enough in size that they can be easily distinguishable after gel electrophoresis (Appendix II, Table. 5). Wild type ftRyR1 was digested in conjunction with the variant constructs as a reference point to confirm successful ligation of the variant pBSKX+ originated insert into ftRyR1. Each construct produced the expected fragments that were comparable to wild type; however, extra fragments could be seen when digesting the p.Arg2458Leu construct with NotI. These fragments each measured roughly 5 kb and 6 kb in length (Fig. 3.4).

Due to their larger size, but lower staining intensity with exposure to UV light, it was thought that these fragments likely arose due to partial digestion of the vector, as although the fragments are larger, the staining intensity was reduced, implying there is less of the product present. While partial digestions can produce extra fragments, both STAR activity and the binding of enzyme to the substrate (gel-shift effect) can result in extra/unexpected bands being present after gel electrophoresis[127, 128]. While STAR activity and the binding of the enzyme to DNA can both result from a high enzyme to DNA ratio, a partial digestion would likely result from a shortened incubation time, or a low enzyme to DNA ratio. The presence of undigested plasmid DNA in each of the constructs suggests that the enzyme to DNA ratio was too low for complete digestion, implying these extra bands are not a result of STAR activity.

Digestion of each construct with NdeI produced an unexpected band roughly 5 kb in length, although this band is nearly invisible in the p.Gly2183Glu construct. Again, it being both larger, and a lower intensity than the expected fragment at roughly 4 kb suggests that it is the result of a partial digestion. As previously mentioned, cloning of the full-length p.Arg2458Leu was performed in a way that removed 1 kb of vector backbone, inadvertently bringing 2 BamHI sites within 21 bp of one another (Appendix V, Fig. 7.20). As a result, BamHI digestion produces fragments of slightly different sizes compared to the other full-length constructs, with one fragment being too small to see via agarose gel electrophoresis. While the differences in cloning strategies created some complexities, the full-length clones generated all contained the complete coding sequence of *RYR1* and the features of pcDNA5/FRT/TO© required for effective recombination with the Flp-In™ T-REx™ 293 cell line, making them adequate for generating stable cell lines.

4.4 Expression of RYR1

4.4.1 Selecting stable cell lines

While incorporation of the FRT site into the host cell genome during the generation of the Flp-In™ cell line is random, once incorporated, monoclonal cell lines with the gene of interest (GOI) at the same locus can be selected for further use. After a Flp-In™ cell line has been generated, incorporation of the GOI becomes rapid and efficient and allows for the generation of isogenic cell lines that stably express the GOI. Although other techniques, such as viral transduction are commonly used, the incorporation of the gene of interest is random and varies between transformants, thus increasing the potential for deleterious effects on cell function, such as the disruption of genes integral to the cell cycle.

Using the Flp-In™ system allows each variant to be incorporated at the same locus, minimising positional effects on expression. Fortunately, a Flp-In™ 293 cell line had previously been generated, therefore, transfection of the GOI was the only step required. Transfection of the Flp-In™ T-REx™ cell line with pcDNA5/FRT/TO/CAT© can be performed in conjunction with transfections with the GOI as a positive control. This positive control vector contains chloramphenicol acetyl transferase (CAT) which can be expressed in an inducible manner at the same genomic loci of the GOI. Used primarily to compare protein expression between different cell lines, it was decided this control was not required, as protein expression was compared via immunoblot analysis of RyR1 itself rather than through CAT activity.

Three cell lines stably expressing variant RyR1 were generated over the course of this project using the Flp-In™ system: p.Gly2183Glu, p.Cys2237Tyr and p.Arg2458Leu. After transfection, monoclonal recombinants were selected and their relative expression of RyR1 was measured before further analysis was performed. While each clone should theoretically express RyR1 equally, immunoblot analysis showed the p.Cys2237Tyr and p.Arg2458Leu clones each appeared to have varied expression. This variation was likely due to inconsistencies in the immunoblot process, such as an insufficient transfer of the protein to the PVDF membrane. Regardless, to minimise any limiting factors, the difference in expression seen between the clones was treated as a product of the transfection, and therefore the clones that appeared to express RyR1 most abundantly were chosen for further analysis. Clones p.Gly2183Glu_3, and p.Arg2458Leu_4 were chosen to propagate the cell lines for the respective variants, while the p.Cys2237Tyr_2 clone was chosen for downstream applications. Unfortunately, during initial immunoblot analysis, the p.Cys2237Tyr_1 clone displayed less expression than the p.Cys2237Tyr_2 clone (Appendix III, Fig. 7.11), leading to the first clone being discarded prematurely,

therefore all experimentation of the p.Cys2237Tyr cell line was performed on the p.Cys2237Tyr_2 clone despite appearing to express less RyR1. This should not have impacted the functional analysis as fluorescence data collected from functional assays were normalised to account for differences in expression as outlined in chapter 2.2.4.1

4.4.2 Expression of RYR1 and co-localisation to the endoplasmic reticulum.

All cell lines were shown to express RyR1 in a comparable manner, except for the cell line p.Pro2793Leu, which displayed substantially reduced expression of the transgene. The cell lines: p.Phe539Leu and p.Arg1707Cys also displayed reduced expression of RyR1, although to a lesser extent. Interestingly, the diminished expression of the p.Arg1707Cys and p.Pro2793Leu variants aligned with a previous student's analysis of the same cell lines.

The immunoblots depicted in Fig.3.6 differ from that in Fig.3.5 in two key ways. The first being an apparent reduction of RyR1 expression despite both blots using identical protein extracts; the second is observed in Fig.3.6B wherein the bands corresponding to α-tubulin display a distinct "wavy" pattern. It is important to recognise that immunoblot analysis is an intricate technique, wherein small changes to parameters can have substantial effects on protein visualisation. Such parameters range from the relatively simple, such as the quality of the antibodies and/or ECL substrate used (both of which depreciate over time), to the more complex. These include the conditions in which the polyacrylamide gel sets and the components of the buffers used for both the electrophoresis of protein extracts, and the transfer of the protein to a PVDF membrane.

As previously mentioned RyR1 is comprised of 4 identical 565 kDa subunits; subsequently, transfer of the channel protein from a polyacrylamide gel to a PVDF membrane is less efficient than smaller proteins such as α-tubulin[129]. Therefore, the size of RyR1 may be preventing its successful transfer to the membrane. The apparent reduction in RyR1 expression is likely a result of this in conjunction with the transfer buffer used. Methanol (10%) is often added to the Tris-Glycine buffer commonly used for transfer of protein to PVDF membranes as it aids in protein adsorption. Importantly, the buffer used to transfer the protein extracts to the PVDF membrane in Fig.3.6 did not contain methanol, and while this had no observable effect on the transfer of α-tubulin (Fig. 3.6), the absense of methanol likely effected the transfer of the substantially larger RyR1.

A distinct "wavy" pattern of the bands corresponding to α-tubulin were observed in Fig.3.6B. This may also be due to an inadequate transfer; however, it is more likely a result of the gel in which the protein was resolved during SDS-PAGE, as the transfer parameters were identical between Fig. 3.6A and Fig. 3.6B.

The pH of the gels as well as the temperature and duration in which they set all effect the correct formation of the acrylamide matrix through which the samples migrate. Because of this, any changes to these parameters can result in an inconsistent matrix, resulting in the non-uniform resolution of proteins. Changes like these would logically effect smaller proteins such as α-tubulin more as they migrate faster during electrophoresis.

While polyacrylamide gels solidify within 30 minutes to one hour, it is recommended that the gels be left at room temperature overnight as the matrix is still forming over this time period[130]. Electrophoresis of the protein visualised in Fig. 3.6B was performed using an acrylamide gel that had not been allocated this time to properly set; therefore, it may be that the samples migrated through an inconsistent gel matrix, resulting in the α-tubulin resolving non-uniformly.

It should be noted that a high concentration of salts in the protein extracts themselves can also effect the migration of protein through an acrylamide matrix[131]. It is, however, more probable that the cause of the non-uniform resolution of the α-tubulin bands is a result of the polyacrylamide gel, rather than the samples, as identical extracts from cell lines p.Gly2183Glu, p.Cys2237Tyr, and p.Arg2458Leu were used in Fig. 3.5, in which this "wavy" pattern was not observed. Immunoblot analysis of RyR1 resulted in a third observation, which was of doublet bands representing the Ca^{2+} channel (Fig. 3.5, Fig. 3.6A). This phenomenon is apparent in multiple blots from separate laboratories and is generally accepted as a feature of RyR1 immunoblots[121-123].

The manufacturer of the α-RyR1 antibody used during this project states that doublets occur in non-mammalian vertebrate extracts as it can not distinguish between the organisms α- and β-isoforms. However, it has been observed that the same antibody also cannot distinguish between the mammalian type 1 and type 3 isoforms[123]. It may therefore be possible that the immunoblot is detecting endogenous expression of RyR3; however, the bands observed in Fig. 3.5 and Fig. 3.6 appear to be of equal intensity. Therefore, this reasoning is predicated on the implication that cells are expressing endogenous RyR3 to the same extent as the over-expressed RyR1; an unlikely occurrence. Fig.3.6 also displays triplet bands at the ~565 kDa location, which, following this logic would suggest the antibody is interacting with more than just two isoforms. Instead, it is more likely that the multiple bands displayed in Fig. 3.5 and Fig. 3.6 arise as a result of extensive post-translational modification to the Ca^{2+} channel, or partial degradation of the protein upon storage.

As a monoclonal Flp-In™ cell line was used for transfection of each construct, all cell lines examined over the course of this project should have the *RYR1* cDNA incorporated at an identical locus of the host cell genome, making differences in expression an unlikely occurrence. Importantly, bands corresponding to α-tubulin appear to be equal in intensity across each cell line (Fig. 3.6). This would suggest the variation in RyR1 band intensity is a function of its expression, rather than overall protein synthesis in the cell lines. It also indicates that an equal mass of protein in respect to each variant was separated via SDS-PAGE, though not necessarily transferred to the PVDF membrane. While the molecular weight of a protein, along with its hydrophobicity are determining factors in its transfer to a PVDF membrane, it is unlikely that the reduced expression of RyR1 seen in the p.Arg1707Cys, and p.Pro2793Leu protein extracts is due to such phenomena. Indeed, reduced RyR1 expression in these cell lines is a perpetual occurrence spanning multiple projects, indicating a mechanism that may be intrinsic to the variants themselves.

A previous student's initial attempts to produce a cell line stably expressing the p.Arg1707Cys variant resulted in no visible RyR1 expression in immunoblot analysis. However, a transient transfection of a HEK293 cell line with the same ftRyR1 (p.Arg1707Cys) vector did result in detectable expression of RyR1. It may be that the integration of the GOI such as the c.5119 C>T (p.Arg1707Cys) variant at the FRT loci in the Flp-In™ T-REx™ 293 cell line has an unknown effect on expression. As a result of the repetitive nature of the *RYR1* sequence, there is a possibility that during homologous recombination, the *RYR1* cDNA is being altered, and shifting the sequence into an alternative reading frame, producing an unstable product that is subsequently degraded[132, 133]. RT-qPCR of the host cell transcriptome may therefore elucidate the reason for the reduced expression in these cell lines by quantifying the cell's production of mRNA. Importantly, successful transfections of each cell line were confirmed through PCR of genomic DNA using primers that flank the variant locus. As a result, any affects to the cDNA at the FRT site remains unknown.

No discernible difference in RyR1 expression could be seen between the cell lines during confocal microscopy for immunolocalisation. Each cell line displayed expression of RyR1 which was shown to co-localise with PDI at the endoplasmic reticulum, indicating that RyR1 is being deposited in the endoplasmic reticulum membrane. The discrepency between the results of the immunoblot and immunofluorescence assays may be a result of differences in the visualisation process itself. Visualisation of RyR1 via immunoblot analysis was performed via chemiluminescence, using a horse-radish peroxidase (HRP) conjugated secondary antibody at a substantially lower dilution than the FITC fluorophore-conjugated secondary antibody used for detection of RyR1 during the immunofluorescence assay.

Also, while HRP produces light via enzymatic cleavage of its substrate, the FITC fluorophore produces light via fluorescence, a process wherein light is emitted after excitation at a specific wavelength. It is important to recognise that the concentrations of each secondary antibody, the mechanism through which each antibody produces light, and the mode of detection all vary greatly between immunoblot and immunofluorescence analysis, making direct comparison of the results from each assay impractical.

While the results are not directly comparable, one would expect that cell lines that showed more abundant expression of RyR1 in the immunoblot to also exhibit increased expression of the transgene in the immunostain; however, this does not occur. It may be that the over-expression of the recombinant protein is encountering a bottleneck event wherein the ER is unable to accommodate the increased expression of RyR1. Also, considering the immense size of RyR1, and its targeting to the ER/SR membrane, it is possible that the over-expression of the Ca^{2+} channel is activating the eukaryotic unfolded protein response (UPR).

The UPR is an adaptive cellular mechanism designed to monitor protein folding within the ER. Importantly, while this response is induced during incidences of ER stress such as the accumulation of unfolded proteins, increased expression of membrane bound proteins such as RyR1 has also been observed to incite the response[134]. It is therefore possible that over-expression of the membrane bound Ca^{2+} channel may increase ER stress, priming the cell lines susceptibility to the UPR. If, in this case, the p.Pro2793Leu substitution results in the misfolding of RyR1, the increase in ER stress may subsequently trigger the UPR in this cell line[135].

The defining feature of the UPR is an upregulation of protein chaperone synthesis; therefore, the apparent equal expression of RyR1 seen in the immunostain may be a result of increased protein deposition to the endoplasmic reticulum membrane[135]. This would still allow for the variation in RyR1 expression seen in the immunoblot, as protein expression remains the same; however, deposition of RyR1 to the ER membrane in cell lines that have triggered the UPR would increase, resulting in an apparent equal expression of the transgene. It should be noted that while functional analysis was performed in uninduced cell lines, co-localisation of RyR1 to the endoplasmic reticulum was confirmed in induced cells. This was not seen as an issue as co-localisation is a function of properties intrinsic to the protein as well as the chaperones that aid its deposition; therefore, any effects on co-localisation to the ER membrane should be a result of the variant itself and not its induction status.

During expression analysis, it was also found that the uninduced p.Phe539Leu cell line produced visible RyR1, albeit to a lower extent than in the induced cell line. When analysing transgenes in heterologous systems, it remains unknown where the

integration of the gene within the host cell genome takes place. Although, the Flp-In™ system allows for the incorporation of transgenes at identical loci, it does so via homologous recombination at a transgenic FRT site which is incorporated randomly into the host cell genome. It is therefore possible that the *RYR1* cDNA is incorporated at a transcriptionally active locus; an event that is likely to result in the basal expression seen in the uninduced cell lines. While expression of RyR1 in other uninduced cell lines could not be detected, it was assumed that basal expression in all cell lines was occurring, an assumption that was supported by the results of the functional analyses described in chapter 3.3. The discrepancies seen between the expression levels of p.Pro2793Leu and other cell lines, as well as between each of the uninduced cell lines highlights possible pitfalls of the Flp-In™ system which may influence functional analysis of transgenes. As previously mentioned, representing fluorescence data gathered during functional analysis as a percentage of the fluorescence measured at the maximum concentration of 4-c*m*c (1000 µM) normalises the data and thereby resolves the discrepancies seen in protein expression between the cell lines.

4.5 Functional analysis of RYR1 variants

During the course of this project, the functional characterisation of RyR1 variants proved to be challenging, with many technical difficulties occurring along the way. Initial attempts to analyse the function of these variants were complicated by observations that induced Ca^{2+} release was sustained rather than transient. A result like this implies that the Ca^{2+} release measured isn't indicative of the function of RyR1 for multiple reasons. The first being the implication that Ca^{2+} stores within the ER are not being replenished, as the fluorescence data indicates cytosolic [Ca^{2+}] is not diminishing. Secondly, fura2-AM, the fluorescent dye used to measure [Ca^{2+}], detects Ca^{2+} in a ratiometric fashion via excitation at two wavelengths corresponding to unbound and bound Ca^{2+}. Therefore, it would be expected that the ratio of fluorescence detected would decrease over time as more Ca^{2+} binds to fura2, an occurrence that was not initially observed. This problem was resolved by preparing a new solution of 4-c*m*c after it was found that the solution used in initial experimentation had produced a precipitate. This precipitate was likely interfering with light detection hence the sustained Ca^{2+} release observed was likely to be an artifact.

The replacement of the 4-c*m*c, however, did not resolve the most crucial technical issue that occurred. That being each of the RyR1 variants except p.Arg1707Cys exhibited a hypersensitive reaction to the agonist, including the hypersensitive (p.Thr4826Ile) and negative controls (wild type) which were indistinguishable from

one another. Many attempts to resolve this issue were conducted in vain, including sequencing of the wild type cell line for known variants to rule out possible contamination, of which there were none. Ratiometric analyses of the fluorescence data were also re-conducted with a focus on a more inclusive region of interest (ROI). The ROI at which initial analyses were conducted comprised single cells. It was found during functional analysis that not all cells release Ca^{2+} equally, therefore, defining ROIs on single cells can introduce a bias by only measuring regions at which there was substantial fluorescence, and thus not being representative of the cell line as a whole. This was resolved by defining an ROI that comprised the microscopes complete field of view, thus accounting for variation in fluorescence. Other variants previously shown to behave in a fashion indicative of wild type RyR1 were also functionally characterised by a summer student, and these too produced a hypersensitive reaction. As each variant continued to exhibit a hypersensitive response to 4-c*m*c, the problem may not have been intrinsic to the cell lines, but rather the detection method itself.

Functional characterisation of RyR1 variants has been carried out in multiple projects spanning many years within the research group, with the only difference between this project and previous projects being that the detection of fluorescence was performed on a new camera/wavelength switcher system with different software. It appeared that the new system was substantially more sensitive than its predecessor, thus the over-expression of RyR1 produced a Ca^{2+} release profile which appeared to over-saturate the new system. This over-saturation would, in-turn, mimic a hypersensitive channel as the system is unable to discern any difference between the fluorescence observed at the lowest and highest concentrations of 4-c*m*c. Importantly, tetracycline inducible systems have been widely observed to result in basal expression of transgenes, an occurrence exhibited in the uninduced p.Phe539Leu cell line (Fig. 3.6)[136, 137]. As a potential solution, functional analyses were performed on uninduced cell lines which resulted in the detected Ca^{2+} release by the well-established positive control p.Thr4826Ile variant and wild type RyR1 being significantly different from one another. It should be noted that while basal expression was shown, not inducing the cells with tetracycline abrogates control over expression, meaning that each cell line may express varying amounts of RyR1. It is therefore important to account for this during data analysis such as by normalising the data as previously outlined.

Of the 6 variants functionally characterised, 2 were shown to result in a hypersensitive channel. The p.Cys2237Tyr and p.Pro2793Leu variants were each characterised by an EC_{50} of 128.66 µM 4-c*m*c ± 13.37 and 218.97 µM 4-c*m*c ± 17.67 respectively compared to wild type that displayed an EC_{50} of 377.1 µM 4-c*m*c ± 31.73. The significant difference seen between these variants and wild type RyR1, is consistent

with a gain of function effect indicative of MH susceptibility. After functional characterisation an analysis of these variants according to the Variant Curation Expert Panel's (VCEP) guidelines[138] classified the p.Cys2237Tyr variant as likely pathogenic for MH (PS4 supporting, PM1, PP3 moderate, PS3 moderate), while the significance of the p.Pro2793Leu variant remains unknown (PS4 supporting, PP3 moderate, PS3 moderate). Upgrading the p.Cys2237Tyr classification to pathogenic would require further functional characterisation in a knock-in mouse system and/or additional segregation analysis in multiple families[138].

Interestingly, the variant p.Arg1707Cys displayed a significant decrease in channel activity compared to wild type, with an EC_{50} of 621.55 µM 4-c*mc* ± 29.50. While this loss of function is consistent with the myopathy phenotype of the proband in which the variant was identified, it is inconsistent with the diagnostic requirements for MHS, that being a gain of function effect on RyR1 activity. It should be noted that the proband carried two variants, those being p.Arg1707Cys and p.Val4849Ile. One variant being inherited from each of the parents. The p.Val4849Ile variant is regarded as pathogenic by the EMHG; however, neither parent who carried these variants displayed any myopathies, suggesting the p.Arg1707Cys associated myopathy actually may arise from the presence of both variants[100].

4.6. VCEP classification of RYR1 variants

Table 4.1 VCEP classifications

	Prevalence	Functional data	Segregation	Bioinformatic prediction	Grantham score	Mutational hot-spot	Points	Classification	Reference
p.Cys2237Tyr	PS4_Moderateg, two families, 2 points	PS3_Moderate, Functional data hypersensitive		PP3_Moderate, REVEL>0.85, 2 points		PM1, central, 2 points	8	LP	PMID:24433488, and Unpublished, or this study
p.Pro2793Leu	PS4_Supporting, One family, 1 point	PS3_Moderate, Functional data hypersensitive. 2 points					3	VUS	Unpublished, or this study
p.Phe539Leu	PS4_Moderate, Two unrelated families, 2 points	BS3_supporting, functional data as wild-type , -1 point		PP3_Moderate, REVEL>0.85, 2 points		PM1, N-terminal, 2 points	5	VUS	PMID:30236257, and unpublished or this study
p.Arg1707Cys	None, only associates with CCD	BS3_supporting, functional data as wild-type , -1 point					0	VUS	Unpublished, or this study
p.Arg2458Leu	PS4_Supporting, One family, 1 point	BS3_supporting, functional data as wild-type , -1 point		PP3_Moderate,REVEL>0.85, 2 points	PM5, p.(Arg2458His) is pathogenic, 2 points	PM1, central, 2 points	7	LP	PMID:21965348, PMID:30236257 and Unpublished, or this study

Table 4.2 VCEP classifications continued

	Prevalence	Functional data	Segregation	Bioinformatic prediction	Grantham score	Mutational hot-spot	Points	Classification	Reference
p.Gly2183Glu	PS4_Supporting, One family, 1 point	BS3_supporting, functional data as wild-type , -1 point				PM1, central, 2 points	2	VUS	PMID:25735680
p.Val2627Met	PS4_Strong, Eight unrelated families, 4 points						4	VUS	PMID:30236257, and unpublished or this study
p.Arg2676Trp	PS4_Strong, Eight unrelated families, 4 points		PP1_Strong, Segregates in 10 individuals in one family, 4 points				8	LP	PMID:30236257, PMID:16163667, PMID:19191329, PMID:25960145, PMID:21157159, and unpublished or this study

Table 4.3 VCEP classifications continued

	Prevalence	Functional data	Segregation	Bioinformatic prediction	Grantham score	Mutational hot-spot	Points	Classification	Reference
p.Arg3348His	PS4_Supporting, One family, 1 point						1	VUS	PMID:15731587, PMID:25735680
p.Phe4808Ser	PS4_Supporting, One family, 1 point			PP3_Moderate,REVEL>0.85, 2 points			3	VUS	Unpublished or this study
p.Gly4835Gly	PS4_Supporting, One family, 1 point			PP3_Moderate,REVEL>0.85, 2 points		PM1, C-term hotspot, 1 point	4	VUS	Unpublished or this study

4.7 Structure/function relationships of variants

4.7.1 p.Phe539Leu RYR1

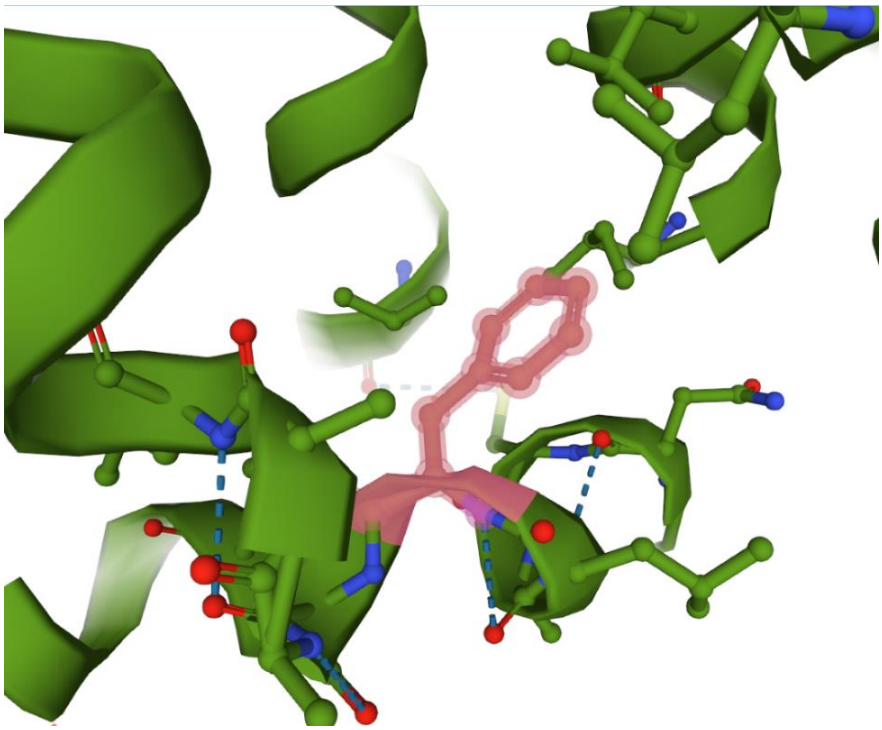

Figure 4.1. RyR1 protein structure (Phe539)

Wild type RyR1 protein structure showing the Phe539 residue highlighted in red. Oxygen depicted in red, nitrogen depicted in blue. Hydrogen bonds depicted in dotted blue lines. Structure retrieved from Protein data bank (https://www.rcsb.org/structure/5TAZ). Protein code: 5TAZ.

The p.Phe539Leu variant was shown to result in a hypersensitive channel in a previous project; however, that result was not reproduced over the course of this project. Instead, with an EC_{50} of 304.82 µM 4-c*m*c ± 18.12, the p.Phe539Leu variant was shown to behave like wild type. This observation is consistent with the presence of hydrophobic side chains that make phenylalanine and leucine of similar structure and biochemical properties. Before performing functional analysis in this project, sequencing of genomic DNA revealed that the cell line actually contained the p.Pro2793Leu variant. Due to the p.Pro2793Leu variant confering hypersensitivity onto the RyR1 channel, along with the previous student's diagnostic restriction digest of the p.Phe539Leu construct, it was determined that during the previous project, the p.Pro2739Leu cell line was mislabelled as p.Phe539Leu. Therefore the results generated from the new p.Phe539Leu cell line used in this project are novel and the data outlined should be regarded as characteristic for this variant.

4.7.2 p.Arg1707Cys

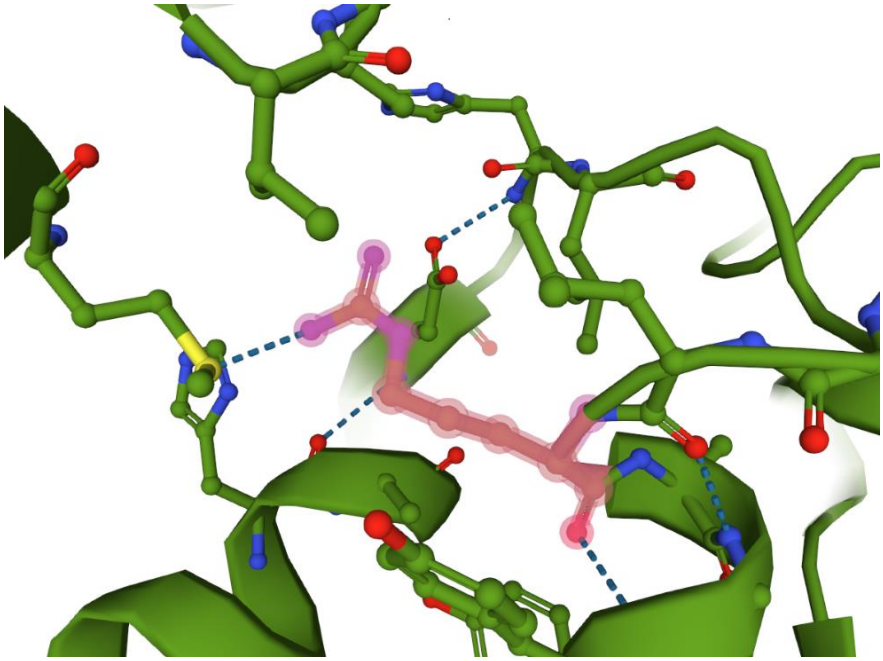

Figure 4.2. RyR1 protein structure (Arg1707)

Wild type RyR1 protein structure showing the Arg1707 residue highlighted in red. Oxygen depicted in red, nitrogen depicted in blue, sulfur depicted in yellow. Hydrogen bonds depicted in dotted blue lines. Structure retrieved from Protein data bank (https://www.rcsb.org/structure/5TAZ). Protein code: 5TAZ.

The Arg1707 residue resides in a turn structure connecting two α-helices located near a putative FKBP12 binding site[61]. It forms a single hydrogen bond with the sulfur containing R-group of Met1637 via its amino group as well as 2 more hydrogen bonds with the side chain of Asp1700. Due to the p.Arg1707Cys substitution residing in proximity to the putative FKBP12 binding site, it is possible the amino acid change may stabilise the channel in its closed state, essentially mimicking the binding of FKBP12 to RyR1. However, if this were true one would expect Ca^{2+} release to be similar to that seen in the wild type cell line when the calstabin is over-expressed. While the p.Arg1707Cys substitution may not identically mimic the effects of FKBP12 binding, its reduced Ca^{2+} release and proximity to a site fundamental to the stabilisation of the closed state of RyR1 implies that the residue may play an integral role in stabilisation/maintainance of the closed state of the channel.

4.7.3 p.Gly2183Glu RYR1

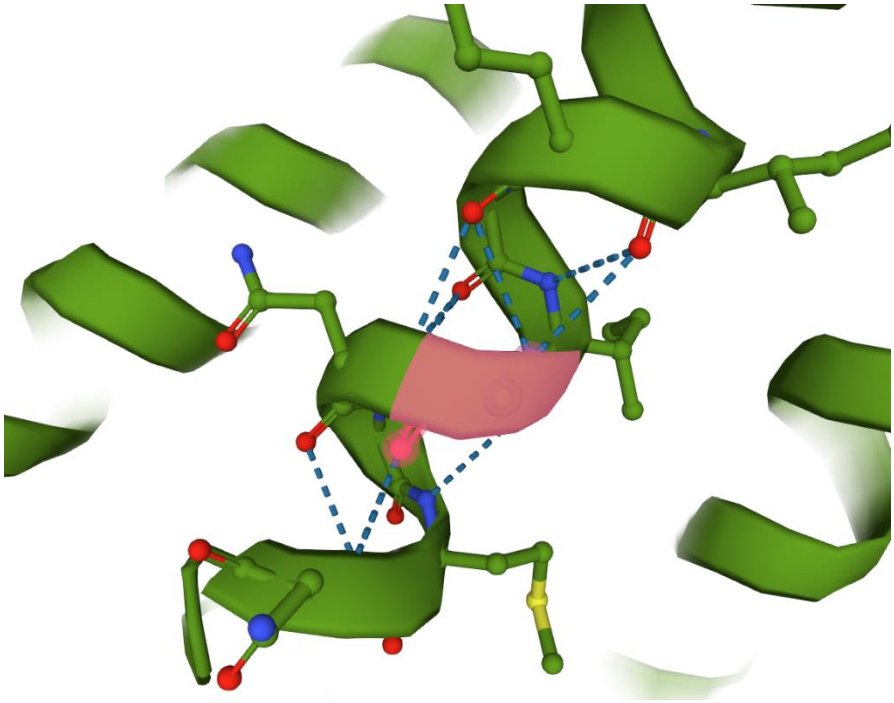

Figure 4.3. RyR1 protein structure (Gly2183)

Wild type RyR1 protein structure showing the Gly2183 residue highlighted in red. Oxygen depicted in red, nitrogen depicted in blue, sulfur depicted in yellow. Hydrogen bonds depicted in dotted blue lines. Structure retrieved from Protein data bank (https://www.rcsb.org/structure/5TAZ). Protein code: 5TAZ.

Residue Gly2183 is also part of an α-helix located near a putative FKBP12 binding site[61]. It forms two hydrogen bonds via its backbone amino group to the backbone carbonyl groups of residues Ile2179 and Gln2180. One would expect that a substitution of two substantially different amino acids such as glycine for glutamic acid would alter the proteins structure, and therefore function; however, the substitution does not confer hypersensitivity to 4-c*m*c on RyR1 in the experimental system used. While glycine and glutamic acid are substantially different, the structural integrity of the protein likely remains the same, as the hydrogen bonds within the α-helix of which Gly2183 resides are formed between the backbone amino and carbonyl groups of the amino acid, rather than the R-group, which protrudes out from the α-helix. The location of the residue also makes its side chain unlikely to interact with other R-groups, thus the substitution would likely not result in a substantial change to the protein structure/function.

4.7.4 p.Cys2237Tyr RYR1

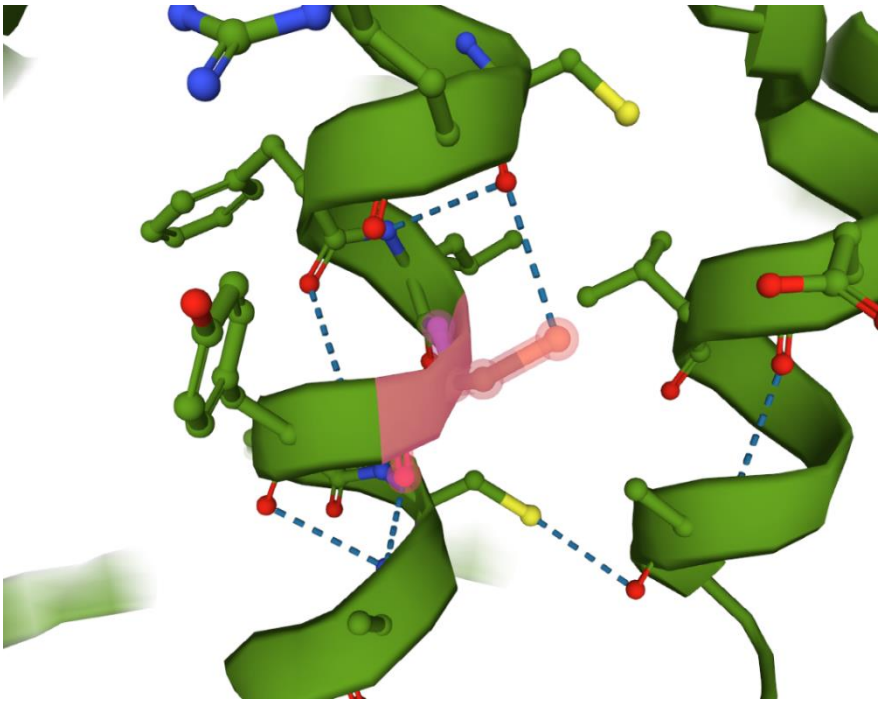

Figure 4.4. RyR1 protein structure (Cys2237)

Wild type RyR1 protein structure showing the Cys2237 residue highlighted in red. Oxygen depicted in red, nitrogen depicted in blue, sulfur depicted in yellow. Hydrogen bonds depicted in dotted blue lines. Structure retrieved from Protein data bank (https://www.rcsb.org/structure/5TAZ). Protein code: 5TAZ.

The Cys2237 residue resides in an α-helix closer in proximity to the putative FKBP12 binding site than Gly2183[61]. It forms many bonds with the surrounding residues including two hydrogen bonds between the backbone amino groups and the backbone carbonyl groups of Cys2233 and Arg2234. The backbone carbonyl group of Cys2237 also forms 2 hydrogen bonds with the backbone amino groups of Cys2240 and Arg2241. These interactions generate and stabilise the α-helix structure in which the residues reside. While the secondary structure of a protein is determined by interactions of the peptide backbone, the α-helix structure is also heavily dependent on the steric conformation of the amino acids, including the R-group. Large R-groups such as in tryptophan, phenylalanine and tyrosine can destabilise α-helices due to steric hindrance between surrounding amino acids[139, 140]. The proximity of the Cys2237 residue to the large R-group containing residues Phe2235, Arg2234, Tyr2238 and Phe2239 may therefore provide an environment in which a p.Cys2237Tyr substitution destablises the protein structure and thereby confers hypersensitivity to 4-c*m*c on RyR1.

It is also possible that, while at physiological pH tyrosine is protonated ($Pka_2 = 10.46$), the high electronegativity of oxygen in combination with the aromatic ring it is attached to will produce a partial positive charge at the end of the R-group. Weak interactions may therefore arise between this partial charge and the deprotonated side chain of the nearby Asp2274 (Pka_2 3.9), which may influence the functionality of RyR1. Of course, without solving the crystal structure of the mutant RyR1, the precise mechanism through which hypersensitivity is confered will remain as speculative.

4.7.5 p.Arg2458Leu RYR1

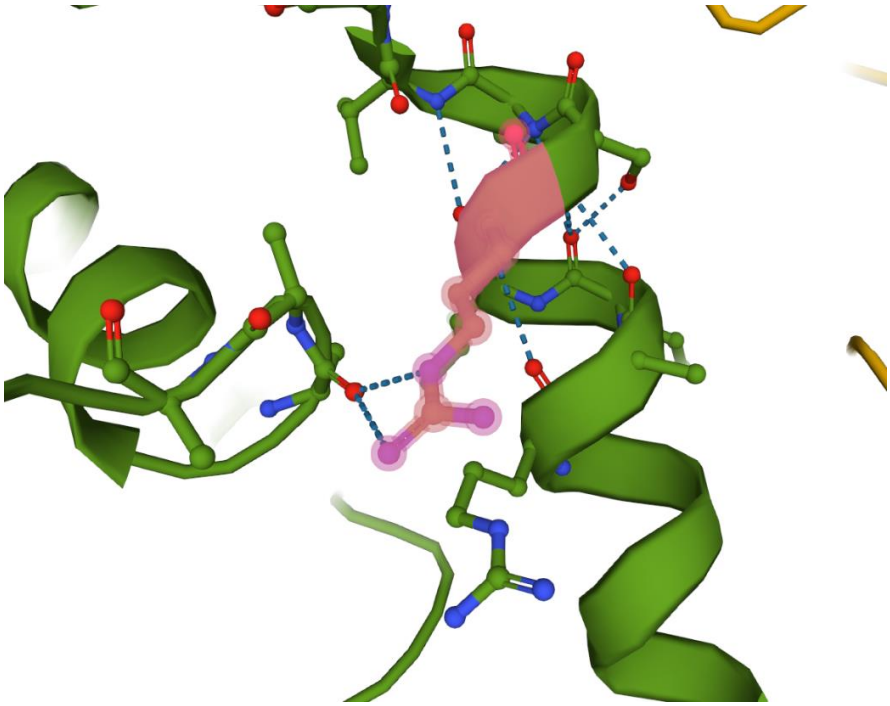

Figure 4.5. RyR1 protein structure (Arg2458)

Wild type RyR1 protein structure showing the Arg2458 residue highlighted in red. Oxygen depicted in red, nitrogen depicted in blue. Hydrogen bonds depicted in dotted blue lines. Structure retrieved from Protein data bank (https://www.rcsb.org/structure/5TAZ). Protein code: 5TAZ.

The Ca^{2+} release mediated by the p.Arg2458Leu variant was indicative of wild type functionality. This was unexpected, as other substitutions of this residue have resulted in a hypersensitive channel, including p.Arg2458His and p.Arg2458Cys[124, 125]. Although cysteine possesses a polar sufhydryl group on its side chain, the amino acid has been shown to behave in a hydrophobic manner[141]. As a result, one might expect that substituting the same arginine residue for leucine, a true hydrophobic amino acid,

would result in a similar effect on protein function; however, that is not what is seen here. Similarly, arginine and histidine are both positively charged amino acids with only slight differences between the R-groups. Because of this, the finding that a p.Arg2458His substitution results in a hypersensitive channel suggests that the residue plays an important role in RyR1 activity, as relatively slight changes in biochemical properties have significant effects on protein function.

The Arg2458 residue forms hydrogen bonds with Val2509 via the amino group of the arginine side chain and the backbone carbonyl group of the valine. One might expect the abrogation of this interaction with the p.Arg2458Leu substitution may have a larger effect on protein function than p.Arg2458His, and result in a hypersensitive channel as well; however, this was not the case.

While the data shows that the p.Arg2458Leu substitution does not result in a hypersensitive channel, it is possible that the discrepency seen between these substitutions may be the product of variations in protocols. It should be noted that although the p.Arg2458Cys substitution was found to be hypersensitive in the same heterologous system used in this project (HEK293 cells), caffeine and halothane were used to induce Ca^{2+} release as opposed to 4-c*m*c[124]. While each act as RyR1 agonists, the Ca^{2+} release profile produced varies between them which may result in the discrepancies seen between these results. In a similar manner, the results of the p.Arg2458His substitution may vary to the p.Arg2458Leu substitution as although 4-c*m*c was used in both experiments, the variant was characterised in myotubes, thus there may be limiting factors within HEK293 cells that are not present in their experimentation which causes this discrepency; such as proteins expressed in myotubes being absent in HEK293 cells[125].

4.7.6 p.Pro2793Leu RYR1

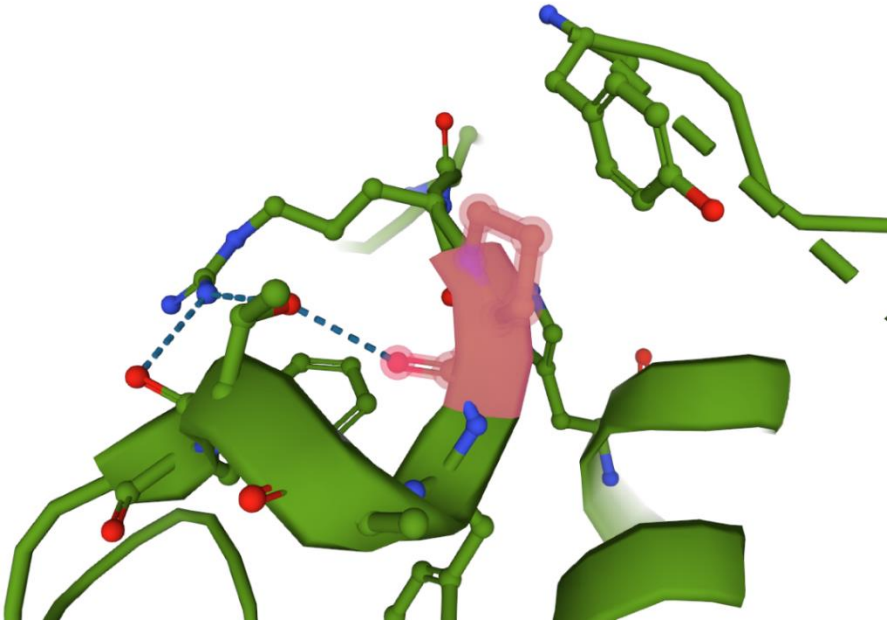

Figure 4.6. RyR1 protein structure (Pro2793)

Wild type RyR1 protein structure showing the Pro2793 residue highlighted in red. Oxygen depicted in red, nitrogen depicted in blue. Hydrogen bonds depicted in dotted blue lines. Structure retrieved from Protein data bank (https://www.rcsb.org/structure/5TAZ). Protein code: 5TAZ.

Proline has a pKa_2 of 10.60 therefore it is deprotonated *in vivo*. The deprotonation of the amino group and its interactions with its side chain produces a unique ring structure that confers special properties onto the amino acid. Indeed, these properties result in proline residues being heavily implicated in protein folding via their "kinking" of α-helices[142]. This may therefore provide an explanation for the small α-helix structure in which the Pro2793 residue resides. A p.Pro2793Leu substitution confers hypersensitivity to 4-c*m*c onto RyR1 indicating that this residue plays an important role in protein function. Such a result was expected as changing the relatively small, kink-inducing proline for a substantially larger amino acid such as leucine has the propensity to destabilise the protein structure.

While the residue does not interact with nearby side-chains, properties intrinsic to the amino acids themselves such as their size and polarity also effect protein folding. Therefore, while the R-group of leucine does not have the capacity to form bonds with proximal amino acids, the substantial change in properties of the residue at position 2793 may be altering the secondary structure of RyR1.

While leucine is hydrophobic, the p.Pro2793Leu substitution does not result in the formation of a hydrophobic pocket, therefore affinity to water likely has a minimal effect on the structure of this region. However, the change in protein function may be a result of the relative size of leucine. Pro2793 resides within a pocket of amino acids with substantially large R-groups such as arginine, tyrosine and lysine. Therefore, the p.Pro2793Leu substitution may produce a string of residues that may induce steric hindrance that destabilises the α-helix, and as a result imparts hypersensitivity to 4-c*m*c onto RyR1.

4.8 Effects of FKBP12 on RyR1 function

Although it is well documented that FKBP12 interacts with RyR1, the discordance in the literature about the consequences of this interaction highlights a large gap in knowledge yet to be filled. Due to the proximity of three of the RyR1 variants to a putative binding site for FKBP12, functional analysis of these variants was carried out in the presence of over-expressed FKBP12 as a means to further elucidate the generally accepted notion that the calstabin stabilises the closed state of RyR1[37]. The p.Thr4826Ile substitution was analysed here as a positive control as Thr4826 is located near the pore region of RyR1. This distal location of the residue to the putative FKBP12 binding site should therefore limit any effects of the substitution on the activity of the calstabin.

As expected, the p.Thr4826Ile cell line exhibited a decrease in sensitivity to 4-c*m*c in the presence of FKBP12, as indicated by the increased EC_{50} (Appendix IV, Table. 11), suggesting that binding of the calstabin may revert a hypersensitive channel back to wild type functionality[30]. Although this effect was not evident in the fitted curve (Fig. 3.15), the hypersensitivity of each variant was calculated by producing a fitted curve of the individual Ca^{2+} release assays, then averaging the EC_{50} of each experiment.

While the p.Phe539Leu variant did not produce a hypersensitive channel, over-expression of FKBP12 did result in a higher EC_{50}, suggesting further stabilisation of the channel; however, this was not deemed significant after a Bonferroni correction for multiple tests ($p = 0.0217$, $\alpha = 0.01$). Importantly, over-expression of the calstabin in each of the hypersensitive cell lines resulted in a return to wild type functionality except for the p.Cys2237Tyr cell line which remained hypersensitive.

Unlike p.Thr4826Ile, p.Pro2793Leu is closer in proximity to the putative FKBP12 binding site and therefore may have an effect on FKBP12 binding/function; however, over-expression of the calstabin resulted in a return of this variant to wild-type functionality (Fig.3.20)[61]. This may suggest that the Pro2793 residue is not integral

to FKBP12 binding. The most interesting results were observed for the p.Cys2237Tyr cell line. Over-expression of FKBP12 had no effect on the hypersensitive Ca^{2+} release characteristic of this variant. As over-expression of the calstabin was observed to revert the hypersensitive p.Thr4826Ile variant to wild type functionality, it is plausible that the Cys2237 residue of RyR1 may be integral for FKBP12 binding as substitution of the residue abrogates its function. However, the location of Cys2237 likely makes its role indirect, helping to maintain the correct structure of the channel protein to allow FKBP12-RyR1 interactions rather than acting more directly, as a residue at which the calstabin chemically binds.

As mentioned previously, the p.Cys2237Tyr substitution has the potential to destabilise the α-helix in which the residue resides. The potential destabilisation of the α-helix may have substantial effects on the surrounding structure of RyR1 by abrogating the hydrogen bonds between it and the surrounding α-helices. It is therefore a possibility that the p.Cys2237Tyr substitution may not abrogate FKBP12 binding but may limit its function by interfering in the subsequent intra-protein interactions that occur after binding of the calstabin. It is important to recognise that the exact physical mechanism behind the functional change of this variant is only speculation until a structure of the variant is solved. Despite this, more detail on the mechanism behind the effects of the p.Cys2237Tyr substitution on FKBP12 function may be gained via protein binding assays to further investigate the interactions between the variant RyR1 and FKBP12.

Chapter 5. Final summary

5.1 Conclusions

Over the course of this project six RyR1 variants were functionally characterised: p.Phe539Leu, p.Arg1707Cys, p.Gly2183Glu, p.Cys2237Tyr, p.Arg2458Leu and p.Pro2793Leu. Of these variants, p.Cys2237Tyr and p.Pro2793Leu displayed a hypersensitive response to the RyR1 agonist, 4-c*m*c, while the variant p.Arg1707Cys displayed a hyposensitive response.

According to the Variant Curation Expert Panel's guidelines, the functional analysis data of the p.Cys2237Tyr variant classifies it as likely pathogenic for malignant hyperthermia. Subsequently, familial diagnostics for MH susceptibility should now include the p.Cys2237Tyr variant. Although the p.Pro2793Leu variant displayed a hypersensitive response to 4-c*m*c, its classification remains as a variant of unknown significance. A more descriptive classification of p.Pro2793Leu could be attained by performing a number of analyses, including: segregation analysis to determine the inheritance pattern of the variant as well as an analysis of the frequency in which the variant is present within the general population [138].

While substitution of the p.Arg2458 residue with amino acids such as cysteine and histidine results in a hypersensitive channel, no such effect was observed here with the p.Arg2458Leu substitution. Variants p.Gly2183Glu and p.Phe539Leu each displayed a response to 4-c*m*c comparable to wild type, and while the results of the p.Gly2183Glu variant were interesting, results of the p.Phe539Leu variant were in disagreement with a previous analysis. However, sequencing of the p.Phe539Leu cell line proved it actually contained the p.Pro2793Leu variant, causing the previous functional analysis of p.Phe539Leu to be a misrepresentation of the channel function.

In all but one hypersensitive cell line, over-expression of FKBP12 resulted in a return to wild type RyR1 functionality, supporting the suggestion that FKBP12 confers a stabilising effect onto the closed state of the channel. While the Pro2793 residue resides close to a putative FKBP12 binding site on RyR1, the p.Pro2793Leu substitution was not enough to abrogate FKBP12 function, as indicated by the response no longer being significantly different to wild type, suggesting the residue is not integral to binding of the calstabin. However, over-expression of FKBP12 in the p.Cys2237Tyr cell line did not result in a return to wild type functionality, suggesting the Cys2237 residue has a substantial role in conventional FKBP12-RyR1 interactions.

5.2 Future directions

5.2.1 Generate full-length constructs

Six variants were generated over the course of this project; however, only p.Arg2458Leu was incorporated into the full-length vector. Variants p.Arg2676Trp and p.Gly4835Glu were each cloned into half-length vectors, while variants p.Val2627Met, p.Arg3348His and p.Phe4808Ser remain in the initial vector that SDM was carried out on. Cloning of each of these variants into the full-length vector should be carried out, then stable cell lines generated in order to perform subsequent functional analysis. Especially p.Arg2676Trp which has a predictive VCEP classification as likely pathogenic.

5.2.2 Binding assays of FKBP12/RYR1

It was found during this project that FKBP12 appears to confer a stabilising effect on RyR1, reverting the hypersensitive variants to wild type functionality. This was shown in all variants except p.Cys2237Tyr, suggesting that this variant interferes with FKBP12 function on RyR1. To determine whether this loss of function is due to the abrogation of FKBP12-RyR1 binding or if it is a result of the loss of an intramolecular mechanism, the binding affinity of FKBP12 to the p.Cys2237Tyr variant should be analysed. Protein interaction assays utilising GST-tagged FKBP12 and glutathione conjugated magnetic beads could be used to "pull down" variant RyR1 for immunoblot analysis. The results of these initial binding assays could then be corroborated via bio-layer interferometry[143].

5.2.3 Over-expression of FKBP12.6 in cell lines

As suggested by the current literature, while FKBP12 and its isoform FKBP12.6 are expressed at varying levels in skeletal and cardiac muscles respectively, both have been implicated in the stabilisation of RyR1. While the research conducted over the course of this projects suggests this is the case for FKBP12, it would be worth over-expressing FKBP12.6 in each cell line to determine its capability as an RyR1 stabiliser. If this indicates that FKBP12.6 does confer stability, it would also be worth performing the binding assays outlined above with this isoform to further characterise the interaction.

5.2.4 Functionally characterise RYR1 response to caffeine

Although 4-c*m*c is commonly used as an agonist for functional analysis of RyR1, performing the assays with a second agonist such as caffeine would further confirm the function of each variant. The use of a second agonist would provide a characterisation of the function of each variant as a response to two separate mechanisms, thus giving a more detailed representation of the channel. It would also have the added benefit of characterising the variant in the context of the *in vitro* contracture test, the current "gold-standard" diagnostic technique for malignant hyperthermia susceptibility.

5.2.5 Optimise functional characterisation assays

While the functional analysis of variants during this project was met with many technical difficulties, reliable results were eventually obtained by performing the assays on uninduced cell lines. It was thought that the new system was too sensitive to accurately distinguish Ca^{2+} release at low and high concentrations of agonist, leading to all but one variant being regarded as hypersensitive. The substantially lower expression of RyR1 in uninduced cells seemed to have diminished the Ca^{2+} release, allowing for accurate detection of Ca^{2+} transients. While this method was sufficient for the requirements of this project, attempts to publish the results may be thwarted by the lack of control over expression. Further optimisation of the protocol may have allowed for the use of induced cell lines during functional characterisation. Changing the concentrations of 4-c*m*c from 200 µM increments ranging between 0-1000 µM to 20 µM increments ranging from 0-100 µM may have produced distinguishable results for each variant. While the length of time for induction with tetracyclin had been changed in an attempt to solve these technical issues, the concentration of tetracyline had not been altered, therefore this would be a logical next step in the optimisation of the protocol.

5.2.6 Ex vivo Functional analysis

The use of HEK-293 cells as a heterologous system for the characterisation of protein function is a highly established and valuable tool in protein analysis. The system is affordable and cell lines are relatively easy to generate and maintain. Subsequently, they are widely used for the functional analysis of RyR1 variants. While data gathered in this fashion is adequate for the characterisation of new variants, further analysis of said variants can be attained by performing similar experimentation within the context of a more physiologically relevant system.

Functional analysis within patient-derived myotubes would provide data in the physiological context of human muscle, making for a more descriptive analysis of each variant by allowing the effects of each substitution on the nuances of RyR1 function to be characterised. However, each variants will have to be analysed in myotubes derived from separate individuals, thus requiring extensive funding. In addition, the genetic background of the individuals would have to be established to mitigate the effects of any indirect changes to RyR1 function.

Similarly, further analysis could be performed on dyspedic mouse myotubes[144]. While not as physiologically relevant as patient-derived myotubes, the genetic background of a mouse model can be more accurately controlled. Mouse myotubes also allow for a more optimised methodology in which the cell line can be transfected with *RYR1* variants generated internally following the protocols established over the course of this project.

5.2.7 Characterise resting cytosolic [Ca^{2+}] and ER Ca^{2+} stores

While the pathogenesis of malignant hyperthermia is defined by a gain of function in RyR1 mediated Ca^{2+} release, substitutions within RyR1 may effect Ca^{2+} homeostasis in a manner that does not fit this definition. During functional analysis, the p.Arg1707Cys substitution was found to result in changes in fluorescence that were smaller in comparison to wild type, indicating a decrease in Ca^{2+} release in response to 4-c*m*c (Appendix IV, Table. 7). This observation could be explained by the substitution causing the channel to either "favour" the closed state, or become "leaky"; however, the precise mechanism is indistinguishable in the methodology used.

Further analysis on the Ca^{2+} profile of the p.Arg1707Cys cell line would help to further define how the variant effects Ca^{2+} homeostasis. While analysing the resting cytosolic [Ca^{2+}], may help define a channel such as RyR1 (p.Arg1707Cys) as "leaky", it would be beneficial to conduct this analysis on each variant studied over the course of this project as it would provide a more descriptive characterisation of how each variant effects Ca^{2+} homeostasis.

In the context of a "leaky" RyR1, diminished ER Ca^{2+} stores would subsequently appear to reduce the channels response to 4-c*m*c as the channel would be incapable of releasing Ca^{2+} to the extent of a wild type channel which has access to a more Ca^{2+} enriched store. Characterising resting cytosolic [Ca^{2+}] as well as the Ca^{2+} stores within the endoplasmic reticulum would produce a more definitive description of the p.Arg1707Cys substitution that may aid in describing its role in the pathogenesis of the myopathy the proband in which the variant was found suffers from.

Resting cytosolic [Ca^{2+}] can be measured in a variety of ways, not dissimilar to the methodology used to characterise Ca^{2+} release during this project. Once production of a cell line containing the variant of interest has been established, a plethora of experimentation can be conducted. Resting cytosolic [Ca^{2}] could be characterised following a modified methodology outlined by Sheu *et al* (1984) in which cells would be incubated with the Ca^{2+} dye fura2, then centrifuged and resuspended in Krebs-Henseleit solution to remove any extracellular dye[145]. Intraceullular [Ca^{2+}] would then determined using the Olympus I X 2 UCB microscope to excite the dye at wavelengths 340 nm and 380 nm (bound and unbound Ca^{2+} respectively) and measure the subsequent fluorescence at 510 nm.

While effective, this methodology is arguably outdated and restrictive. The use of genetically encoded Ca^{2+} indicators (GECI) such as the calmodulin-green fluorescent fusion protein (GCaMP) can allow for more targeted measurements of Ca^{2+} such as the resting cytosolic [Ca^{2+}] or the endoplasmic reticulum Ca^{2+} stores of the cell. While a separate cell line would have to be generated which contains both the variant of interest and the GECI, this is another potential methodology in which Ca^{2+} homeostasis can be characterised. In this methodology, binding of Ca^{2+} to calmodulin, modulates the protonation state, conformation and spectral chromophore properties of green fluorescent protein (GFP), allowing for the measurement of [Ca^{2+}] through changes in the fluorescence profile of GFP[146].

Chapter 6. Bibliography

1. Sweeney, H.L. and Hammers, D.W., *Muscle contraction.* Cold Spring Harbor Perspectives in Biology, 2018. **10**(2): p. a023200.

2. Kuo, I.Y. and Ehrlich, B.E., *Signaling in muscle contraction.* Cold Spring Harbor Perspectives in Biology, 2015. **7**(2): p. a006023.

3. Tanabe, T., Beam, K.G., Powell, J.A., and Numa, S., *Restoration of excitation—contraction coupling and slow calcium current in dysgenic muscle by dihydropyridine receptor complementary DNA.* Nature, 1988. **336**(6195): p. 134-139.

4. Adams, B.A., Tanabe, T., Mikami, A., Numa, S., et al., *Intramembrane charge movement restored in dysgenic skeletal muscle by injection of dihydropyridine receptor cDNAs.* Nature, 1990. **346**(6284): p. 569-572.

5. Rebbeck, R.T., Karunasekara, Y., Gallant, E.M., Board, P.G., et al., *The β1a subunit of the skeletal DHPR binds to skeletal RyR1 and activates the channel via its 35-residue C-terminal tail.* Biophysical Journal, 2011. **100**(4): p. 922-930.

6. Ebashi, S. and Kodama, A., *A new protein factor promoting aggregation of tropomyosin.* The Journal of Biochemistry, 1965. **58**(1): p. 107-108.

7. Ebashi, S., Ebashi, F., and Kodama, A., *Troponin as the Ca++-receptive protein in the contractile system.* The Journal of Biochemistry, 1967. **62**(1): p. 137-138.

8. Eisenberg, E. and Hill, T.L., *A cross-bridge model of muscle contraction.* Progress in Biophysics and Molecular Biology, 1979. **33**: p. 55-82.

9. Xu, C., Craig, R., Tobacman, L., Horowitz, R., et al., *Tropomyosin positions in regulated thin filaments revealed by cryoelectron microscopy*. Biophysical journal, 1999. **77**(2): p. 985-992.

10. Scott, W., Stevens, J., and Binder–Macleod, S.A., *Human skeletal muscle fiber type classifications.* Physical Therapy, 2001. **81**(11): p. 1810-1816.

11. Toyoshima, C., Nakasako, M., Nomura, H., and Ogawa, H., *Crystal structure of the calcium pump of sarcoplasmic reticulum at 2.6 Å resolution.* Nature, 2000. **405**(6787): p. 647-655.

12. Clarke, D.M., Loo, T.W., Inesi, G., and Maclennan, D.H., *Location of high affinity Ca2+-binding sites within the predicted transmembrane domain of the sarco-plasmic reticulum Ca2+-ATPase.* Nature, 1989. **339**(6224): p. 476-478.

13. Liou, J., Kim, M.L., Do Heo, W., Jones, J.T., et al., *STIM is a Ca2+ sensor essential for Ca2+-store-depletion-triggered Ca2+ influx.* Current Biology, 2005. **15**(13): p. 1235-1241.

14. Stathopulos, P.B., Schindl, R., Fahrner, M., Zheng, L., et al., *STIM1/Orai1 coiled-coil interplay in the regulation of store-operated calcium entry.* Nature Communications, 2013. **4**(1): p. 2963.

15. Zhang, S.L., Yu, Y., Roos, J., Kozak, J.A., et al., *STIM1 is a Ca2+ sensor that activates CRAC channels and migrates from the Ca2+ store to the plasma membrane.* Nature, 2005. **437**(7060): p. 902-905.

16. Cherednichenko, G., Hurne, A.M., Fessenden, J.D., Lee, E.H., et al., *Conformational activation of Ca2+ entry by depolarization of skeletal myotubes.* Proceedings of the National Academy of Sciences of the United States of America, 2004. **101**(44): p. 15793.

17. Dirksen, R.T. and Beam, K.G., *Role of calcium permeation in dihydropyridine receptor function: Insights into channel gating and excitation–contraction coupling.* Journal of General Physiology, 1999. **114**(3): p. 393-404.

18. Bannister, R.A., Pessah, I.N., and Beam, K.G., *The skeletal l-type Ca(2+) current is a major contributor to excitation-coupled Ca(2+) entry.* The Journal of General Physiology, 2009. **133**(1): p. 79-91.

19. Lyfenko, A.D. and Dirksen, R.T., *Differential dependence of store-operated and excitation-coupled Ca2+ entry in skeletal muscle on STIM1 and Orai1*. The Journal of Physiology, 2008. **586**(20): p. 4815-4824.

20. Otsu, K., Willard, H.F., Khanna, V.K., Zorzato, F., et al., *Molecular cloning of cDNA encoding the Ca2+ release channel (ryanodine receptor) of rabbit cardiac muscle sarcoplasmic reticulum.* Journal of Biological Chemistry, 1990. **265**(23): p. 13472-13483.

21. Takeshima, H., Nishimura, S., Matsumoto, T., Ishida, H., et al., *Primary structure and expression from complementary DNA of skeletal muscle ryanodine receptor.* Nature, 1989. **339**(6224): p. 439-445.

22. Nakai, J., Imagawa, T., Hakamata, Y., Shigekawa, M., et al., *Primary structure and functional expression from cDNA of the cardiac ryanodine receptor/calcium release channel.* FEBS Letters, 1990. **271**(1-2): p. 169-177.

23. Hakamata, Y., Nakai, J., Takeshima, H., and Imoto, K., *Primary structure and distribution of a novel ryanodine receptor/calcium release channel from rabbit brain.* FEBS Letters, 1992. **312**(2-3): p. 229-235.

24. Caswell, A.H. and Brandt, N.R., *Does muscle activation occur by direct mechanical coupling of transverse tubules to sarcoplasmic reticulum?* Trends in Biochemical Sciences, 1989. **14**(5): p. 161-165.

25. Cannell, M.B., Cheng, H., and Lederer, W.J., *The control of calcium release in heart muscle.* Science, 1995. **268**(5213): p. 1045.

26. Santulli, G., Pagano, G., Sardu, C., Xie, W., et al., *Calcium release channel RyR2 regulates insulin release and glucose homeostasis.* The Journal of Clinical Investigation, 2015. **125**(5): p. 1968-1978.

27. Supnet, C., Noonan, C., Richard, K., Bradley, J., et al., *Up-regulation of the type 3 ryanodine receptor is neuroprotective in the TgCRND8 mouse model of alzheimer's disease.* Journal of Neurochemistry, 2010. **112**(2): p. 356-365.

28. Protasi, F., Takekura, H., Wang, Y., Chen, S.R., et al., *RYR1 and RYR3 have different roles in the assembly of calcium release units of skeletal muscle.* Biophysical Journal, 2000. **79**(5): p. 2494-2508.

29. Mukund, K. and Subramaniam, S., *Skeletal muscle: A review of molecular structure and function, in health and disease.* Wiley Interdisciplinary Reviews. Systems Biology and Medicine, 2020. **12**(1): p. e1462.

30. Des Georges, A., Clarke, O.B., Zalk, R., Yuan, Q., et al., *Structural basis for gating and activation of RyR1*. Cell, 2016. **167**(1): p. 145-157.e17.

31. Fan, G., Baker, M.L., Wang, Z., Baker, M.R., et al., *Gating machinery of insP3R channels revealed by electron cryomicroscopy.* Nature, 2015. **527**(7578): p. 336-341.

32. Gomez, A.C., Holford, T.W., and Yamaguchi, N., *Malignant hyperthermia-associated mutations in the S2-S3 cytoplasmic loop of type 1 ryanodine receptor calcium channel impair calcium-dependent inactivation.* American Journal of Physiology. Cell Physiology, 2016. **311**(5): p. C749-C757.

33. Zalk, R., Clarke, O.B., Des Georges, A., Grassucci, R.A., et al., *Structure of a mammalian ryanodine receptor*. Nature, 2015. **517**(7532): p. 44-49.

34. O'reilly, F.M., Robert, M., Jona, I., Szegedi, C., et al., *FKBP12 modulation of the binding of the skeletal ryanodine receptor onto the II-III loop of the dihydropyridine receptor.* Biophysical Journal, 2002. **82**(1 Pt 1): p. 145-155.

35. Wong King Yuen, S.M., Campiglio, M., Tung, C.-C., Flucher, B.E., et al., *Structural insights into binding of STAC proteins to voltage-gated calcium channels.* Proceedings of the National Academy of Sciences of the United States of America, 2017. **114**(45): p. e9520-e9528.

36. Horstick, E.J., Linsley, J.W., Dowling, J.J., Hauser, M.A., et al., *STAC3 is a component of the excitation-contraction coupling machinery and mutated in Native American myopathy.* Nature Communications, 2013. **4**: p. 1952-1952.

37. Gaburjakova, M., Gaburjakova, J., Reiken, S., Huang, F., et al., *FKBP12 binding modulates ryanodine receptor channel gating.* Journal of Biological Chemistry, 2001. **276**(20): p. 16931-16935.

38. Ponting, C., Schultz, J., and Bork, P., *SPRY domains in ryanodine receptors (Ca2+-release channels).* Trends in Biochemical Sciences, 1997. **22**(6): p. 193-194.

39. Grabner, M., Dirksen, R.T., Suda, N., and Beam, K.G., *The II-III loop of the skeletal muscle dihydropyridine receptor is responsible for the bi-directional coupling with the ryanodine receptor.* Journal of Biological Chemistry, 1999. **274**(31): p. 21913-21919.

40. Rebbeck, R.T., Willemse, H., Groom, L., Casarotto, M.G., et al., *Regions of ryanodine receptors that influence activation by the dihydropyridine receptor β1a subunit.* Skeletal Muscle, 2015. **5**(1): p. 23.

41. Cheng, W., Altafaj, X., Ronjat, M., and Coronado, R., *Interaction between the dihydropyridine receptor Ca2+ channel beta-subunit and ryanodine receptor type 1 strengthens excitation-contraction coupling.* Proceedings of the National Academy of Sciences of the United States of America, 2005. **102**(52): p. 19225-19230.

42. Tripathy, A., Xu, L., Mann, G., and Meissner, G., *Calmodulin activation and inhibition of skeletal muscle Ca2+ release channel (ryanodine receptor).* Biophysical Journal, 1995. **69**(1): p. 106-119.

43. Beard, N.A., Casarotto, M.G., Wei, L., Varsányi, M., et al., *Regulation of ryanodine receptors by calsequestrin: Effect of high luminal Ca2+ and phosphorylation.* Biophysical Journal, 2005. **88**(5): p. 3444-3454.

44. Reiken, S., Lacampagne, A., Zhou, H., Kherani, A., et al., *PKA phosphorylation activates the calcium release channel (ryanodine receptor) in skeletal muscle: Defective regulation in heart failure.* The Journal of Cell Biology, 2003. **160**(6): p. 919-928.

45. Dilworth, D., Gudavicius, G., Xu, X., Boyce, A.K.J., et al., *The prolyl isomerase FKBP25 regulates microtubule polymerization impacting cell cycle progression and genomic stability.* Nucleic Acids Research, 2018. **46**(5): p. 2459-2478.

46. Pirkl, F. and Buchner, J., *Functional analysis of the hsp90-associated human peptidyl prolyl cis/trans isomerases FKBP51, FKBP52 and cyp4011.* Journal of Molecular Biology, 2001. **308**(4): p. 795-806.

47. Heitman, J., Movva, N.R., and Hall, M.N., *Targets for cell cycle arrest by the immunosuppressant rapamycin in yeast.* Science, 1991. **253**(5022): p. 905.

48. Hidalgo, M. and Rowinsky, E.K., *The rapamycin-sensitive signal transduction pathway as a target for cancer therapy.* Oncogene, 2000. **19**(56): p. 6680-6686.

49. Obata, K., Koide, M., Nagata, K., Iio, A., et al., *Role of FK506-binding protein 12 in development of the chick embryonic heart.* Biochemical and Biophysical Research Communications, 2001. **283**(3): p. 613-620.

50. Sehgal, S.N., Baker, H., and Vézina, C., *Rapamycin (AY-22, 989), a new antifungal antibiotic II. Fermentation, isolation and characterization.* The Journal of Antibiotics, 1975. **28**(10): p. 727-732.

51. Robinson, J., Lai, C., Martin, A., Nye, E., et al., *Oral rapamycin reduces tumour burden and vascularization in Lkb1+/− mice.* The Journal of Pathology, 2009. **219**(1): p. 35-40.

52. Yang, H., Rudge, D.G., Koos, J.D., Vaidialingam, B., et al., *mTOR kinase structure, mechanism and regulation.* Nature, 2013. **497**(7448): p. 217-223.

53. Brunn, G.J., Hudson, C.C., Sekulić, A., Williams, J.M., et al., *Phosphorylation of the translational repressor PHAS-I by the mammalian target of rapamycin.* Science, 1997. **277**(5322): p. 99.

54. Hara, K., Yonezawa, K., Kozlowski, M.T., Sugimoto, T., et al., *Regulation of EIF-4E BP1 phosphorylation by mTOR.* Journal of Biological Chemistry, 1997. **272**(42): p. 26457-26463.

55. Marx, S.O., Reiken, S., Hisamatsu, Y., Jayaraman, T., et al., *PKA phosphorylation dissociates FKBP12.6 from the calcium release channel (ryanodine receptor): Defective regulation in failing hearts.* Cell, 2000. **101**(4): p. 365-376.

56. Barg, S., Copello, J.A., and Fleischer, S., *Different interactions of cardiac and skeletal muscle ryanodine receptors with FK-506 binding protein isoforms.* American Journal of Physiology-Cell Physiology, 1997. **272**(5): p. C1726-C1733.

57. Galfré, E., Pitt, S.J., Venturi, E., Sitsapesan, M., et al., *FKBP12 activates the cardiac ryanodine receptor Ca2+-release channel and is antagonised by FKBP12.6.* PloS one, 2012. **7**(2): p. e31956.

58. Masumiya, H., Wang, R., Zhang, J., Xiao, B., et al., *Localization of the 12.6-kDa FK506-binding protein (FKBP12.6) binding site to the NH2-terminal domain of the cardiac Ca2+ release channel (ryanodine receptor).* Journal of Biological Chemistry, 2003. **278**(6): p. 3786-3792.

59. Zissimopoulos, S. and Lai, F.A., *Interaction of FKBP12.6 with the cardiac ryanodine receptor C-terminal domain.* Journal of Biological Chemistry, 2005. **280**(7): p. 5475-5485.

60. Wagenknecht, T., Grassucci, R., Berkowitz, J., Wiederrecht, G.J., et al., *Cryoelectron microscopy resolves FK506-binding protein sites on the skeletal muscle ryanodine receptor.* Biophysical Journal, 1996. **70**(4): p. 1709-1715.

61. Girgenrath, T., Mahalingam, M., Svensson, B., Nitu, F.R., et al., *N-terminal and central segments of the type 1 ryanodine receptor mediate its interaction with FK506-binding proteins.* The Journal of Biological Chemistry, 2013. **288**(22): p. 16073-16084.

62. Campiglio, M., Kaplan, M.M., and Flucher, B.E., *STAC3 incorporation into skeletal muscle triads occurs independent of the dihydropyridine receptor.* Journal of Cellular Physiology, 2018. **233**(12): p. 9045-9051.

63. Babu, Y.S., Bugg, C.E., and Cook, W.J., *Structure of calmodulin refined at 2.2 Å resolution.* Journal of Molecular Biology, 1988. **204**(1): p. 191-204.

64. Zhu, X., Ghanta, J., Walker, J.W., Allen, P.D., et al., *The calmodulin binding region of the skeletal ryanodine receptor acts as a self-modulatory domain.* Cell Calcium, 2004. **35**(2): p. 165-177.

65. Moore, C.P., Rodney, G., Zhang, J.-Z., Santacruz-Toloza, L., et al., *Apocalmodulin and Ca2+ calmodulin bind to the same region on the skeletal muscle Ca2+ release channel.* Biochemistry, 1999. **38**(26): p. 8532-8537.

66. Zhang, L., Kelley, J., Schmeisser, G., Kobayashi, Y.M., et al., *Complex formation between junctin, triadin, calsequestrin, and the ryanodine receptor: Proteins of the cardiac junctional sarcoplasmic reticulum membrane.* Journal of Biological Chemistry, 1997. **272**(37): p. 23389-23397.

67. Wang, S., Trumble, W.R., Liao, H., Wesson, C.R., et al., *Crystal structure of calsequestrin from rabbit skeletal muscle sarcoplasmic reticulum.* Nature Structural Biology, 1998. **5**(6): p. 476-483.

68. Cozens, B. and Reithmeier, R.A., *Size and shape of rabbit skeletal muscle calsequestrin.* Journal of Biological Chemistry, 1984. **259**(10): p. 6248-6252.

69. Szegedi, C., Sárközi, S., Herzog, A., Jóna, I., et al., *Calsequestrin: More than 'only' a luminal Ca2+ buffer inside the sarcoplasmic reticulum.* The Biochemical Journal, 1999. **337 (Pt 1)**(Pt 1): p. 19-22.

70. Wei, L., Varsányi, M., Dulhunty, A.F., and Beard, N.A., *The conformation of calsequestrin determines its ability to regulate skeletal ryanodine receptors.* Biophysical Journal, 2006. **91**(4): p. 1288-1301.

71. Gehlert, S., Bungartz, G., Willkomm, L., Korkmaz, Y., et al., *Intense resistance exercise induces early and transient increases in ryanodine receptor 1 phosphorylation in human skeletal muscle.* PLOS ONE, 2012. **7**(11): p. e49326.

72. Stange, M., Xu, L., Balshaw, D., Yamaguchi, N., et al., *Characterization of recombinants skeletal muscle (Ser-2843) and cardiac muscle (Ser-2809) ryanodine receptor phosphorylation mutants.* Journal of Biological Chemistry, 2003. **278**(51): p. 51693-51702.

73. Kim, H.W., Steenaart, N.A., Ferguson, D.G., and Kranias, E.G., *Functional reconstitution of the cardiac sarcoplasmic reticulum Ca2(+)-ATPase with phospholamban in phospholipid vesicles.* Journal of Biological Chemistry, 1990. **265**(3): p. 1702-1709.

74. Masterson, L.R., Yu, T., Shi, L., Wang, Y., et al., *Camp-dependent protein kinase A selects the excited state of the membrane substrate phospholamban.* Journal of Molecular Biology, 2011. **412**(2): p. 155-164.

75. Fajardo, V.A., Bombardier, E., Vigna, C., Devji, T., et al., *Co-expression of SERCA isoforms, phospholamban and sarcolipin in human skeletal muscle fibers.* PLOS ONE, 2013. **8**(12): p. e84304.

76. Aracena, P., Tang, W., Hamilton, S.L., and Hidalgo, C., *Effects of S-glutathionylation and S-nitrosylation on calmodulin binding to triads and FKBP12 binding to type 1 calcium release channels.* Antioxidants & Redox Signaling, 2005. **7**(7-8): p. 870-881.

77. Aracena, P., Sánchez, G., Donoso, P., Hamilton, S.L., et al., *S-glutathionylation decreases Mg2+ inhibition and S-nitrosylation enhances Ca2+ activation of RyR1 channels.* Journal of Biological Chemistry, 2003. **278**(44): p. 42927-42935.

78. Joseph, M.M., Shah, K., and Viljoen, J.F., *Malignant hyperthermia associated with isoflurane anesthesia.* Anesthesia & Analgesia, 1982. **61**(8).

79. Otsuka, H., Komura, Y., Mayumi, T., Yamamura, T., et al., *Malignant hyperthermia during sevoflurane anesthesia in a child with central core disease.* Anesthesiology, 1991. **75**(4): p. 699-700.

80. Fu, E.S., Scharf, J.E., Mangar, D., and Miller, W.D., *Malignant hyperthermia involving the administration of desflurane.* Canadian Journal of Anaesthesia, 1996. **43**(7): p. 687.

81. Ellis, F.R., Keaney, N.P., Harriman, D.G., Sumner, D.W., et al., *Screening for malignant hyperpyrexia.* British Medical Journal, 1972. **3**(5826): p. 559-561.

82. Litman, Ronald s., Flood, Christopher d., Kaplan, Richard f., Kim, Yung l., et al., *Postoperative malignant hyperthermia: An analysis of cases from the North American malignant hyperthermia registry.* Anesthesiology, 2008. **109**(5): p. 825-829.

83. Rosenberg, H., Pollock, N., Schiemann, A., Bulger, T., et al., *Malignant hyperthermia: A review.* Orphanet Journal of Rare Diseases, 2015. **10**: p. 93.

84. Gupta, P.K. and Hopkins, P.M., *Diagnosis and management of malignant hyperthermia.* BJA Education, 2017. **17**(7): p. 249-254.

85. Rosenberg, H., Davis, M., James, D., Pollock, N., et al., *Malignant hyperthermia*. Orphanet Journal of Rare Diseases, 2007. **2**: p. 21.

86. Glahn, K.P.E., Ellis, F.R., Halsall, P.J., Müller, C.R., et al., *Recognizing and managing a malignant hyperthermia crisis: Guidelines from the european malignant hyperthermia group.* British Journal of Anaesthesia, 2010. **105**(4): p. 417-420.

87. Kolb, Mary e., Horne, M.L., and Martz, R., *Dantrolene in human malignant hyperthermia a multicenter study.* Anesthesiology, 1982. **56**(4): p. 254-262.

88. Choi, R.H., Koenig, X., and Launikonis, B.S., *Dantrolene requires Mg(2+) to arrest malignant hyperthermia.* Proceedings of the National Academy of Sciences of the United States of America, 2017. **114**(18): p. 4811-4815.

89. Ratto, D. and Joyner, R.W., *Statpearls*. 2021.

90. Jiang, D., Chen, W., Xiao, J., Wang, R., et al., *Reduced threshold for luminal Ca2+ activation of RyR1 underlies a causal mechanism of porcine malignant hyperthermia.* Journal of Biological Chemistry, 2008. **283**(30): p. 20813-20820.

91. Ørding, H., *Incidence of malignant hyperthermia in Denmark.* Anesthesia & Analgesia, 1985. **64**(7).

92. Urwyler, A. and Hartung, E., *Malignant hyperthermia.* Der Anaesthesist, 1994. **43**(8): p. 557-569.

93. Wappler, F., *Anesthesia for patients with a history of malignant hyperthermia.* Current Opinion in Anesthesiology, 2010. **23**(3).

94. Kim, D.-C., *Malignant hyperthermia.* Korean Journal of Anesthesiology, 2012. **63**(5): p. 391-401.

95. Brady, J.E., Sun, L.S., Rosenberg, H., and Li, G., *Prevalence of malignant hyperthermia due to anesthesia in New York State, 2001-2005*. Anesthesia & Analgesia, 2009. **109**(4): p. 1162-1166.

96. Strazis, K.P. and Fox, A.W., *Malignant hyperthermia: A review of published cases.* Anesthesia & Analgesia, 1993. **77**(2).

97. European Malignant Hyperthermia Group. *Testing for MH susceptibility*. 2015; Available from: https://www.emhg.org/testing-for-mh/2017/12/28/in-vitro-contracture-testing-ivct.

98. Ording, H., Brancadoro, V., Cozzolino, S., Ellis, F.R., et al., *In vitro contracture test for diagnosis of malignant hyperthermia following the protocol of the European MH group: Results of testing patients surviving fulminant MH and unrelated low-risk subjects. The European Malignant Hyperthermia Group.* Acta Anaesthesiologica Scandinavica, 1997. **41**(8): p. 955-966.

99. Suzumori, N., Inagaki, H., Ohtani, A., Kumagai, K., et al., *Compound heterozygous RYR1 mutations by whole exome sequencing in a family with three repeated affected fetuses with fetal akinesia.* European Journal of Obstetrics & Gynecology and Reproductive Biology, 2018. **230**: p. 200-202.

100. European Malignant Hyperthermia Group. *Diagnostic MH mutations*. Available from: https://www.emhg.org/diagnostic-mutations.

101. European Malignant Hyperthermia Group. *Scoring matrix for classification of genetic variants in malignant hyperthermia susceptibility*. Available from: https://www.emhg.org/genetic-scoring-matrix.

102. Wu, S., Ibarra, M.C.A., Malicdan, M.C.V., Murayama, K., et al., *Central core disease is due to RYR1 mutations in more than 90% of patients.* Brain, 2006. **129**(6): p. 1470-1480.

103. Girard, T., Cavagna, D., Padovan, E., Spagnoli, G., et al., *B-lymphocytes from malignant hyperthermia-susceptible patients have an increased sensitivity to skeletal muscle ryanodine receptor activators*. Journal of Biological Chemistry, 2001. **276**(51): p. 48077-48082.

104. Yang, T., Riehl, J., Esteve, E., Matthaei, Klaus i., et al., *Pharmacologic and functional characterization of malignant hyperthermia in the R163C RyR1 knock-in mouse.* Anesthesiology, 2006. **105**(6): p. 1164-1175.

105. Durham, W.J., Aracena-Parks, P., Long, C., Rossi, A.E., et al., *RyR1 S-nitrosylation underlies environmental heat stroke and sudden death in y522s ryr1 knockin mice.* Cell, 2008. **133**(1): p. 53-65.

106. Loy, R.E., Orynbayev, M., Xu, L., Andronache, Z., et al., *Muscle weakness in RyR1I4895T/WT knock-in mice as a result of reduced ryanodine receptor Ca2+ ion permeation and release from the sarcoplasmic reticulum.* The Journal of General Physiology, 2011. **137**(1): p. 43-57.

107. Lawal, T.A., Wires, E.S., Terry, N.L., Dowling, J.J., et al., *Preclinical model systems of ryanodine receptor 1-related myopathies and malignant hyperthermia: A comprehensive scoping review of works published 1990–2019.* Orphanet Journal of Rare Diseases, 2020. **15**(1): p. 113.

108. Yuen, B., Boncompagni, S., Feng, W., Yang, T., et al., *Mice expressing T4826I-RyR1 are viable but exhibit sex- and genotype-dependent susceptibility to malignant hyperthermia and muscle damage.* FASEB Journal: Official Publication of the Federation of American Societies for Experimental Biology, 2012. **26**(3): p. 1311-1322.

109. Boncompagni, S., Loy, R.E., Dirksen, R.T., and Franzini-Armstrong, C., *The I4895T mutation in the type 1 ryanodine receptor induces fiber-type specific alterations in skeletal muscle that mimic premature aging.* Aging cell, 2010. **9**(6): p. 958-970.

110. Schiemann, A.H., Roesl, C., Pollock, N., Langton, E., et al., *Identification and functional analysis of RYR1 variants in a family with a suspected myopathy and associated malignant hyperthermia.* Journal of Neuromuscular Diseases, 2020. **7**(1): p. 51-60.

111. Magee, K.R. and Shy, G.M., *A new congenital non-progressive myopathy.* Brain, 1956. **79**(4): p. 610-21.

112. Dubowitz, V. and Pearse, A.G., *Oxidative enzymes and phosphorylase in central-core disease of muscle.* Lancet, 1960. **2**(7140): p. 23-24.

113. Romero, N.B., Monnier, N., Viollet, L., Cortey, A., et al., *Dominant and recessive central core disease associated with RYR1 mutations and fetal akinesia.* Brain, 2003. **126**(11): p. 2341-2349.

114. Jungbluth, H., Sewry, C., Brown, S.C., Manzur, A.Y., et al., *Minicore myopathy in children: A clinical and histopathological study of 19 cases.* Neuromuscular Disorders, 2000. **10**(4): p. 264-273.

115. Shuaib, A., Martin, J.M.E., Mitchell, L.B., and Brownell, A.K.W., *Multicore myopathy: Not always a benign entity.* Canadian Journal of Neurological Sciences / Journal Canadien des Sciences Neurologiques, 1988. **15**(1): p. 10-14.

116. Bailey, A.G. and Bloch, E.C., *Malignant hyperthermia in a three-month-old American Indian infant.* Anesthesia & Analgesia, 1987. **66**(10).

117. Stamm, D.S., Aylsworth, A.S., Stajich, J.M., Kahler, S.G., et al., *Native American myopathy: Congenital myopathy with cleft palate, skeletal anomalies, and susceptibility to malignant hyperthermia.* American Journal of Medical Genetics Part A, 2008. **146A**(14): p. 1832-1841.

118. Barnes, C., Stowell, K.M., Bulger, T., Langton, E., et al., *Safe duration of postoperative monitoring for malignant hyperthermia patients administered non-triggering anaesthesia: An update.* Anaesthesia and Intensive Care, 2015. **43**(1): p. 98-104.

119. Chang, A.Y., Chau, V.W.Y., Landas, J.A., and Pang, Y., *Preparation of calcium competent Escherichia coli and heat-shock transformation.* JEMI methods, 2017. **1**: p. 22-25.

120. Sato, K., Pollock, N., and Stowell, K.M., *Functional studies of RYR1 mutations in the skeletal muscle ryanodine receptor using human RYR1 complementary DNA.* Anesthesiology, 2010. **112**(6): p. 1350-1354.

121. Cacheux, M., Blum, A., Sébastien, M., Wozny, A.S., et al., *Functional characterization of a central core disease RyR1 mutation (p.Y4864H) associated with quantitative defect in RyR1 protein.* Journal of Neuromuscular Diseases, 2015. **2**(4): p. 421-432.

122. Chugun, A., Taniguchi, K., Murayama, T., Uchide, T., et al., *Subcellular distribution of ryanodine receptors in the cardiac muscle of carp (Cyprinus carpio).* American Journal of Physiology-Regulatory, Integrative and Comparative Physiology, 2003. **285**(3): p. R601-R609.

123. Fessenden, J.D., Wang, Y., Moore, R.A., Chen, S.R.W., et al., *Divergent functional properties of ryanodine receptor types 1 and 3 expressed in a myogenic cell line.* Biophysical Journal, 2000. **79**(5): p. 2509-2525.

124. Tong, J., Oyamada, H., Demaurex, N., Grinstein, S., et al., *Caffeine and halothane sensitivity of intracellular Ca2+ release is altered by 15 calcium release channel (ryanodine receptor) mutations associated with malignant hyperthermia and/or central core disease.* Journal Biological Chemistry, 1997. **272(**42): p. 26332-26339.

125. Yang, T., Ta, T.A., Pessah, I.N., and Allen, P.D., *Functional defects in six ryanodine receptor isoform-1 (RyR1) mutations associated with malignant hyperthermia and their impact on skeletal excitation-contraction coupling.* Journal of Biological Chemistry, 2003. **278(**28): p. 25722-25730.

126. Chan, V., Dreolini, L.F., Flintoff, K.A., Lloyd, S.J., et al., *The effect of increasing plasmid size on transformation efficiency in Escherichia coli.* Journal of Experimental Microbiology and Immunology, 2002. **2**: p. 207-223.

127. Tikchonenko, T.I., Karamov, E.V., Zavizion, B.A., and Naroditsky, B.S., *EcoRI activity: Enzyme modification or activation of accompanying endonuclease?* Gene, 1978. **4**(3): p. 195-212.

128. Hellman, L.M. and Fried, M.G., *Electrophoretic mobility shift assay (EMSA) for detecting protein–nucleic acid interactions.* Nature Protocols, 2007. **2**(8): p. 1849-1861.

129. Ghosh, R., Gilda, J.E., and Gomes, A.V., *The necessity of and strategies for improving confidence in the accuracy of western blots.* Expert Review of Proteomics, 2014. **11**(5): p. 549-560.

130. Westermeier, R., *Frequently made mistakes in electrophoresis.* Proteomics, 2007. **7**(S1): p. 60-63.

131. See, Y.P., Olley, P.M., and Jackowski, G., *The effects of high salt concentrations in the samples on molecular weight determination in sodium dodecyl sulfate polyacrylamide gel electrophoresis*. Electrophoresis, 1985. **6**(8): p. 382-387.

132. Strathern, J.N., Shafer, B.K., and Mcgill, C.B., *DNA synthesis errors associated with double-strand-break repair*. Genetics, 1995. **140**(3): p. 965-72.

133. Rosenberg, S.M., Longerich, S., Gee, P., and Harris, R.S., *Adaptive mutation by deletions in small mononucleotide repeats.* Science, 1994. **265**(5170): p. 405-407.

134. Griffith, D.A., Delipala, C., Leadsham, J., Jarvis, S.M., et al., *A novel yeast expression system for the overproduction of quality-controlled membrane proteins.* FEBS Letters, 2003. **553**(1): p. 45-50.

135. Kozutsumi, Y., Segal, M., Normington, K., Gething, M.J., et al., *The presence of malfolded proteins in the endoplasmic reticulum signals the induction of glucose-regulated proteins.* Nature, 1988. **332**(6163): p. 462-464.

136. Pham, D.H., Moretti, P.a.B., Goodall, G.J., and Pitson, S.M., *Attenuation of leakiness in doxycycline-inducible expression via incorporation of 3 ′ AU-rich mRNA destabilizing elements.* BioTechniques, 2008. **45**(2): p. 155-162.

137. Costello, A., Lao, N.T., Gallagher, C., Capella Roca, B., et al., *Leaky expression of the TET-On system hinders control of endogenous mirna abundance.* Biotechnology Journal, 2019. **14**(3): p. e1800219.

138. Richards, S., Aziz, N., Bale, S., Bick, D., et al., *Standards and guidelines for the interpretation of sequence variants: A joint consensus recommendation of the American College of Medical Genetics and Genomics and the Association for Molecular Pathology.* Genetics in Medicine, 2015. **17**(5): p. 405-423.

139. Creamer, T.P. and Rose, G.D., *Side-chain entropy opposes alpha-helix formation but rationalizes experimentally determined helix-forming propensities.* Proceedings of the National Academy of Sciences, 1992. **89**(13): p. 5937.

140. Chakrabartty, A., Kortemme, T., and Baldwin, R.L., *Helix propensities of the amino acids measured in alanine-based peptides without helix-stabilizing side-chain interactions.* Protein Science, 1994. **3**(5): p. 843-852.

141. Nagano, N., Ota, M., and Nishikawa, K., *Strong hydrophobic nature of cysteine residues in proteins.* FEBS Letters, 1999. **458**(1): p. 69-71.

142. Barlow, D.J. and Thornton, J.M., *Helix geometry in proteins.* Journal of Molecular Biology, 1988. **201**(3): p. 601-619.

143. Abdiche, Y., Malashock, D., Pinkerton, A., and Pons, J., *Determining kinetics and affinities of protein interactions using a parallel real-time label-free biosensor, the Octet.* Analytical Biochemistry, 2008. **377**(2): p. 209-217.

144. Lefebvre, R., Legrand, C., Groom, L., Dirksen, R.T., et al., *Ca2+ release in muscle fibers expressing R4892W and G4896V type 1 ryanodine receptor disease mutants.* PLOS ONE, 2013. **8**(1): p. e54042.

145. Sheu, S.S., Sharma, V.K., and Banerjee, S.P., *Measurement of cytosolic free calcium concentration in isolated rat ventricular myocytes with quin 2.* Circulation Research, 1984. **55**(6): p. 830-834.

146. Zhong, C. and Schleifenbaum, J., *Genetically encoded calcium indicators: A new tool in renal hypertension research.* Frontiers in Medicine, 2019. **6**: p. 128.

Chapter 7. Appendices

Appendix I: Generating variant *RYR1* cDNA

Table 1. Primer sequences for site-directed mutagenesis.

Name	Size	Sequence (5'-3')	Annealing Temp (°C)	Variant	Vector
R2458L Mut for	27bp	CGCGCCA TCCTCCT CTCCCTT GTGCCC	67	c.7374 G>T p.Arg2458Leu	pBSKO+
R2458L Mut rev	27bp	GGGCACA AGGGAGA GGAGGAT GGCGCG			
V2627M Mut for	30bp	CTGTTGC GCCGCCT GATGTTC GACGTGC CC	67	c.7879 G>A p.Val2627Met	pBSKO+
V2627M Mut rev	30bp	GGGCACG TCGAACA TCAGGCG GCGCAAC AG			
R2676W Mut for	31bp	GAGCTGC ACCTCAC ATGGAAA CTCTTCT GGG	57	c.8026 C>T p.Arg2676Trp	pBSKO+
R2676W Mut rev	31bp	CCCAGAA GAGTTTC CATGTGA GGTGCAG CTC			
R3348H Mut for	30bp	CAGCCCA TTGTGAG CCATGCA CGGCCGG AG	57	c.10042 G>A p.Arg3348His	pBSKO+
R2248H Mut rev	30bp	CTCCGGC CGTGCAT GGCTCAC AATGGGC TG			

F4808S mut for	30bp	GACACTAC AACAACTC CTTCTTTGC TGCCC	57	c.14423 T>C p.Phe4808Ser	pBSH+
F4808S mut rev	30bp	GGGCAGCA AAGAAGGA GTTGTTGTA GTGTC			
G4835E Mut for	34bp	CTCTGTCAC CCACAATG AGAAACAG CTGGTGAT G	59	c.14504 G>A p.Gly4835Glu	pBSH+
G4835E Mut rev	34bp	CATCACCA GCTGTTTCT CATTGTGG GTGACAGA G			

7.1 Site-directed mutagenesis technical issues.

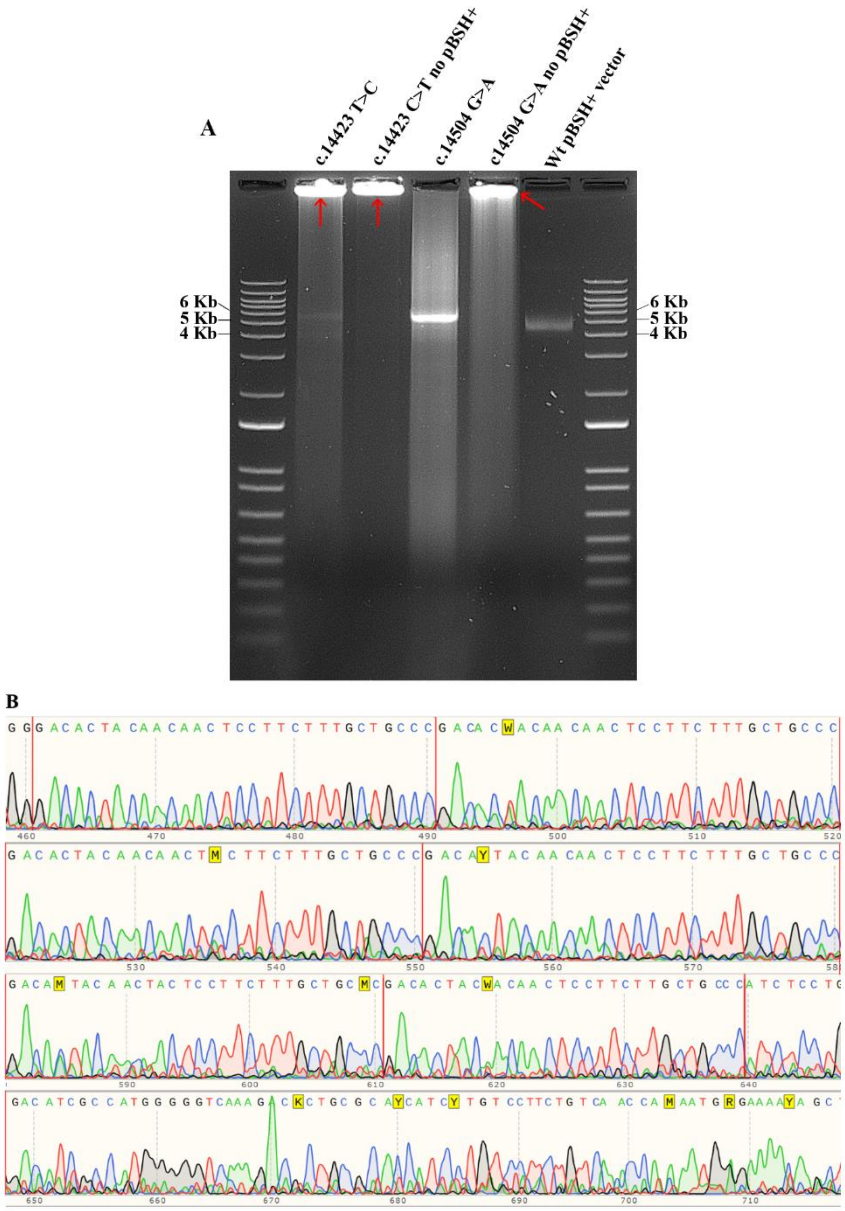

Figure 7.1. Technical issues during site-directed mutagenesis.

Product analysis of c.14423 T>C (p.Phe4808Ser) variant after site-directed mutagenesis **(A)** 0.8% agarose gel electrophoresis of site-directed mutagenesis products with red arrows showing the large molecular weight bands [that] did not traverse from the wells. **(B)** Sequence chromatogram showing the repeating sequence of the mutagenic primer for the c.14423 T>C variant. Repeats are outlined in red. Chromatogram was generated in Snapgene® 5.3 and images were compiled in Adobe Photoshop.

Table 2. Primer sequences for sequencing of pBSKO+ constructs.

Name	Size	Sequence (5'-3')	Vector
Exon44	19bp	CGAGAGCGTGGAGGAGAAC	pBSKO+
TM7361	20bp	CCATCCTCCGCTCCCTTGTG	pBSKO+
TM7642	20bp	GCCGTGAACCGCTACCTGTG	pBSKO+
RyR2729	20bp	AAATACGACCCGGAGCTGTA	pBSKO+
TM8273	21bp	CGGAGTACACACACGAGAAGT	pBSKO+
RyR2862F-Cfol	21bp	CCTCGAGAAGGCTACAACCCT	pBSKO+
TM9178	20bp	GCCCCAGCTGTGGTCAACTG	pBSKO+
TM9234	21bp	TCAGGGCCTGACTTCATCACT	pBSKO+
TM9485	20bp	CAGCGTTCGGTAGCAAGAGA	pBSKO+
TM9769	21bp	TGTGTAGCGGGCACCTGACTC	pBSKO+
TM10109	20bp	CTCCTCCTCGGACACCACCT	pBSKO+
TM10518	21bp	GGCAGCATCTTCTTCAGTGTG	pBSKO+
TM10884	21bp	AGGGGCGTCATACGGAAACAG	pBSKO+
TM11213	20bp	GACCTCAACCTCCTCTTCAG	pBSKO+
TM11359	20bp	AGCTTCAGGGTGGAGGACAC	pBSKO+
TM11787	21bp	ATGACATCCTTGCCCGAGTAG	pBSKO+

Table 3. Primer sequences for sequencing of pBSH+ constructs.

Name	Size	Sequence	Vector
T7 forward	20bp	TAATACGACTCACTATAGGG	pBSH+
TM13377	19bp	GCCCACACCCGAGGGCTCTC	pBSH+
TM13903	21bp	GAACCCGCCCTGCGGTGTCTG	pBSH+
T4826I HRM for	17bp	ACTTCTTCTTTGCTGCC	pBSH+
M13 reverse	16bp	CAGGAACAGCTATGAC	pBSH+
TM14512	21bp	GTAGACGACCACCGCCAGAAG	pBSH+
TM13973	21bp	TTACCAGGGGCACCTTGAGAC	pBSH+
TM13356	21bp	GGTTCCGCAGGCGTCGTGTCC	pBSH+

Figure 7.2 Sequencing of pBSKO+ (c.7374 G>T) (p.Arg2458Leu).

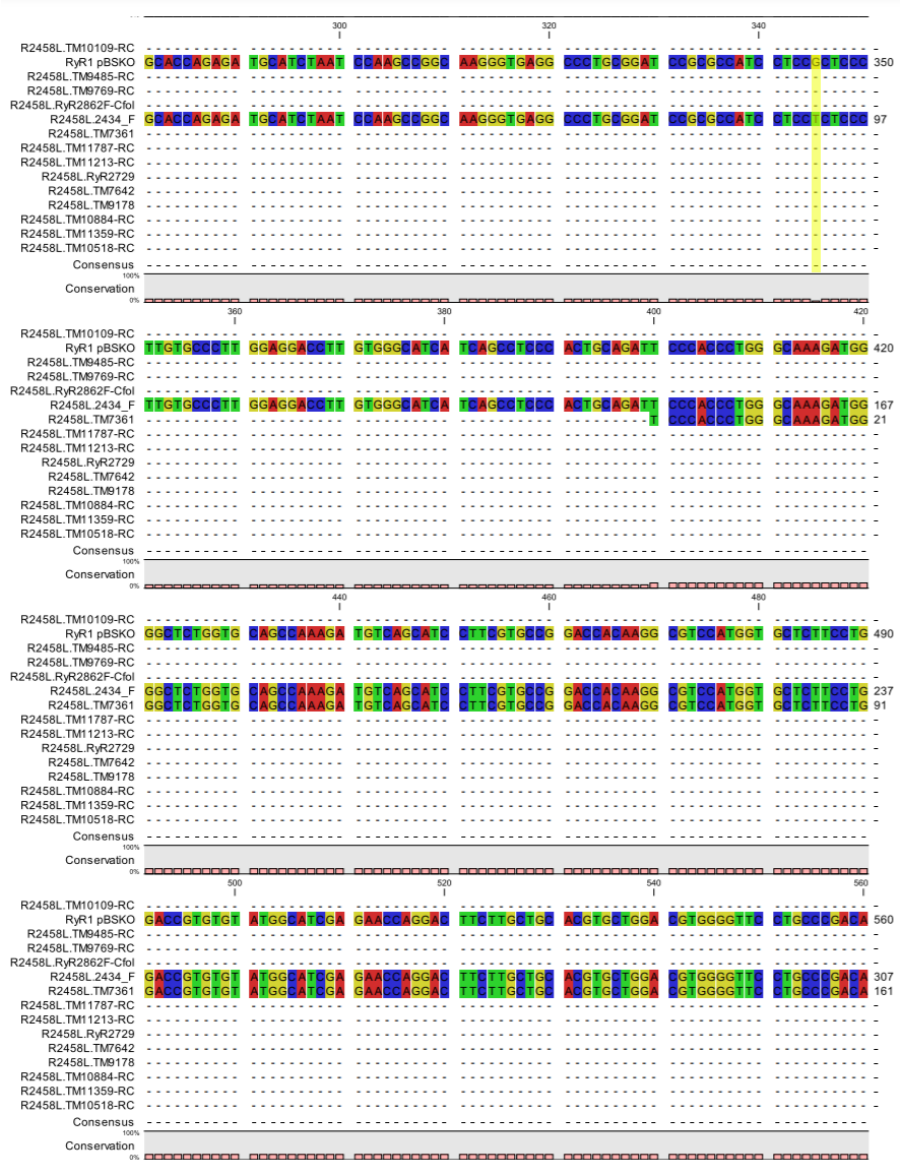

Figure 7.2. Multiple sequence alignment confirming absence of unwanted missense mutations in c.7374 G>T (p.Arg2458Leu).

Multiple sequence alignment of pBSKO+ construct after mutagenesis to incorporate the c.7374 G>T substitution. A total of 14 primers were used to sequence between restriction sites MfeI and NsiI used for sub-cloning of pBSKO+ into pBSKX+. Sequences were aligned to wild type *RYR1* NM_000540.3 using CLC sequence viewer 8 with a gap open cost of 25, a gap exit cost of 15, and a free end gap cost. Substitution highlighted in yellow. Dotted lines indicate nucleotide positions.

7.3 Sequencing of pBSKO+ (c.7879 G>A) (p.Val2627Met).

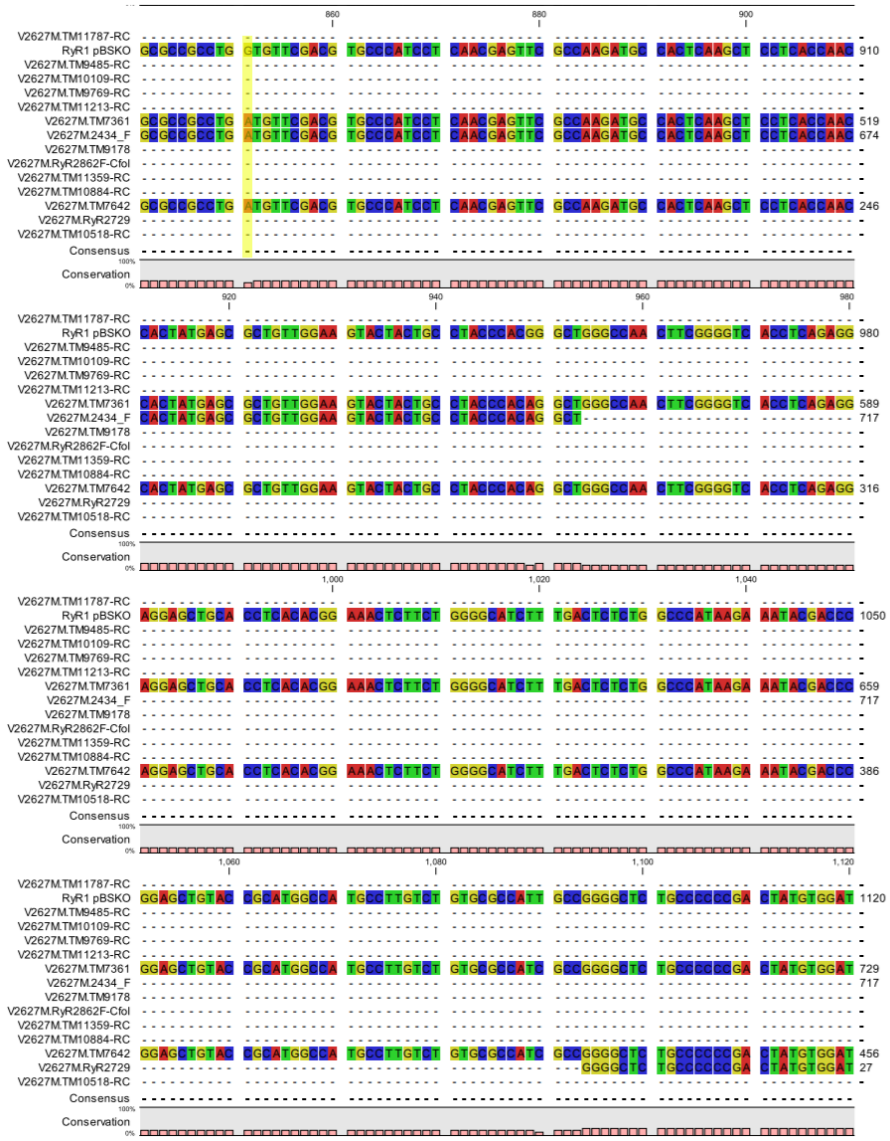

Figure 7.3. Multiple sequence alignment confirming absence of unwanted missense mutations in c.7879 G>A (p.Val2627Met).

Multiple sequence alignment of pBSKO+ construct after mutagenesis to incorporate the c.7879 G>A substitution. A total of 14 primers were used to sequence between restriction sites MfeI and NsiI used for sub-cloning of pBSKO+ into pBSKX+. Sequences were aligned to wild type *RYR1* NM_000540.3 using CLC sequence viewer 8 with a gap open cost of 25, a gap exit cost of 15, and a free end gap cost. Substitution highlighted in yellow. Dotted lines indicate nucleotide positions.

7.4 Sequencing of pBSKO+ (c.8026 C>T) (p.Arg2676Trp).

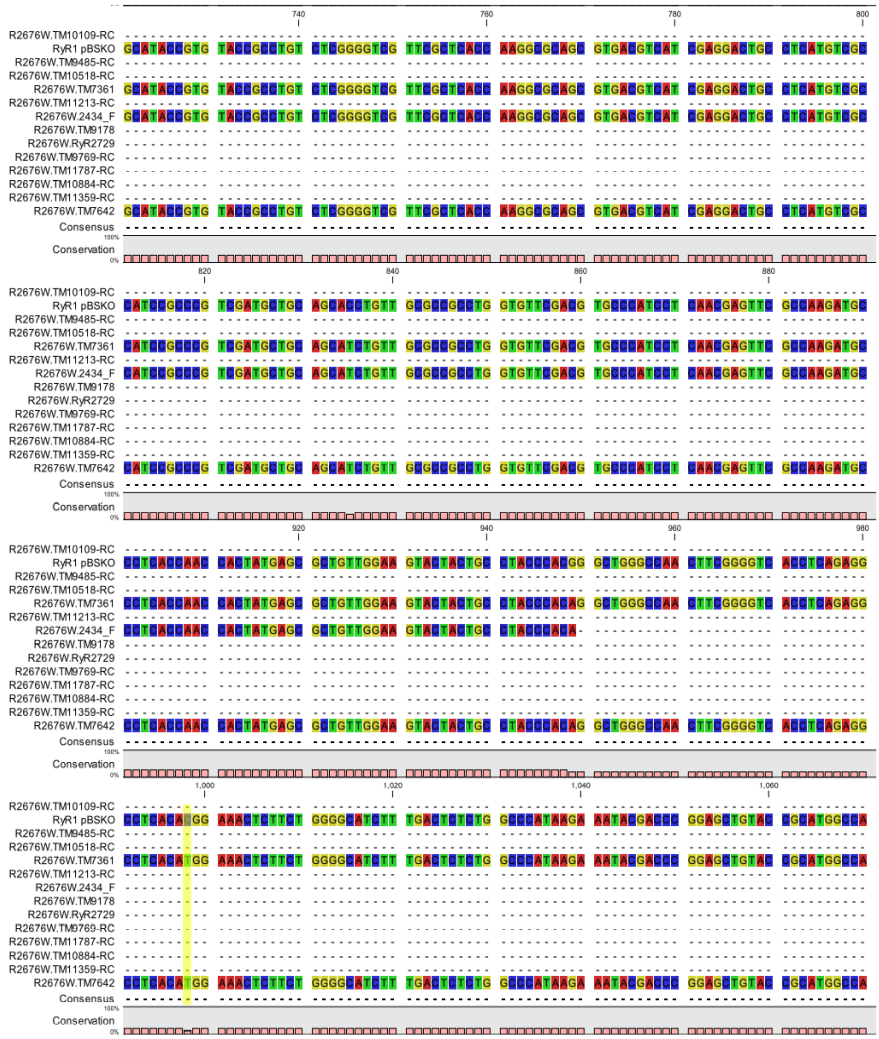

Figure 7.4. Multiple sequence alignment confirming absence of unwanted missense mutations in c.8026 C>T (p.Arg2676Trp).

Multiple sequence alignment of pBSKO+ construct after mutagenesis to incorporate the c.8026 C>T substitution. A total of 14 primers were used to sequence between restriction sites MfeI and NsiI used for sub-cloning of pBSKO+ into pBSKX+. Sequences were aligned to wild type *RYR1* NM_000540.3 using CLC sequence viewer 8 with a gap open cost of 25, a gap exit cost of 15, and a free end gap cost. Substitution highlighted in yellow. Dotted lines indicate nucleotide positions.

7.5 Sequencing of pBSKO+ (c.10042 G>A) (p.Arg3348His).

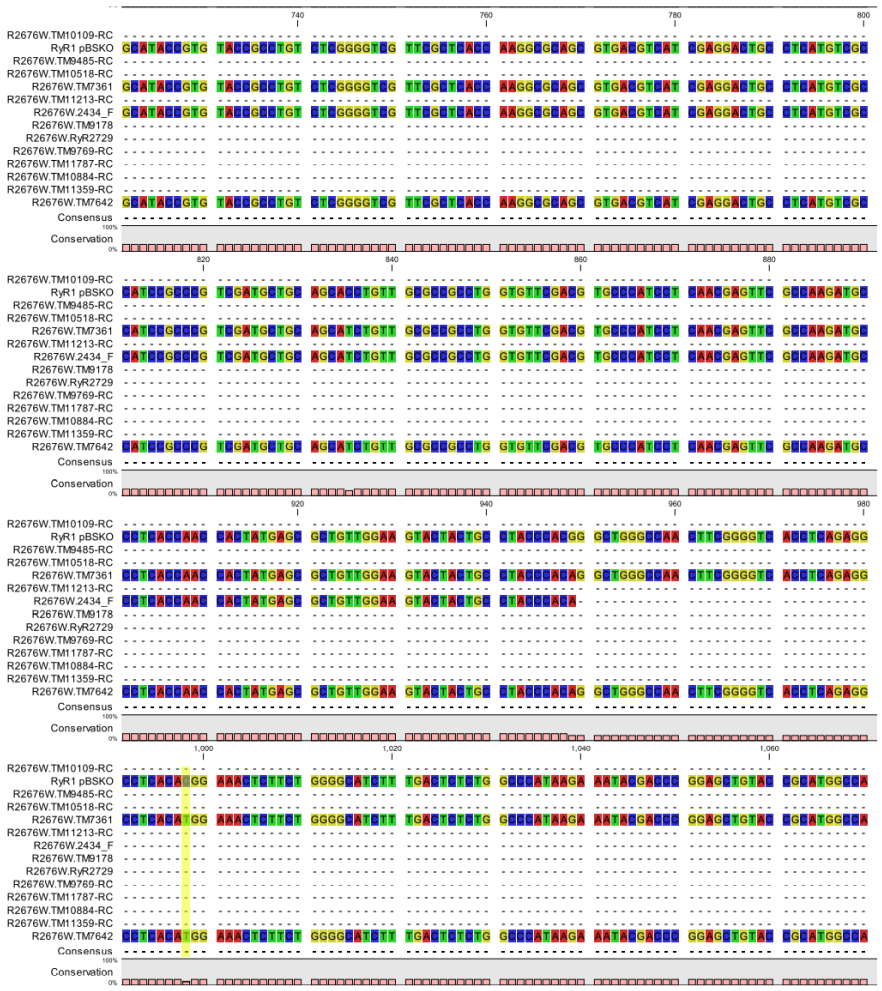

Figure 7.5. Multiple sequence alignment confirming absence of unwanted missense mutations in c.10042 G>A (p.Arg3348His).

Multiple sequence alignment of pBSKO+ construct after mutagenesis to incorporate the c.10042 G>A substitution. A total of 14 primers were used to sequence between restriction sites MfeI and NsiI used for sub-cloning of pBSKO+ into pBSKX+. Sequences were aligned to wild type *RYR1* NM_000540.3 using CLC sequence viewer 8 with a gap open cost of 25, a gap exit cost of 15, and a free end gap cost. Substitution highlighted in yellow. Dotted lines indicate nucleotide positions.

7.6 Sequencing of pBSH+ (c.14423 T>C) (p.Phe4808Ser).

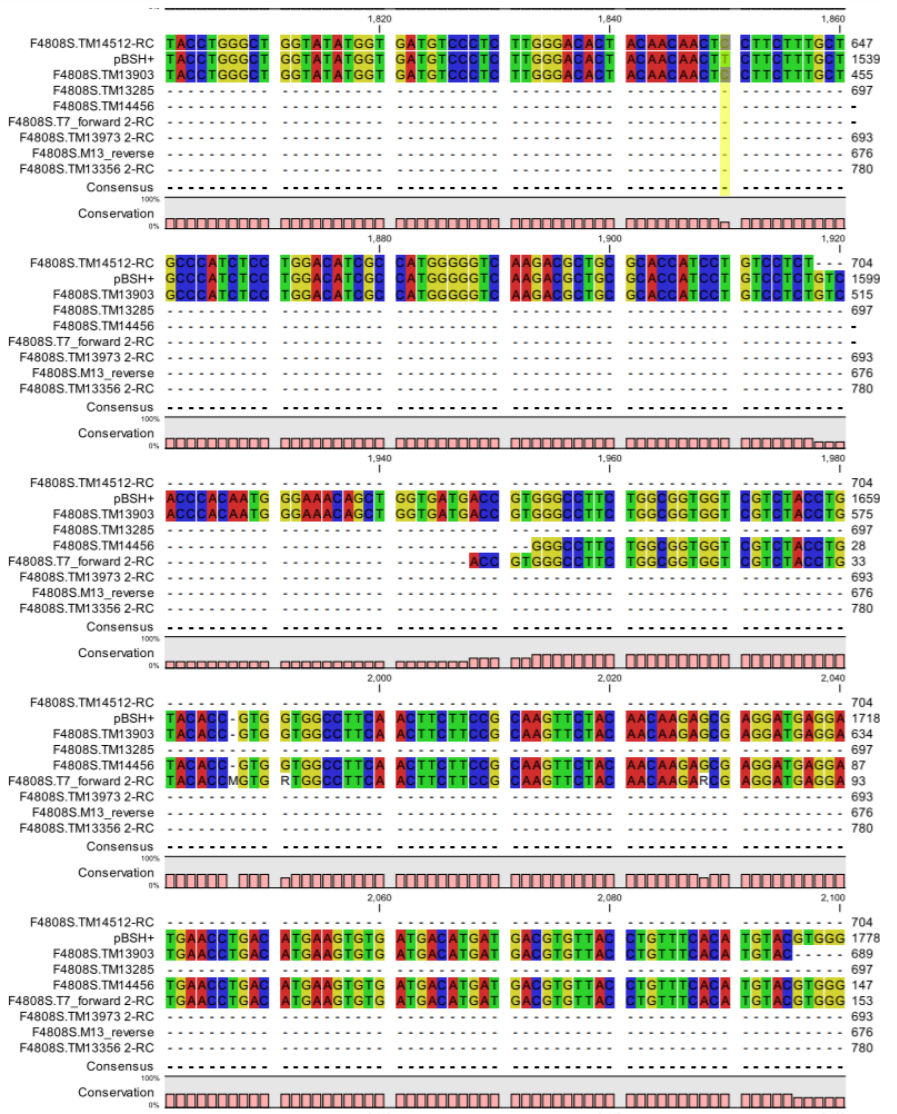

Figure 7.6. Multiple sequence alignment confirming absence of unwanted missense mutations in c.14423 T>C (p.Phe4808Ser).

Multiple sequence alignment of pBSH+ construct after mutagenesis to incorporate the c.14423 T>C substitution. 8 primers were used to sequence between restriction sites XbaI and SphI used for sub-cloning of pBSH+ into pBSKX+. Sequences were aligned to wild type *RYR1* NM_000540.3 using CLC sequence viewer 8 with a gap open cost of 25, a gap exit cost of 15, and a free end gap cost. Substitution highlighted in yellow. Dotted lines indicate nucleotide positions.

7.7 Sequencing of pBSH+ (c.14504 G>A) (p.Gly4835Glu).

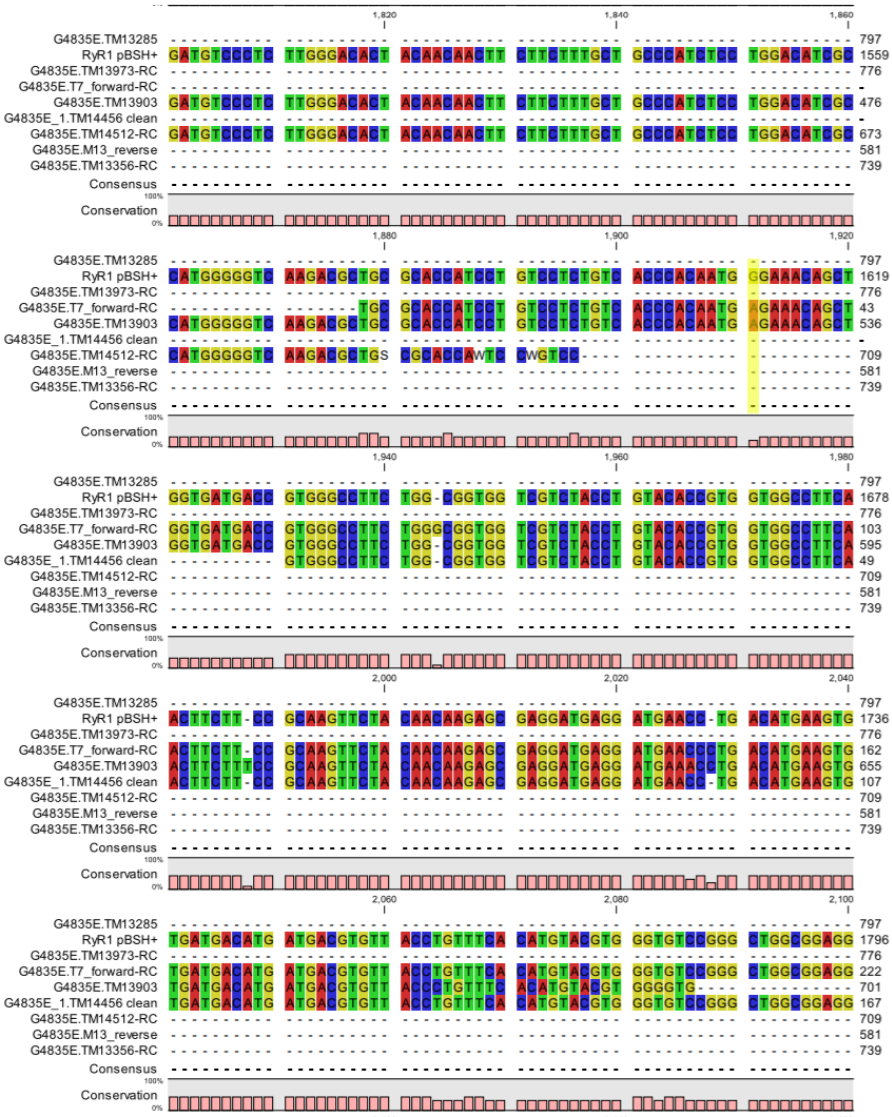

Figure 7.7. Multiple sequence alignment confirming absence of unwanted missense mutations in c.14504 G>A (p.Gly4835Glu).

Multiple sequence alignment of pBSH+ construct after mutagenesis to incorporate the c.14423 T>C substitution. 8 primers were used to sequence between restriction sites XbaI and SphI used for sub-cloning of pBSH+ into pBSKX+. Sequences were aligned to wild type *RYR1* NM_000540.3 using CLC sequence viewer 8 with a gap open cost of 25, a gap exit cost of 15, and a free end gap cost. Substitution highlighted in yellow. Dotted lines indicate nucleotide positions.

Appendix II: Sub-cloning of *RYR1* variants

7.8 Gel purification during sub-cloning.

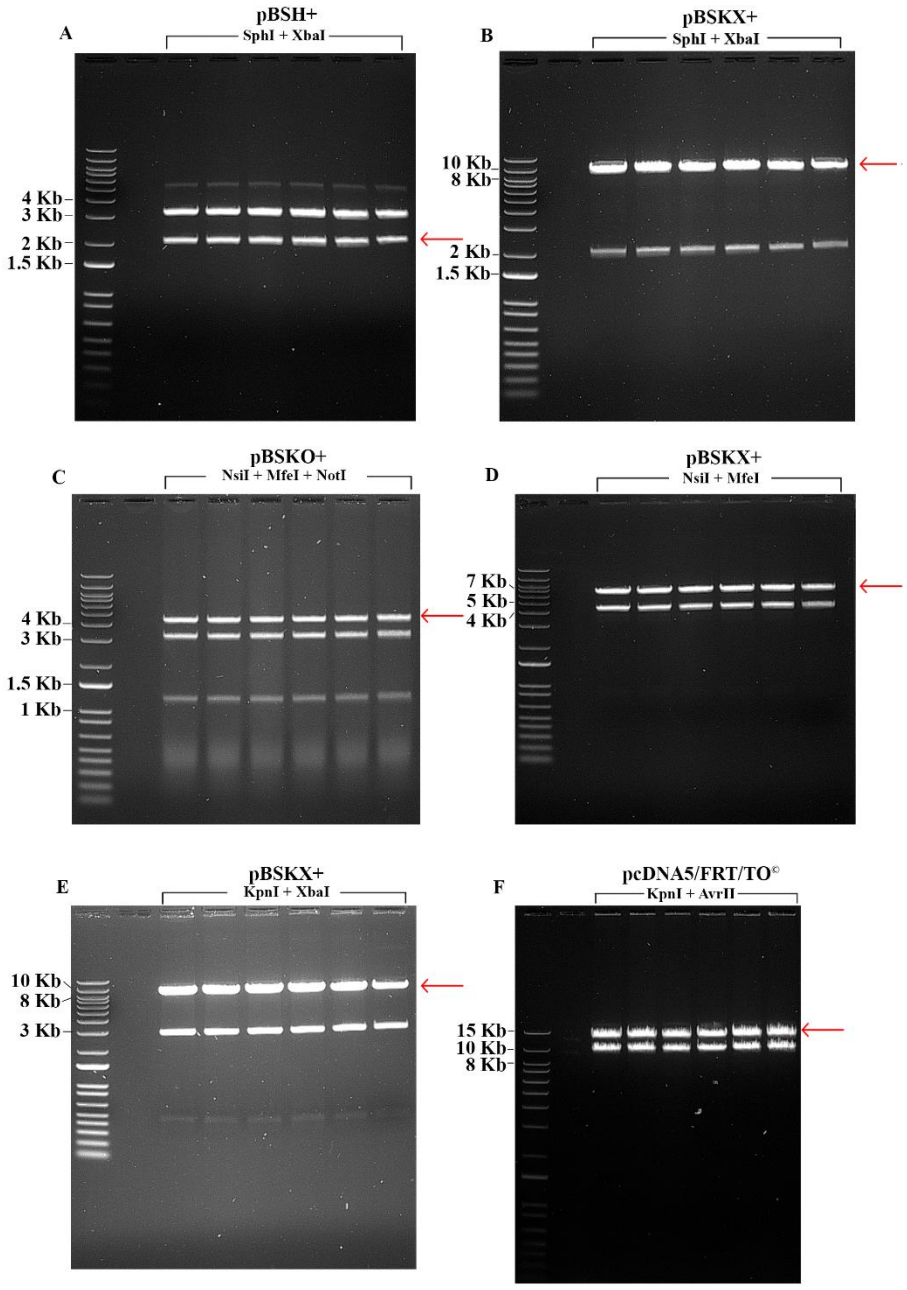

Figure 7.8. Examples of restriction endonuclease digests during sub-cloning process of variants c.14504 G>A (p.Gly4835Glu) and c.7374 G>T (p.Arg2458Leu).

0.8% agarose gel electrophoresis of DNA products after restriction endonuclease (RE) digest. One µg of plasmid DNA was digested for one hour at 37°C with the designated restriction enzymes. **(A)** RE digest of variant (c.14504 G>A) pBSH+ vector with SphI and XbaI. **(B)** RE digest of wild type pBSKX+ vector with SphI and XbaI. **(C)** RE digest of variant (c.7374 G>T) pBSKO+ vector with NsiI, MfeI, and NotI. **(D)** RE digest of wild type pBSKX+ vector with NsiI and MfeI. **(E)** RE digest of variant (c.7374 G>T) pBSKX+ vector with KpnI and XbaI. **(F)** RE digest of pcDNA5/FRT/TO© + full-length wild type *RYR1* cDNA (ftRyR1) with KpnI and XbaI. Red arrows denote the fragment that was purified.

Table 4. Sub-cloning: expected fragment lengths

Vector	Restriction endonucleases	Fragment length (bp)
pBSH+	SphI, XbaI	3200, 2049
pBSH+	XhoI	2958, 2291
pBSKO+	NsiI, MfeI, NotI	4340, 3245, 1234
pBSKX+	SphI, XbaI	9079, 2113
pBSKX+	NsiI, MfeI	6852, 4340
pBSKX+	KpnI, XbaI	8308, 2884
ftRyR1	KpnI, AvrII	12139, 9307

Table 5. ft/axRyR1 restriction digests: expected fragment lengths

Restriction endonuclease	ftRYR1 fragment lengths (bp)	axRYR1 fragment lengths (bp)
Undigested	21446	20383
BamHI	1084, 1261, 2943, 3627, 5140, 7391	21, 1261, 2943, 3627, 5140, 7391
HindIII	1311, 4292, 6233, 9610	1311, 4292, 5170, 9610
NdeI	1225, 3516, 16705	1225, 3516, 15642
NotI	3424, 8378, 9644	2361, 8378, 9644

7.9 Sequence chromatogram of axRyR1 (p.Arg2458Leu).

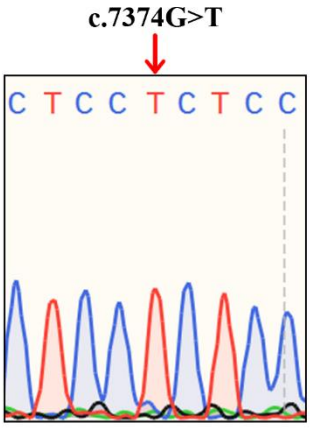

Figure 7.9. c.7374 G>T variant in full-length construct.

Sequence chromatogram showing presence of c.7374 G>T in ftRyR1, indicating successful generation of the full-length p.Arg2458Leu construct. Sequence visualised in Snapgene® 5.3.

Appendix III: Generation of cell lines stably expressing RyR1 variants.

Table 6. Primers for amplification and sequencing of genomic DNA.

Name	Size (bp)	Sequence	Annealing Temp (°C)	Variant
1403M for	16bp	AGGAGGAGTCCCAGGC	64	p.Phe539Leu
R614C rev	18bp	GGTCCGTCGTTCAAGAGT		
Ex 33 2F for	17bp	CGTGCAGTGCCAGGAGC	55	p.Arg1707Cys
Ex 34 2R rev	17bp	TCACGGAACAGGGCGTC		
TM6376 for	21bp	CAGTACGACGGGCTGGGTGAG	55	p.Gly2183Glu
TM6763 rev	21bp	GCCACTGTTCTCCAGCAGGTA		
TM6376 for	21bp	CAGTACGACGGGCTGGGTGAG	55	p.Cys2237Tyr
TM7039 rev	18bp	CACCACATTGGCGTTCTC		
2434 for	22bp	CTTTGTGAGGAACCGCCTGAAG	67	p.Arg2458Leu
TM7699 rev	21bp	GTGTTCTGTGCCCGCAAAGAG		
N2634K HRM for	15bp	GCCGCCTGGTGTTCG	55	p.Pro2793Leu
TM8789 rev	21bp	TAACCGCGTAGCCATTCATCT		
TM13903 for	21bp	GAACCCGCCCTGCGGTGTCTG	60	p.Thr4826Ile
TM14512 rev	21bp	GTAGACGACCACCGCCAGAAG		

7.10 Sequence alignments (genomic DNA from stable cell lines vs wild type *RYR1).*

Figure 7.10. Confirmation of presence of variation in stable cell lines.

Sequence alignment of PCR product from genomic DNA extracts prepared from stable cell lines with wild type *RYR1* NM_000540.3 (Ensembl). PCR product is depicted in purple, wild type *RYR1* is depicted in black, while the variant is indicated in red. Alignments were performed using the Emboss Needle pairwise sequence alignment tool (https://www.ebi.ac.uk/Tools/psa/emboss_needle/).

7.11 Confirmation of RyR1 expression in stable cell line clones.

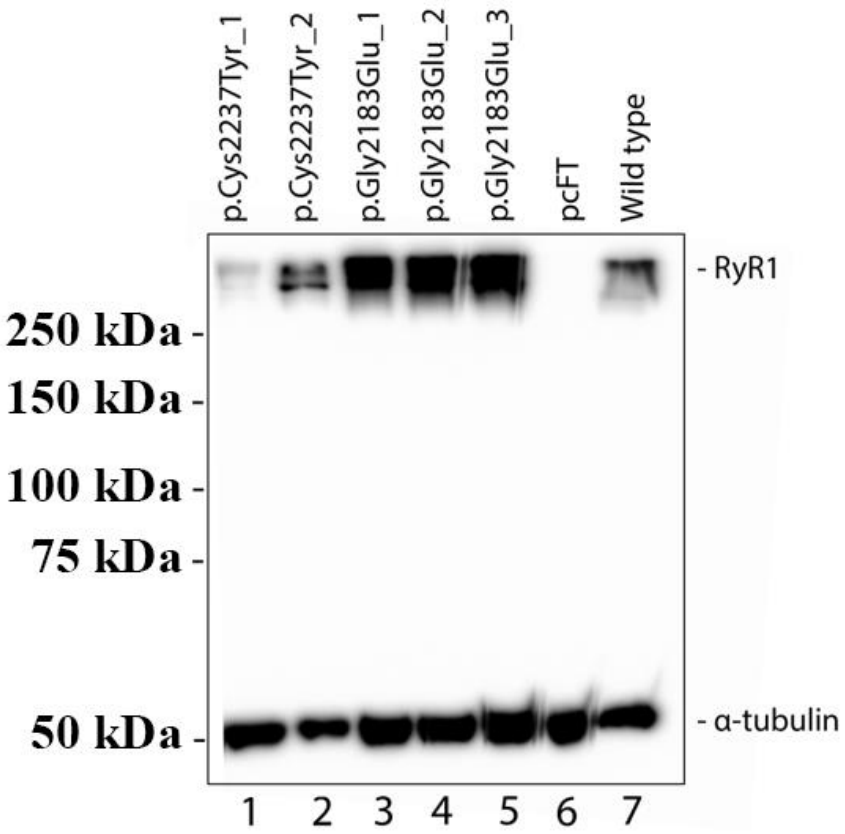

Figure 7.11. Expression of RyR1 in stable cell line clones.

Preliminary RyR1 expression analysis for selection of stable cell line clones. Protein extract from p.Cys2237Tyr and p.Gly2183Glu clones were separated on a 7.5% polyacrylamide gel for 2 ½ hours at 120 V then transferred to a PVDF membrane overnight at 4°C at 70 mA. Blotting for RyR1 was carried out with mouse 34C antibody. α-tubulin was visualised as a loading control using mouse anti-α-tubulin. Protein was visualised using HRP-conjugated anti-mouse secondary antibody. pcFT = protein extract from a cell line transfected with pcDNA5/FRT/TO© without *RYR1* cDNA.

7.12 Presence of RyR1 in uninduced cell line (p.Phe539Leu)

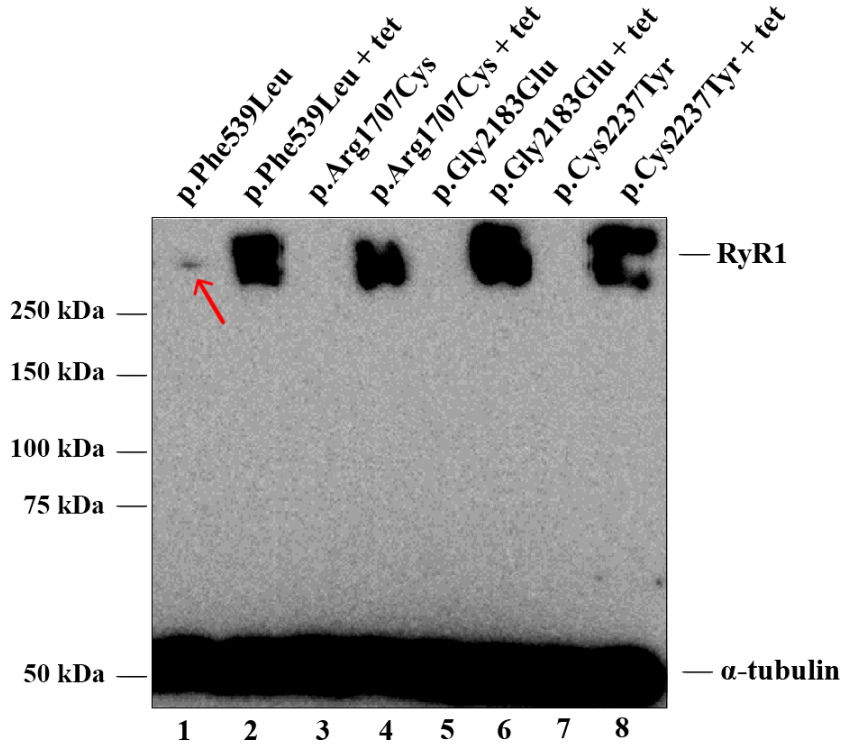

Figure 7.12. Over-exposure of RyR1 expression in Flp-In™ T-REx™ cell lines

Immunoblot analysis of protein extracts retrieved from Flp-In™ T-REx™ cell lines stably expressing RyR1 variants (p.Phe539Leu, p.Arg1707Cys, p.Gly2183Glu, p.Cys2237Tyr). Protein extracted from uninduced and induced (1 $\mu g mL^{-1}$ tetracycline) cell lines were separated via 7.5% SDS-PAGE then immunoblotted for RyR1 and α-tubulin as outlined in chapter 2.2.3.1. Red arrow depicts RyR1 expression in the uninduced p.Phe539Leu cell line. Markers are depicted in kDa. Well numbers are outlined below the figure.

Appendix IV: Functional analysis of RyR1 variants

7.13 Ca^{2+} release profiles in induced stable cell lines**.**

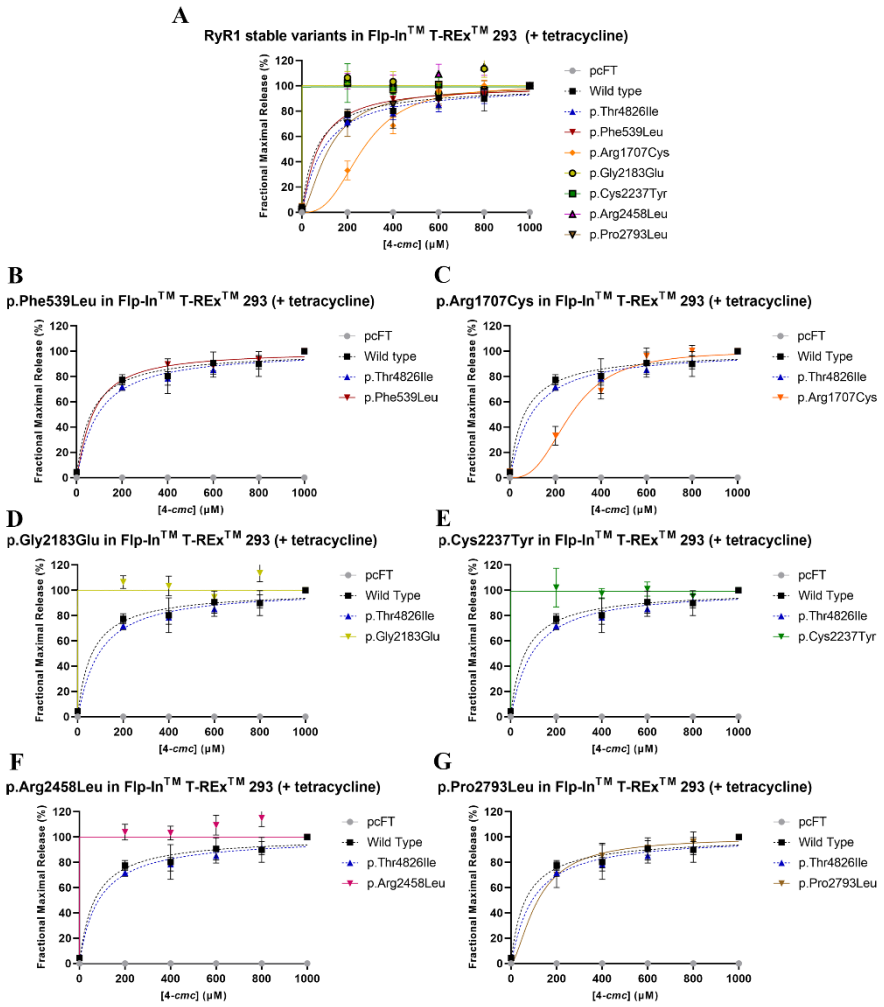

Figure 7.13 Ca^{2+} release profiles in induced cell lines

Ca^{2+} release in response to 4-c*m*c in induced cell lines, represented as a fraction of maximum Ca^{2+} release at exposure to 1000 µM 4-c*m*c. Dotted blue = p.Thr4826Ile, dotted black = wild type, grey = pcFT, red = p.Phe539Leu, orange = p.Arg1707Cys, gold = p.Gly2183Glu, green = p.Cys2237Tyr, pink = p.Arg2458Leu, brown = p.Pro2793Leu **(A)** Ca^{2+} release profile of all induced cell lines. **(B)** Ca^{2+} release profile of p.Phe539Leu. **(C)** Ca^{2+} release profile of p.Arg1707Cys. **(D)** Ca^{2+} release profile of p.Gly2183Glu. **(E)** Ca^{2+} release profile of p.Cys2237Tyr. **(F)** Ca^{2+} release profile of p.Arg2458Leu. **(G)** Ca^{2+} release profile of p.Pro2793Leu. Data compiled in Graphpad Prism 9™ and plotted as a variable slope.

Table 7. Average **Δ** fluorescence measurements during Ca^{2+} transients. (n = 5)

Construct	[4-c*m*c] (μM)	Average delta + tetracycline	Average delta - tetracycline
Wild Type	0	0.04	0
	200	0.82	0.23
	400	0.83	0.55
	600	0.95	0.83
	800	0.93	1.1
	1000	1.1	1.2
p.Phe539Leu	0	0.02	0.02
	200	0.72	0.35
	400	0.86	0.57
	600	0.82	0.72
	800	0.87	0.86
	1000	0.93	1.0
p.ArgR1707Cys	0	0.02	0
	200	0.26	0.025
	400	0.64	0.065
	600	0.91	0.11
	800	0.99	0.25
	1000	1.0	0.31
p.Gly2183Glu	0	0.02	0.033
	200	1.4	0.33
	400	1.7	0.50
	600	1.3	0.65
	800	1.5	0.73
	1000	1.4	0.98
p.Cys2237Tyr	0	0.02	0.03
	200	0.81	0.83
	400	0.77	1.0
	600	0.80	1.1
	800	0.75	1.2
	1000	0.80	1.2
p.Arg2458Leu	0	0.028	0.023
	200	1.1	0.23
	400	1.1	0.30
	600	1.2	0.32
	800	1.2	0.37
	1000	1.1	0.50
p.Pro2793Leu	0	0	0.01
	200	0.74	0.42
	400	0.91	0.66
	600	0.98	0.76
	800	1.0	0.88
	1000	1.1	0.87

p.Thr4826Ile	0	0.02	0
	200	0.60	0.77
	400	0.66	0.98
	600	0.72	1.3
	800	0.77	1.3
	1000	0.84	1.2

Table 8. Functional analysis EC_{50}/p-values (Induced cell lines).

Variant	**EC_{50} ([4-*cmc*] µM) ± SEM**	**P-value (* < 0.05 ** <0.01)**	**Status**
Wild type	114.92 ± 33.39	N/A	N/A
pcFT	0 ± 0	N/A	N/A
p.Phe539Leu	82.42 ± 12.91	0.215	-
p.Arg1707Cys	348.63 ± 38.50	0.00126**	-
p.Gly2183Glu	43.61 ± 0	N/A	N/A
p.Cys2237Tyr	192.7 ± 0	N/A	N/A
p.Arg2458Leu	176.5 ± 0	N/A	N/A
p.Pro2793Leu	207.18 ± 22.78	0.0423 *	-
p.Thr4826Ile	96.09 ± 20.41	0.328	-

Table 9. Functional analysis EC_{50}/p-values (Uninduced cell lines).

Variant	**EC_{50} ([4-*cmc*] µM) ± SEM**	**P-value (* < 0.05 ** < 0.01)**	**Status**
Wild type	377.1 ± 31.73	N/A	-
pcFT	0 ± 0	N/A	-
p.Phe539Leu	304.82 ± 18.12	0.0397 *	-
p.Arg1707Cys	621.55 ± 29.50	0.0247 *	-
p.Gly2183Glu	358.42 ± 38.11	0.358	-
p.Cys2237Tyr	128.66 ± 13.37	$4.56x10^{-5}$ **	+
p.Arg2458Leu	283.86 ± 18.71	0.0161 *	-
p.Pro2793Leu	218.97 ± 17.67	$9.21x10^{-4}$ **	+
p.Thr4826Ile	221.32 ± 38.32	0.00605 **	+

Table 10. Functional analysis EC_{50}/p-values (FKBP12 vs Wt RyR1).

Variant	**EC_{50} ([4-*cmc*] µM) ± SEM**	**P-value (* < 0.05 ** <0.01)**
Wild type	293.80 ± 10.86	0.0210 *
pcFT	0 ± 0	N/A
p.Phe539Leu	367.57 ± 16.62	0.398
p.Cys2237Tyr	123.07 ± 37.56	0.00178 **
p.Pro2793Leu	282.77 ± 32.97	0.0424 *
P.Thr4826Ile	305.54 ± 60.65	0.0607

Table 11. Functional analysis EC_{50}/p-values (pre- vs post- FKBP12).

Variant	**EC_{50} ([4-*cmc*] µM) ± SEM**	**P-value (* < 0.05 ** <0.01)**
Wild type	293.80 ± 10.86	0.0210 *
pcFT	0 ± 0	N/A
p.Phe539Leu	367.57 ± 16.62	0.0217 *
p.Cys2237Tyr	123.07 ± 37.56	0.449
p.Pro2793Leu	282.77 ± 32.97	0.0933
P.Thr4826Ile	305.54 ± 60.65	0.286

Table 12. pcFKBP12 restriction endonuclease digest (expected fragment lengths)

Vector	Restriction endonuclease	Fragment lengths (bp)
pcFKBP12	BamHI + EcoRI	5405, 335

7.14 pcFKBP12 restriction endonuclease digest

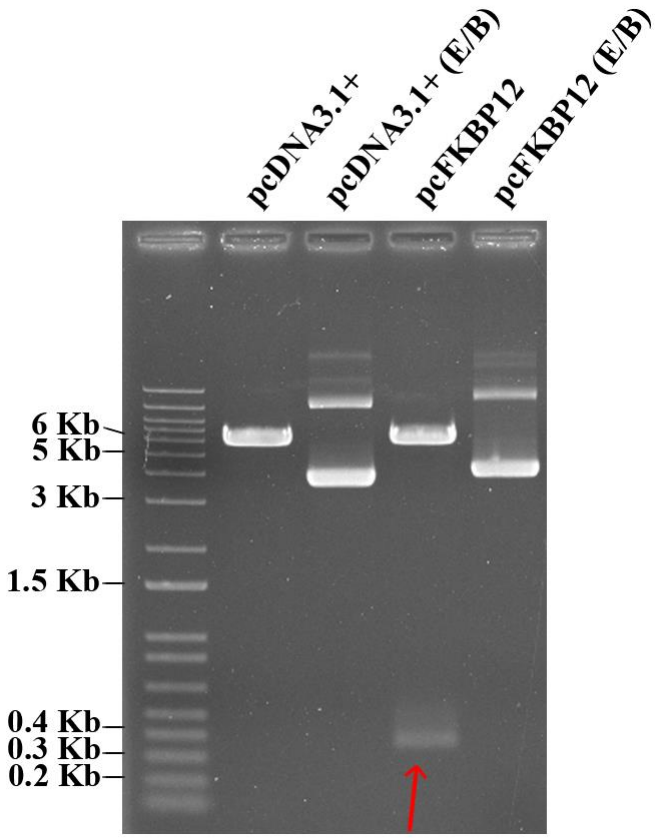

Figure 7.14. Restriction endonuclease digest of *FKBP12* cDNA

Restriction digest of pcDNA^{TM}3.1(+) containing *FKBP12* cDNA. E = EcoRI, B = BamHI. Plasmid DNA was incubated for 2 hours at 37°C with EcoRI and BamHI, the fragments were then separated on a 0.8% agarose gel. 1Kb+ marker bands are denoted in Kb, *FKBP12* cDNA is identified with red arrow. Image was compiled in Adobe Photoshop.

Table 13. Primer sequences for multiplex PCR

Name	Size (bp)	Sequence (5'-3'	Tm (°C)	Target	Product size (bp)
FKBP12 Forward	20	GGTTGCCCAGATG AGTGTGG	59	FKBP12	139
FKBP12 reverse	27	TCATTCCAGTTTTA GAAGCTCCACATC	57	FKBP12	
TUBB forward	21	CAGATCGGTGCCA AGTTCTGG	58	*β-tubulin*	80
TUBB reverse	18	TCGCTGTCCCCGTG GTAG	60	*β-tubulin*	

7.15 Multiplex PCR of *FKBP12* and *β-tubulin*

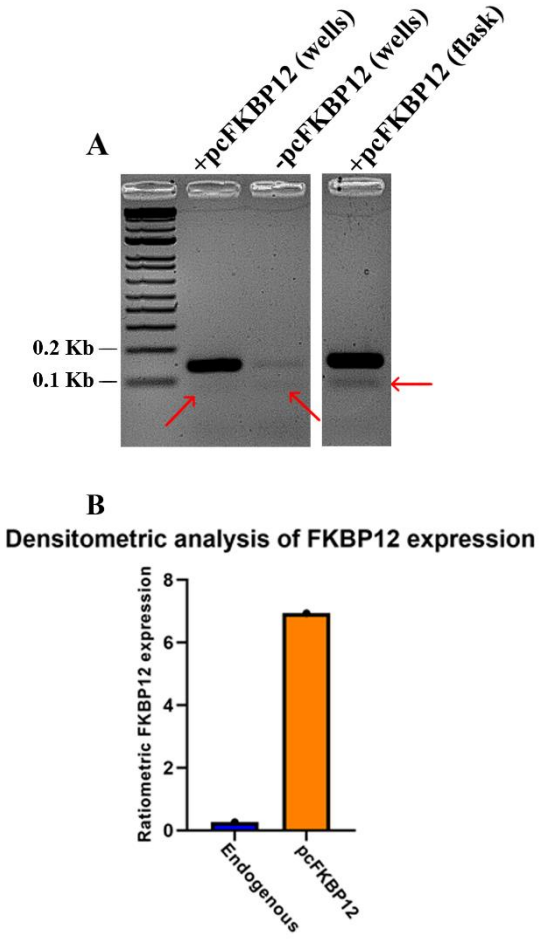

Figure 7.15. Over-expression of FKBP12 in stable cell lines

Confirmation of over-expression of FKBP12 in stable cell lines. **(A)** 2% agarose gel electrophoresis of *FKBP12* and *β-tubulin* RT-PCR products. Red arrows identify *β-tubulin*. Sizes of 1Kb+ marker bands in Kb. **(B)** Densitometric analysis of *FKBP12* expression in untransfected and transfected cells. Expression was normalised to *β-tubulin* expression. Densitometric analysis was carried out using the densitometric analysis tool in ImageJ (Fiji).

Appendix V: Plasmid maps

Plasmid maps were generated using SnapGene® 5.3. Sequences for pBlueScript SK+, pcDNA™3.1(+), pcDNA5/FRT/TO© and pOG44 were retrieved from the SnapGene database (http://www.snapgene.com/resources/plasmid_files/your_time_is_valuable/).

Table 14. List of vectors.

Vector	Size (bp)	Expression system	Mode of expression
pBSH+	5249	DH5-α *E.coli*	-
pBSKO+	8819	DH5-α *E.coli*	-
pBSKX+	11192	DH5-α *E.coli*	-
ftRyR1	21446	DH5-α *E.coli*, Flp-In™ T-REx™ 293	Tetracycline
axRyR1	20383	DH5-α *E.coli*, Flp-In™ T-REx™ 293	Tetracycline
pOG44	5785	DH5-α *E.coli*, Flp-In™ T-REx™ 293	Constitutive
pcFT	5166	DH5-α *E.coli*, Flp-In™ T-REx™ 293	Tetracycline
pcDNA™3.1(+)	5428	DH5-α *E.coli*, Flp-In™ T-REx™ 293	Constitutive
pcFKBP12	5740	DH5-α *E.coli*, Flp-In™ T-REx™ 293	Constitutive

7.16 pBSH+

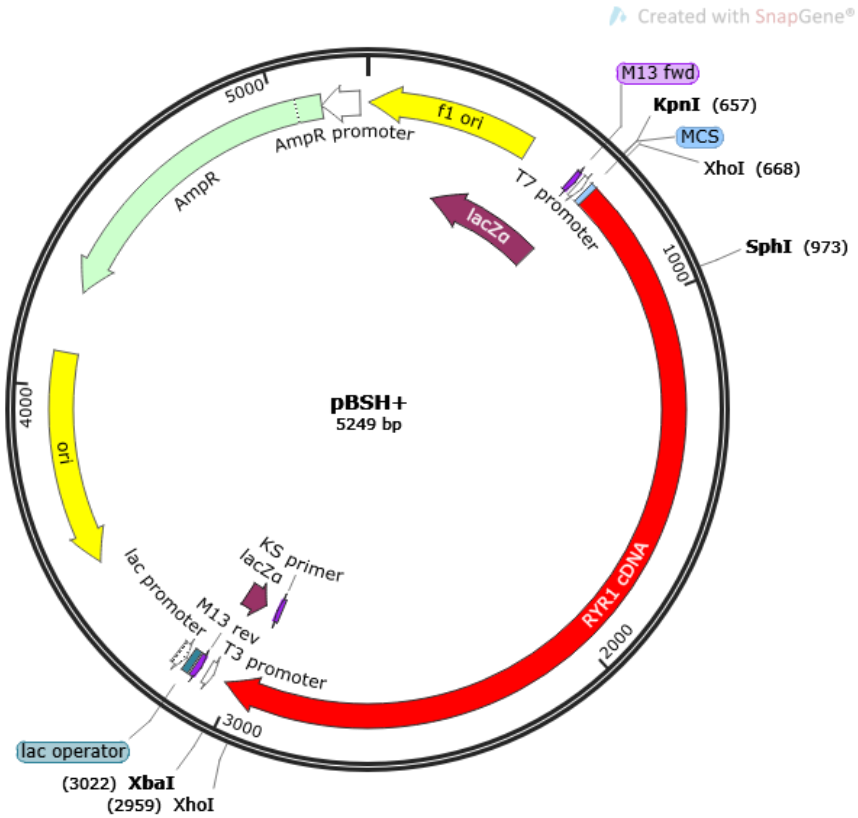

7.17 pBSKO+

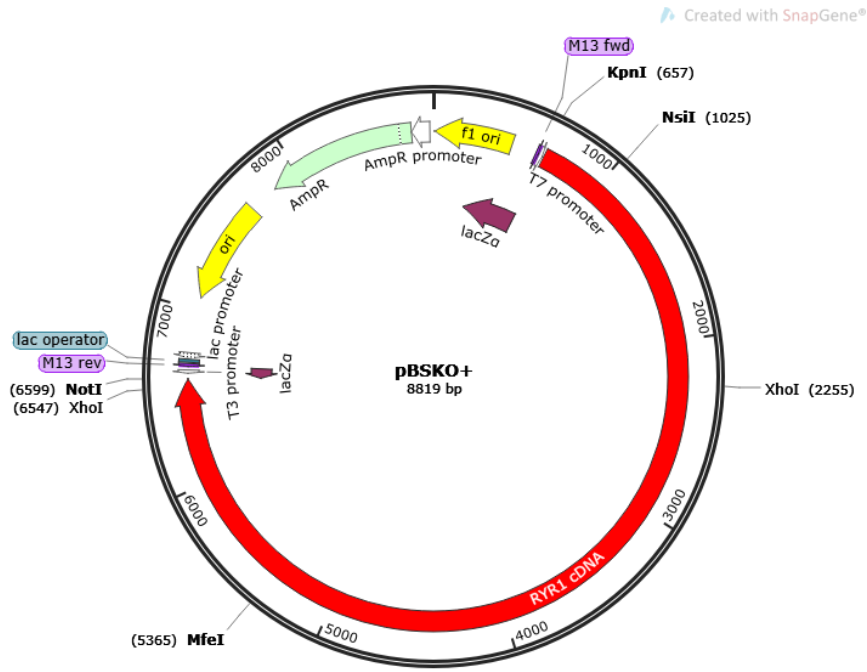

7.18 pBSKX+

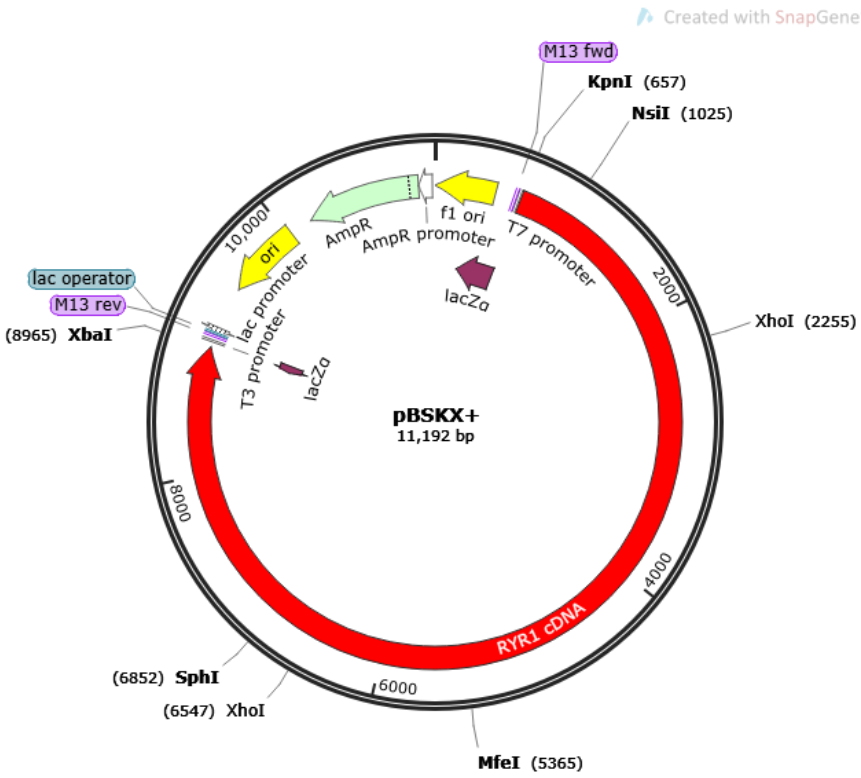

7.19 ftRyR1

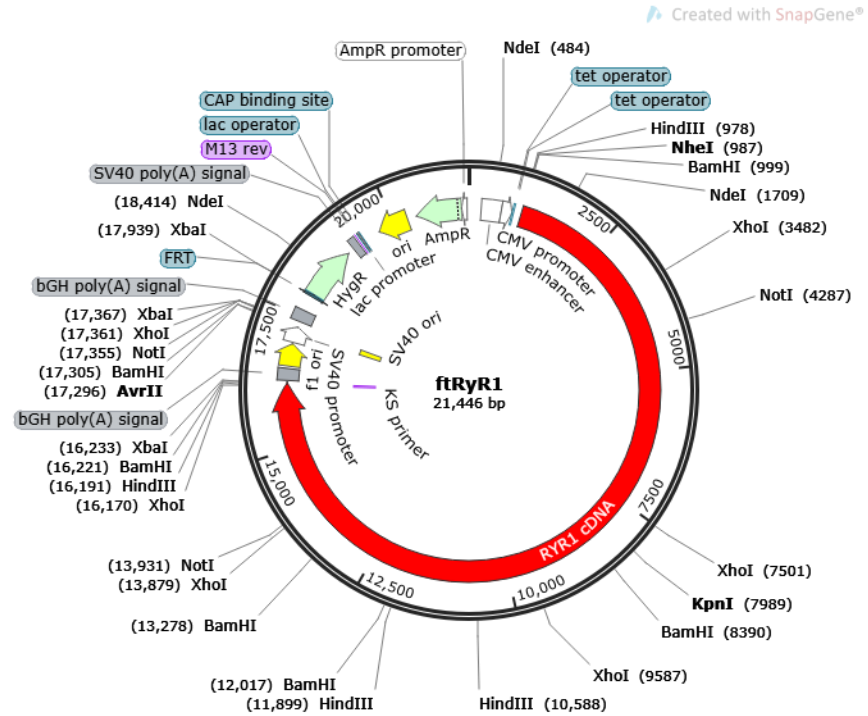

7.20 axRyR1

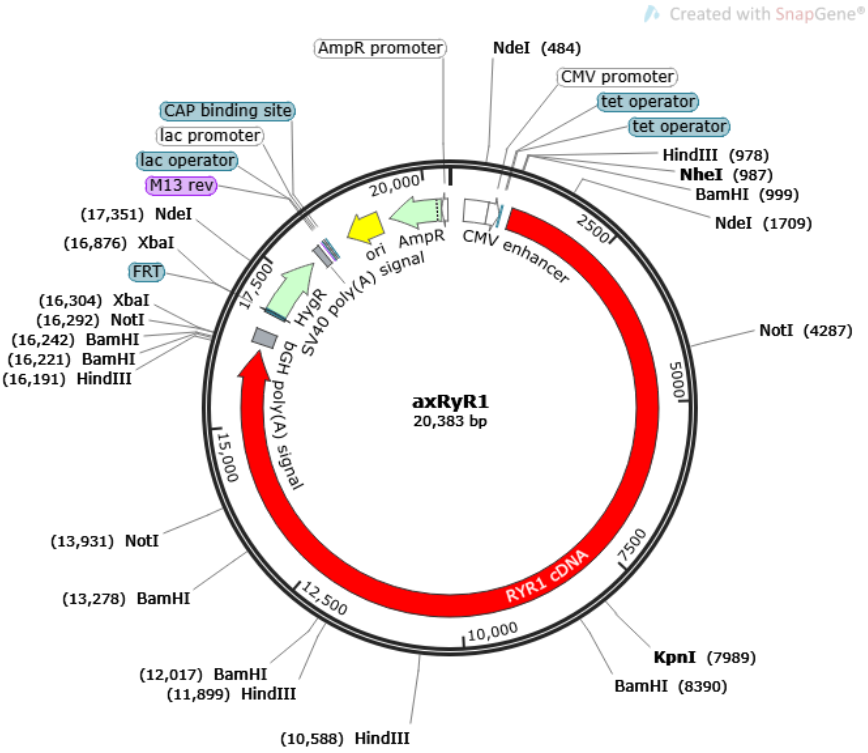

7.21 pcFT

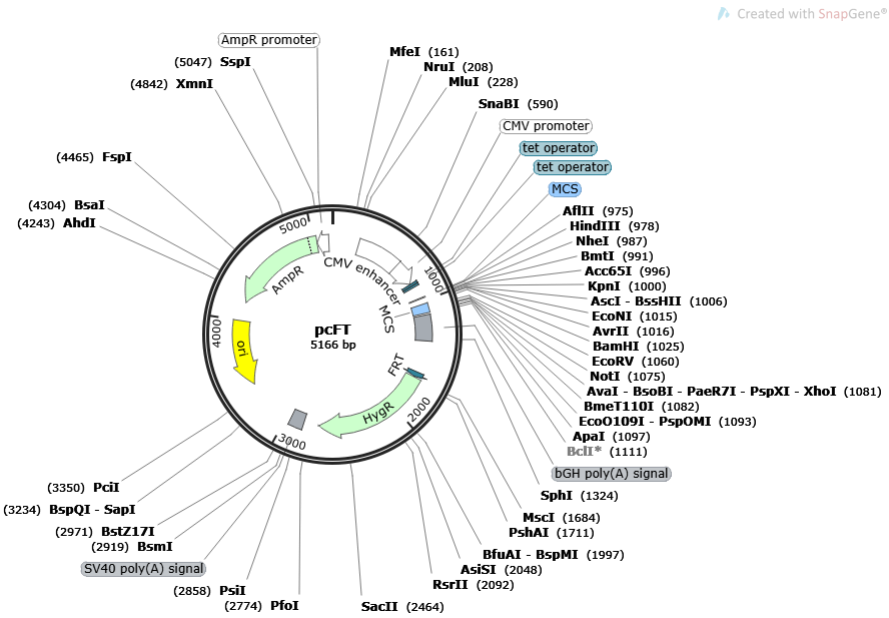

7.22 pOG44

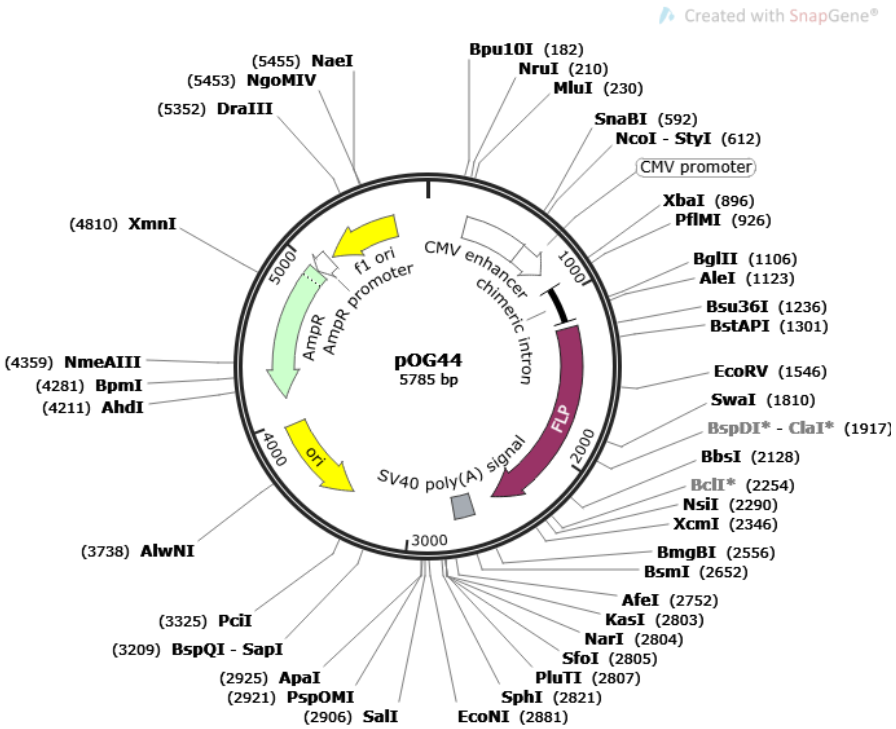

7.23 pcDNA^{TM}3.1(+)

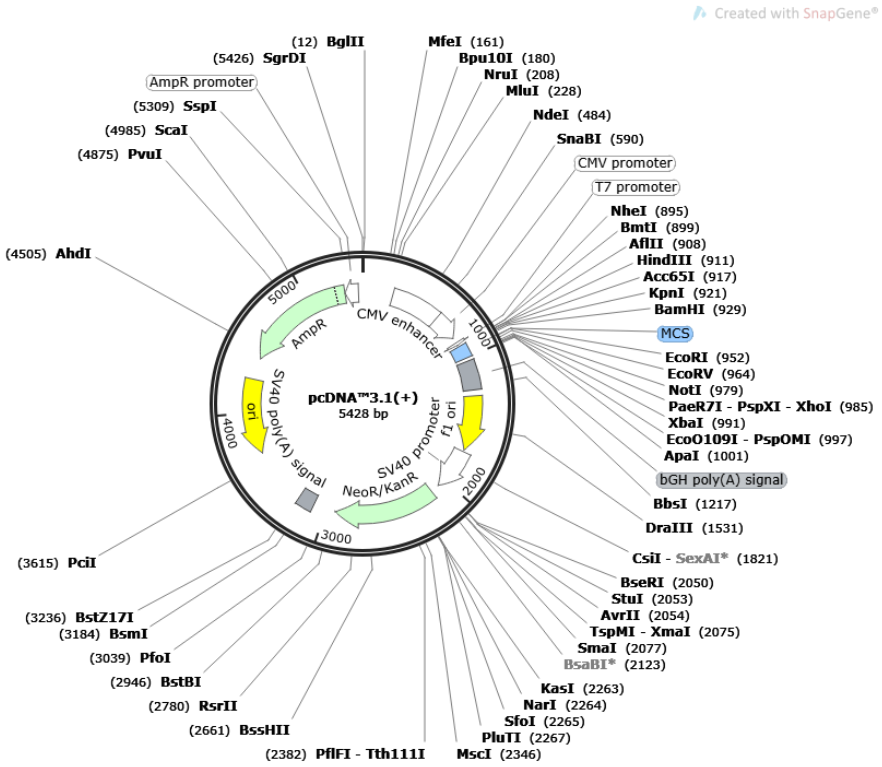

7.24 pcFKBP12